

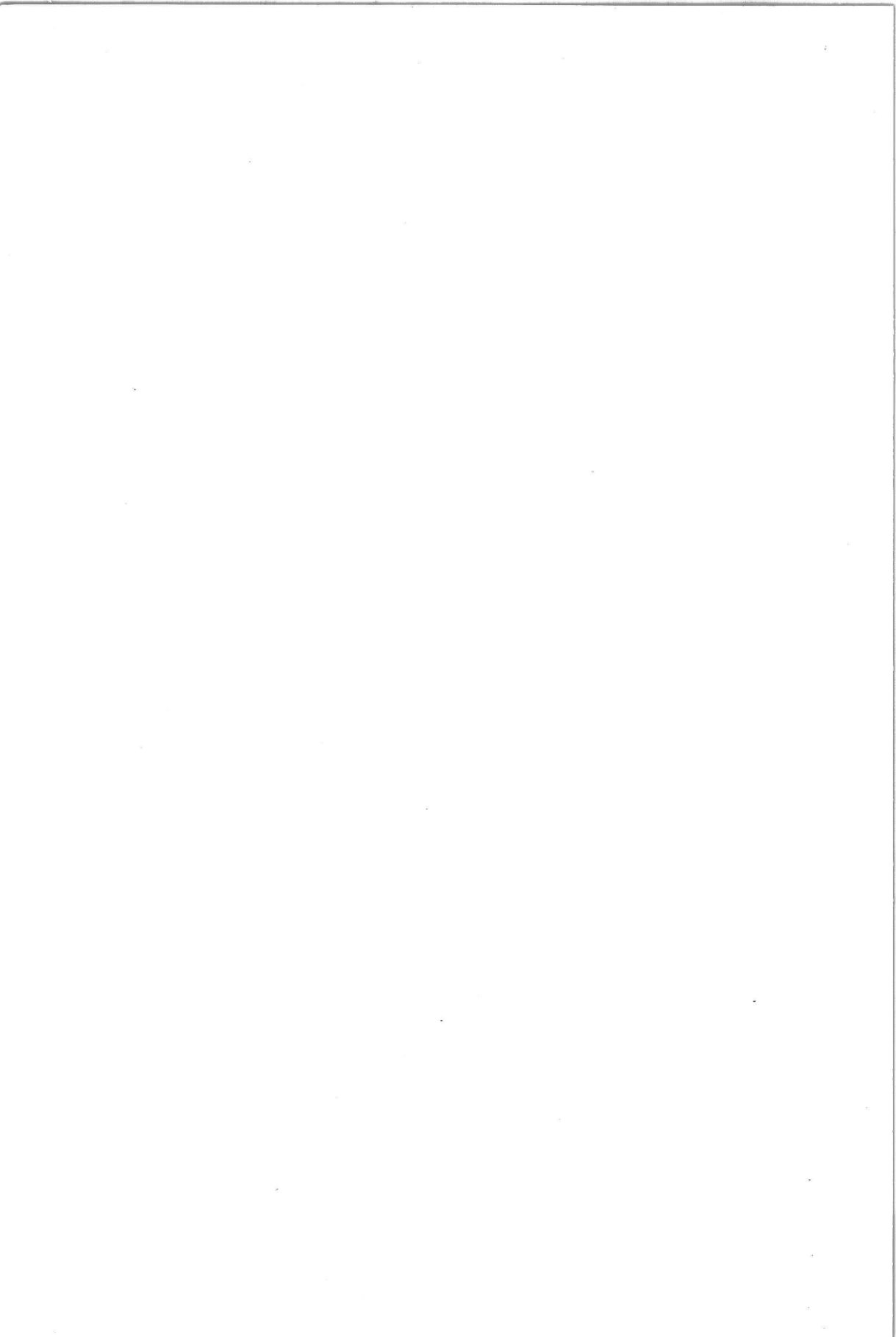
ON THE DETECTION OF COHERENT STRUCTURES IN TURBULENT FLOWS

J.M.G. Kunen

2119 4372

Delft University Press

2110



ON THE DETECTION OF COHERENT STRUCTURES IN TURBULENT FLOWS

Microfilm edition of the book published by Delft University of Technology, Delft, The Netherlands, 1987. 1 volume, 1 microfilm reel, 120 frames. Includes index.

C10C87
51222

BIBLIOTHEEK TU Delft
P 2119 4372



C

875122

ON THE DETECTION OF COHERENT STRUCTURES IN TURBULENT FLOWS

2119 4342



Proefschrift

Ter verkrijging van de graad van doctor
in de technische wetenschappen aan de
Technische Hogeschool Delft, op gezag van
de Rector Magnificus, prof. ir. B.P.Th. Veltman
in het openbaar te verdedigen
ten overstaan van het College van Dekanen
op dinsdag 30 oktober 1984 te 14.00 uur

door

JOSEPH MATHIAS GERARDUS KUNEN

geboren te Venray
vliegtuigbouwkundig ingenieur

Delft University Press/1984

Dit proefschrift is goedgekeurd door de promotor
PROF.DR.IR. G. OOMS

*Aan mijn ouders
Aan Rosette*

TABLE OF CONTENTS

	Quotes	vii
	Summary	viii
I	INTRODUCTION	1
1.1	Brief review of experimental turbulence research	2
1.2	Structure of wall-bounded turbulence	4
1.2.1	Structure of the wall layer	5
1.2.1.1	Flow visualization in the wall layer	5
1.2.1.2	Quantitative measurements in the wall layer	11
1.2.1.3	Comparison between methods of burst detection	16
1.2.2	Structure of the outer layer	16
1.2.2.1	Flow visualization in the outer layer	16
1.2.2.2	Quantitative measurements in the outer layer	18
1.2.3	Structure in the Reynolds stress	20
1.2.4	Organized motion in a turbulent boundary layer	23
1.3	Structure of free turbulence	25
1.3.1	Plane mixing layers	25
1.3.2	Axisymmetric shear layers	28
1.4	Present investigation	32
II	DESCRIPTION OF EXPERIMENTS	34
2.1	Boundary layer	34
2.1.1	Experimental set-up	34
2.1.2	Experimental results	35
2.2	Pipe flow	37
2.2.1	Experimental set-up	37
2.2.2	Experimental results	41
2.3	Channel flow	49
2.3.1	Experimental set-up	49
2.3.2	Experimental results	54
2.4	Axisymmetric jet flow	59
2.4.1	Experimental set-up	59
2.4.2	Experimental results	60

III	DETECTION SCHEMES	65
3.1	Scheme of Ueda and Hinze	65
3.1.1	Description of the scheme	65
3.1.2	Test results	66
3.2	Scheme of Blackwelder and Kaplan	67
3.2.1	Description of the scheme	67
3.2.2	Test results	70
3.2.3	Further tests	73
3.3	Modified scheme of Blackwelder and Kaplan	83
3.3.1	Description of the scheme	83
3.3.2	Test results	83
3.4	Autocorrelation method	89
IV	HYDROGEN BUBBLE VISUALIZATION COMBINED WITH LASER- DOPPLER ANEMOTRY	90
4.1	Observed flow structures	90
4.1.1	Plan view	91
4.1.2	Side view	92
4.2	Characteristic signals of flow structures in the wall layer	94
4.2.1	Low-speed streaks	95
4.2.2	High-speed streaks	96
4.2.3	Eddies	96
4.2.4	Some illustrations	97
4.3	Second quadrant detection method	100
4.3.1	Description and results	100
4.3.2	Comparison with other visualization studies	103
4.4	Detections of Blackwelder and Kaplan's method	105
V	APPLICATION OF QUADRANT ANALYSIS TECHNIQUE TO JET FLOW	107
5.1	Quadrant analysis without hole	108
5.2	Quadrant analysis with hole	110
VI	RECAPITULATION AND DISCUSSION	115

List of symbols	118
References	122
Appendix A: Description of a turbulent boundary layer	130
Appendix B: Description of an axisymmetric jet flow	132
Samenvatting	133
Acknowledgement	135
Levensbericht	135

QUOTES

"Say that a blind man using a road bed sensor attempted to find out what a motor vehicle looked like. Happening to use a road only traveled by airport limousines and motorcycles, he concludes that the average vehicle is a compact car with 2.4 wheels. He might later attempt to construct a theoretical model of the mechanics of such a vehicle, and may attain fame for a tentative model that looks like a motorcycle with a sidecar whose wheel is only in contact with the ground forty percent of the time."

Mollo-Christensen, E. [1971]

"Man, irrespective of whether he is a theologian or scientist, has a strong tendency to see what he hopes to see."

Eiseley, L. [1979]

"Turbulence researchers are very much like archaeologists who seek the origin of man by extrapolative evaluation of bits and pieces of fossilized remains; we try to piece together experimental observations and the 'remains' which our measurement techniques allow us to obtain with the hope that we can establish not only the size and shape of the turbulence 'beast', but its modes of growth, death, reproduction, and interactions with other 'beasts'. Unfortunately, the bits and pieces of information we have for turbulent boundary layers still leave many holes in the morphological puzzle; consequently, current researchers still can't agree whether our 'beast' is large or small, or whether we have more than one beast, or if (like the caterpillar/butterfly) we have a beast which passes through some metamorphosis."

Smith, C. R. [1983]

SUMMARY

This thesis deals with the problem of detecting coherent structures in turbulent flows.

Some Eulerian detection methods were tested; viz. the method of Ueda and Hinze, the method of Blackwelder and Kaplan and a modified version of Blackwelder and Kaplan's method. Hereto measurements were performed in a turbulent boundary layer flow and a turbulent pipe flow. Results show that these methods are not objective; the mean time between successive detections, the distribution of time intervals between successive detections and the conditionally averaged streamwise velocity are very dependent on the parameter values used in the methods. The distribution of time intervals between successive detections and the contribution of detections to the Reynolds stress are also not in agreement with results of visualization studies. Therefore, the only conclusion can be that these Eulerian detection methods are not very appropriate methods to make measurements on coherent structures.

The autocorrelation technique appears also not to be very useful in establishing properties of coherent structures, because this technique can be applied only part of the measuring time.

Flow visualization and Eulerian measurement were combined in an investigation of a turbulent water flow to compare visual and Eulerian detection on a one-to-one basis. Hydrogen bubbles were used to visualize the flow. Only part of the detections of Blackwelder and Kaplan's method appears to coincide with visual detections. Eulerian detections of the so-called second quadrant method, in which only the contributions to the Reynolds stress belonging to the second quadrant are considered, correlate very well with visual detections of ejections. Also bursts are detected in this way, if detections with small time intervals are considered to be detections on the same structures.

The quadrant analysis technique was also applied to a turbulent jet. As this technique does not provide information about origin and orientation of structures, it is only successful in detecting structures in those parts of a jet flow where the influence of the nearby boundary is substantial; viz. the mixing layer region and the outer part of the development region.

Chapter I

INTRODUCTION

It is generally accepted that the time dependent Navier-Stokes equations describe turbulence.

So far it has been impossible to solve these equations, because of the non-linearity of the equations, the essentially three-dimensional character of turbulence and the wide range of scales that controls turbulence.

Reynolds [1895] proposed the decomposition of the velocity components and the pressure in a mean and a fluctuating part. Substitution into the Navier-Stokes equations yields after time-averaging a system of equations almost identical in form to the original system. However, in the new set of equations convective stress terms arise from averaging products of the velocity fluctuations -the so-called Reynolds stresses. Therefore, the set of equations is not closed and an additional equation is needed for the relation between the Reynolds stresses and the mean velocity field.

Until recently much turbulence research was concentrated on finding the additional equation for simple flow configurations hoping the equation could be modified so that it would hold for more complex flow configurations. But until now it has not been possible to construct a more general turbulence model to say nothing of an universal model.

In the following sections first a brief summary of experimental techniques used to investigate turbulence will be given. Further, a review of a new development in turbulence research -the coherent structures in turbulent flows- will be presented. This review will be divided in two parts, one dealing with wall-bounded turbulent flows and one with free turbulent flows. A more complete review of coherent structures can be found in the papers of Willmarth [1975] and Cantwell [1981] -regarding wall-bounded turbulence- and of Hussain [1983] -concerning free turbulence. In the last section the contents of this thesis will be outlined.

1.1 BRIEF REVIEW OF EXPERIMENTAL TURBULENCE RESEARCH

In the 1920's and early 1930's mean velocity measurement was the most important experimental method. Only pressure measuring devices (pitot-tube, venturi-meter) and moving-part instruments (cup anemometer, vane anemometer) were operational. Hot-wire anemometry still was in development.

With these experimental tools it was impossible to check the phenomenological theories of those days.

These theories started from the idea that turbulence was an essentially stochastic phenomenon:

A turbulent flow field exists of a mean velocity field and a randomly fluctuating field.

All scales smaller than the overall dimensions of the flow are important for the turbulent flow.

A well-known theory is the mixing-length theory set up independently by Prandtl [1925] and Taylor [1915, 1932]. In this theory Boussinesq's hypothesis of the eddy viscosity is used. In analogy with the expression for the molecular stress known from the kinetic theory of gases Boussinesq [1877] assumed that the Reynolds stresses can be coupled to the mean flow field by means of an eddy viscosity. The mixing-length theory states that this eddy viscosity is equal to the product of a 'mixing' length and a suitable velocity, again in analogy with the kinetic theory of gases in which the kinematic viscosity is equal to the product of the mean free path of the molecules and their root-mean-square velocity.

(Although this theory cannot be correct in all details, it still proves to be most useful in predicting the distribution of mean quantities of turbulent flows in technical applications.)

In the 1940's and 1950's the hot-wire technique was developed so well that various components of the Reynolds stress and various rate terms occurring in the turbulence-energy equation could be measured.

These measurements resulted in a rejection of the phenomenological theories.

Because of the complexity of inhomogeneous turbulence many researchers turned their attention away to the 'simpler' but more academic homogeneous turbulence (e.g. Taylor [1935]).

In turbulence research the statistical theory dominated the field.

It was noticed that, if the Reynolds number is large enough, the energy-containing structure in homogeneous and isotropic turbulence shows similarity (Batchelor & Townsend [1948 a & b]) and that the small-scale motion is in a state of local equilibrium (Kolmogorov [1941]).

Hot-wire measurements showed that the outer edges of turbulent shear flows -wakes (Townsend [1947]) and jets (Corrsin [1943])- are only intermittently turbulent. This phenomenon was also found in the outer part of turbulent boundary layers (Corrsin & Kistler [1954] and Klebanoff [1954]).

To study the intermittent nature of turbulence a new technique was introduced: selective or conditional sampling.

A new line of approach was initiated by Favre [1946] who used an analog recorder to produce a time-delayed turbulence signal. By expanding this technique -recording two signals simultaneously and reproducing them using a moveable head on one channel- it was possible to measure space-time correlations of turbulent fluctuations (Favre et al. [1957, 1958]).

For the first time in turbulence research Townsend [1956] attempted to draw a picture of a turbulent flow. He introduced a double structure to describe turbulent shear flow:

Turbulent fluid is moved by the convective action of a system of large eddies whose dimensions are comparable to the width of the flow and the small-scale eddies are responsible for the nearly uniform distribution of the turbulence intensity.

The development of a new technology -primarily of electronic devices and computers- guided the experimental research in the 1960's and 1970's.

Using very fast switching circuitries for analog and digital computation it became possible to obtain detailed statistical information of the flow phenomena within the turbulent and non-turbulent regions of an intermittently turbulent flow (Kaplan & Laufer [1969] and Kovaszny et al. [1970]).

Yeh and Cummins [1964] demonstrated that a coherent light source -a laser- can be used to measure steady fluid velocities by observing the Doppler

shift in the frequency of light scattered from small particles moving with the fluid. The great advantage of this measuring technique over hot-wire anemometry is that the flow is not disturbed by a measuring probe.

From spatial-correlations, averaged over long time intervals, a picture was deduced of the large-scale motion in turbulence, resulting in a double-roller large-eddy structure for a general shear flow (Townsend [1970]) and a double-cone structure for a wall-bounded shear flow (Townsend [1976]).

But these approaches did not help to answer the basic question about the generation and maintenance of turbulence.

New light on the turbulence problem was shed by two important observations (Kline & Runstadler [1959] and Brown & Roshko [1974]).

Ironically these observations were not made with sophisticated electronic equipment, but visually with rather simple optical techniques.

The essence of these observations was the discovery that turbulent shear flows are not as chaotic as previously had been assumed:

There is some order in the motion with an observable chain of events reoccurring randomly with a statistically definable mean period.

This chain of events (large-scale vortex motions) dominates the transport properties.

As a result flow visualization (hydrogen bubbles, dye, smoke) was and still is in the centre of interest.

1.2 STRUCTURE OF WALL-BOUNDED TURBULENCE

It is difficult to determine when actually the research of organized structure in turbulence started.

Crucial moments are the discovery of a relatively sharp interface between turbulent and non-turbulent fluid in a jet (Corrsin [1943]), the discovery of the turbulent spots in the transition stage (Emmons [1951]), the discovery of the creation of a horseshoe vortex during transition (Weske & Plankholt [1955]) and the discovery of the streaky behaviour of the sublayer in a turbulent boundary layer (Hama et al. [1957]).

But beyond dispute the work of Kline and his colleagues at Stanford University is the mainspring behind the present interest in organized motion.

In appendix A a description of the various regions in a turbulent boundary layer is given.

1.2.1 Structure of the wall layer

1.2.1.1 Flow visualization in the wall layer

Twenty five years ago, at Stanford University, improved flow visualization methods were developed, using dye and hydrogen bubbles as markers of a turbulent boundary layer along a flat plate.

The early attempts (Kline & Runstadler [1959] and Runstadler et al. [1963]) confirmed the streaky sublayer* structure of a turbulent boundary layer as reported by Hama et al. [1957].

Kline's investigations (Kline et al. [1967]) showed that within a sub-layer an alternating array of high- and low-speed streamwise regions, called streaks, appeared at random locations and times. Some of these streaks interacted with the outer flow. This interacting process is now called a burst. Fig. 1, from typical side views of a dye streak as seen in motion pictures (Kline et al. [1967]), shows the burst-process. The arrow follows a dye parcel.

The process starts with the gradual outflow and liftup (fig. 1 a) of a low-speed streak. When the streak reaches $y^+ = 8 - 12$, it begins to oscillate (fig. 1 b).

[y^+ is the co-ordinate y perpendicular to the wall made dimensionless with the wall friction velocity u_τ ($u_\tau = \sqrt{\tau_w/\rho}$, where τ_w is the wall shear stress and ρ the density of the flow) and the kinematic viscosity ν ($y^+ = yu_\tau/\nu$).]

This oscillation amplifies (fig. 1 c) and terminates in a very abrupt breakup (fig. 1 d), mostly in the region $10 < y^+ < 30$. After breakup the streak is contorted, stretched and ejected outwards along an identifiable trajec-

*The flow in the region very near a smooth wall -usually called the viscous or laminar sublayer- is not laminar as observations showed (Fage & Townsend [1932] and Popovich & Hummel [1967]). In fact in the sublayer the relative turbulence intensity in streamwise direction appears to be higher than everywhere else in the boundary layer (Eckelmann [1974]).

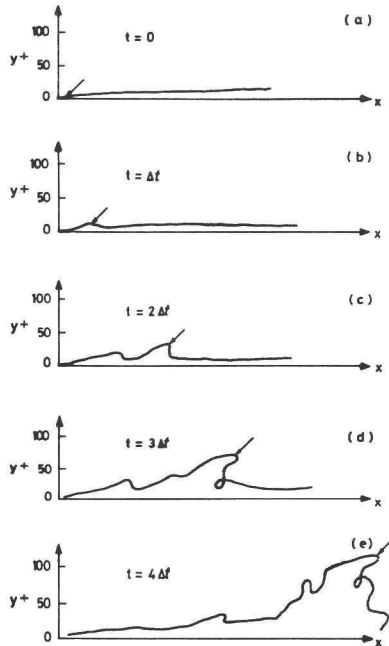


Figure 1: Dye streak breakup, illustration as seen in side view.
From Kline et al. [1967].

tory (fig. 1 e). Fig. 2 shows the distribution and the average trajectories of the contorted streaks. Fluid from the low-speed streak can reach the outer part of the boundary layer.

[δ is the boundary layer thickness.]

Kline et al. deduced from visual data that the average spanwise streak spacing for a smooth wall was approximately $\lambda_z^+ = 100$.

[λ_z^+ is the non-dimensional spanwise streak spacing ($\lambda_z^+ = \lambda_z u_\tau / \nu$).]

At Stanford University Kim et al. [1971] studied the process of production and of Reynolds stress contributions during bursting, using the hydrogen bubble technique. Analyzing motion pictures* they showed that virtually all of the net production of turbulence-energy in the range

* From this visualization method only velocity information in two directions in the boundary layer can be derived. Using a platinum wire normal to the wall the hydrogen bubbles elucidate the motion in a plane in streamwise direction normal to the wall, a wire placed parallel to the wall gives information about the motion in a plane parallel to the wall.

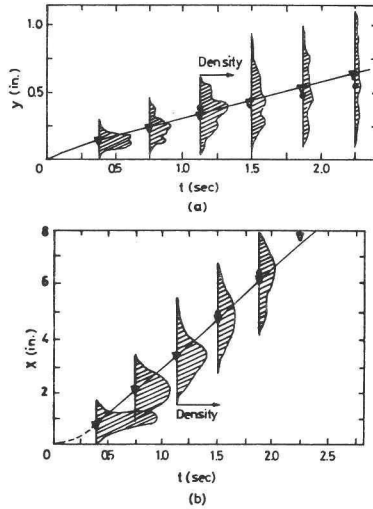


Figure 2: Trajectories of ejected eddies -flat plate flow, $dP/dx = 0$, $\delta = 2.15$ in. From Kline et al. [1967].

$0 < y^+ < 100$ occurred during bursts. They expected that this would also be true for $y^+ > 100$.

From their motion pictures Kim et al. were also able to obtain instantaneous velocity profiles. After breakup there was a return to a more quiescent flow which completed the bursting cycle, creating such flow conditions that a new burst could start.

At the same time Corino and Brodkey [1969] also studied the inner layer of a turbulent boundary layer visually. They used high-speed motion pictures of trajectories of small particles suspended in a liquid flow through a tube at Reynolds numbers in the range $Re_D = 20000$ to 50000 ($Re_\theta = 900$ to 2250).

[Re_D is the Reynolds number based on the diameter D of the tube ($Re_D = U_{av}D/\nu$, where U_{av} is the average flow velocity in the tube). Re_θ is the Reynolds number based on the momentum thickness θ

$$(Re_\theta = U_{av}\theta/\nu, \text{ where } \theta \text{ is defined as } \theta = \int_0^\infty \bar{U}/\bar{U}_{max}(1-\bar{U}/\bar{U}_{max})dy,$$

with R the radius of the tube, \bar{U} the mean velocity at a position y and \bar{U}_{max} the mean velocity at the tube axis).]

The depth of field of their photographs was of the order of $20\nu/u_\tau$, so they could see a slice through the bursting structure. The camera was mounted on a traversing mechanism so the bursting phenomenon could be kept in view as the burst was swept downstream.

The observations of the burst phenomena made by Corino and Brodkey are in agreement with those reported by Kim et al. [1971]. But the use of numerous tracer particles for flow visualization enabled Corino and Brodkey to identify additional features of the bursting process.

According to Corino and Brodkey the sequence of events before and after chaotic breakdown during the bursting process (fig. 3), began with the formation of a low-speed parcel of fluid near the wall in the region $0 \leq y^+ \leq 30$ (fig. 3 a). The velocity of this low-speed region was often only 50% of the local mean velocity with a very small radial velocity gradient within this region. The next phase which occurred after deceleration was called acceleration (fig. 3 b). During this phase a much larger high speed parcel of fluid came into view and began to accelerate the low-speed fluid by 'interaction'. Repeatedly the entering high-speed fluid was within the field of view but at a different spanwise location to one side or the other of the low-speed parcel of fluid (fig. 3 c).

If, in the acceleration phase, the high- and low-speed fluid met at the same spanwise station, the interaction was often immediate, the low-speed fluid above a particular y^+ location was accelerated and a very sharp interface -shear layer- between the accelerated and retarded fluid was formed (fig. 3 d). The next phase in the process was called ejection (fig. 3 e). During ejection an eruption of low-speed fluid occurred immediately or short after the start of the acceleration. Once ejection started, the process proceeded rapidly to a fully developed stage during which ejection of low-speed fluid persisted for varying periods of time and then gradually decayed. The length scale of ejected fluid parcels was small ($7 < z^+ < 20$, $20 < x^+ < 40$) and most of the ejections originated at distances from the wall in the range $5 < y^+ < 15$. Frequently other ejections appeared at adjacent downstream positions of the firstly observed ejection.

[z^+ is the non-dimensional spanwise co-ordinate and x^+ the non-dimensional streamwise co-ordinate ($z^+ = zu_\tau/\nu$, $x^+ = xu_\tau/\nu$).]

When the ejected low-speed fluid encountered the interface between high- and low-speed fluid a violent interaction occurred with intense, abrupt and chaotic movements, resulting in the creation of a relatively large-scale region

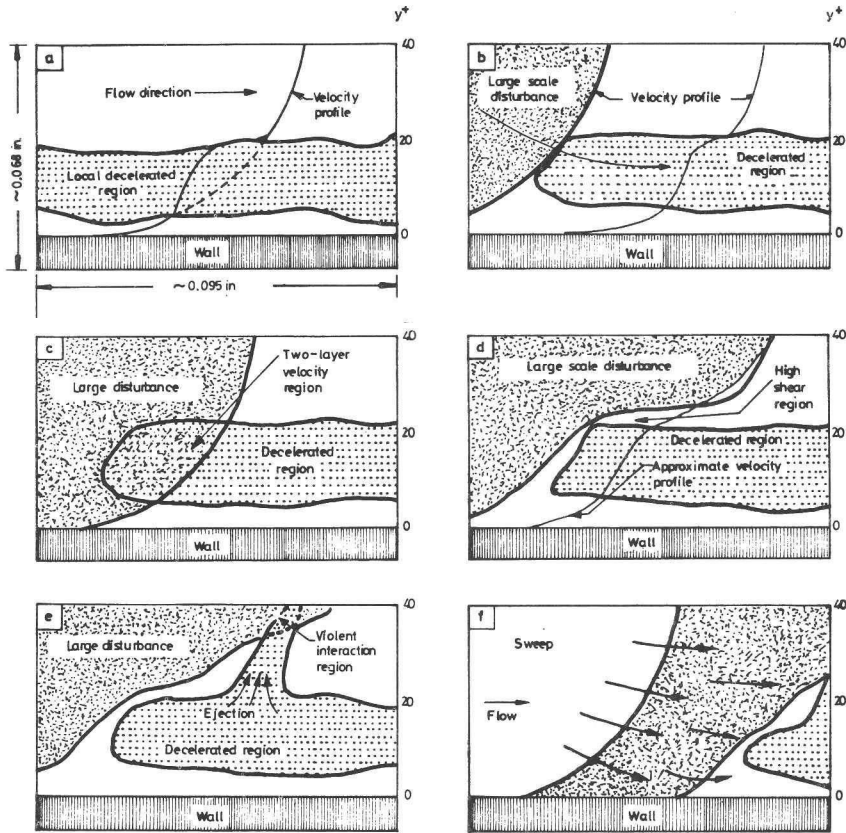


Figure 3: Burst phenomena according to Corino and Brodkey [1969].

of turbulent motion. The ejection or bursting phase ended with the entry from further upstream of fluid directed primarily in the flow direction with approximately the mean velocity profile as velocity distribution (fig. 3 f). The entering high-speed fluid carried away the retarded fluid remaining from the ejection process. This phase was called the sweep.

Both Corino and Brodkey [1969] and Kim et al. [1971] agree that the bursting phenomena are important for turbulence-energy production. Corino and Brodkey estimated from a small sample of bursting events that 70% of the Reynolds stress, measured by Laufer [1954], was produced during ejections.

Grass [1971] studied the structure of turbulent boundary layers developed over smooth and rough surfaces. Motion pictures of hydrogen bubbles were used to calculate instantaneous longitudinal and vertical velocity profiles. From these distributions the mean velocity \bar{U} , the fluctuating velocities u and v and also the contributions to the Reynolds stress were computed.

[The decomposition of Reynolds yields: $U = \bar{U} + u$ and $V = \bar{V} + v$, where U is the instantaneous velocity in streamwise direction, \bar{U} the time-averaged streamwise velocity and u the fluctuating streamwise velocity; V , \bar{V} and v are the corresponding velocities normal to the wall.]

Conditional averaging indicated that not only the ejection contributed to the Reynolds stress but also the sweep. However the ejection events were important throughout the whole boundary layer, while the sweeps events appeared to be mainly confined to a region close to the wall.

The results of the investigation of Grass [1971] agreed well with all that has been reported above. However there is some question regarding the precise role of sublayer streaks in the bursting process. In contrast to Kline et al. [1967], Corino and Brodkey [1969] considered the sublayer to be essentially passive in the bursting process. In the paper of Grass there is some support for the passive role because the same phenomena have been observed irrespective of boundary roughness conditions.

Smith and Schwartz [1983] performed simultaneous top- and end-view visualization studies of the flow behaviour in the near-wall region ($1 < y^+ < 50$) of turbulent boundary layers for $1000 < Re_\theta < 2200$.

[For a boundary layer Re_θ is based on the free stream velocity U_∞ and θ

$$(Re_\theta = U_\infty \theta / \nu, \text{ where } \theta \text{ is defined as } \theta = \int_0^\infty \bar{U} / U_\infty (1 - \bar{U} / U_\infty) dy.)]$$

Using a two-camera, high-speed video system they were able to record simultaneously two different fields-of-view of a plane parallel to the wall visualized with hydrogen bubbles (top- and end-view: looking in normal and upstream direction respectively). This visual study proved the existence of rotating, streamwise structures in the inner region of turbulent boundary layers frequently appearing in counter-rotating pairs. Whenever counter-rotating structures were visible in end-view, they evolved either from or in conjunction with a low-speed streak in the corresponding top-view.

Using the same experimental arrangement as Smith and Schwartz, Smith and Metzler [1983] studied the characteristics of low-speed streaks occurring in the wall layer of turbulent boundary layers for $740 \leq Re_0 < 5830$. The streaks appeared to have a tremendous persistence. In the viscous sub-layer the statistics of non-dimensional spanwise streak spacing was independent of the Reynolds number, having an average value of 100. The streak spacing increased with increasing distance from the wall owing to a merging and intermittency process (apparent disappearance and reappearance of streaks).

1.2.1.2 Quantitative measurements in the wall layer

The detection problem is perhaps the most difficult problem that is encountered in making quantitative measurements of bursts, because the burst near a wall is immersed in the background turbulence. Whether one uses a visual method or a measurement from a probe, or probes, there are two not unrelated aspects of the problem of burst detection: what property (or properties) of the burst should be used for detection and how does one decide from the selected property that a burst is present. The latter issue is really an issue of detecting a signal (or signals) in noise.

Gupta et al. [1971] have performed an experimental investigation to study the streaks with a spanwise rake of ten hot-wires within the sublayer.

The long-time averaged two-point spatial correlations of the streamwise velocity did not show the 'streaky' nature of the viscous sublayer (fig. 4).

[Time averaged two-point spatial correlation $R_{uu}(\Delta z)$ is defined as

$$R_{uu}(\Delta z) = \overline{u(z)u(z+\Delta z)} / u'(z)u'(z+\Delta z), \text{ with } \Delta z \text{ the spanwise separation and}$$

u' the turbulence intensity in streamwise direction ($u' = \sqrt{u^2}$).]

But short-time averaged correlations showed the alternating high- and low-speed streaks (fig. 5). These streaks had a characteristic spacing of the order of $100\nu/u_t$.

Kim et al. [1971] have used the short-time averaged autocorrelation of the streamwise velocity to measure the mean burst period. The measured period agreed with the visual data for the small sample size considered.

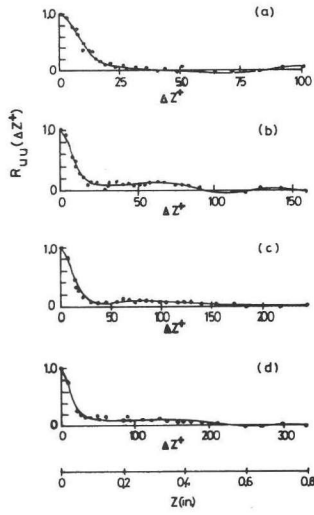


Figure 4: Two-point spanwise long-time average correlations of u fluctuations. (a) $Re_{\theta} = 2200$, $y^+ = 3.4$; (b) $Re_{\theta} = 3300$, $y^+ = 18.8$; (c) $Re_{\theta} = 4700$, $y^+ = 7.8$; (d) $Re_{\theta} = 6500$, $y^+ = 10.8$. From Gupta et al. [1971].

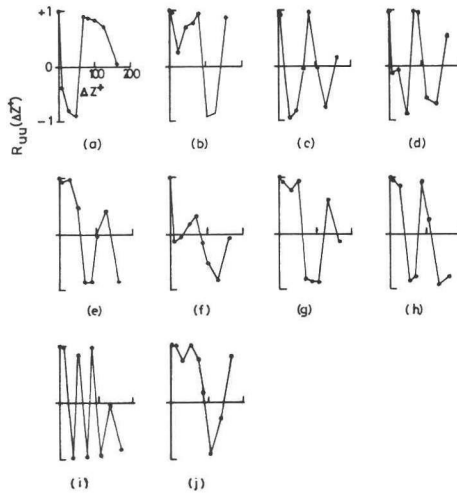


Figure 5: Typical short-time average two-point correlations of u fluctuations. Averaging over 0.375 ms, $Re_{\theta} \approx 3300$, $y^+ = 5.4$. From Gupta et al. [1971].

Blackwelder and Kaplan [1972] employed a detection scheme in which the occurrence of a burst was inferred from a digital processing scheme devised by Kaplan and Laufer [1969]. Using a series of digitized values of the u-signal the variance at a certain time was computed over a short time interval T_m centered around the digitized value of the u-signal corresponding to that time. A burst was presumed to occur if the short time variance was greater than a threshold level -the threshold level equals a threshold parameter k times the variance of the total digitized signal. Then the calculation was repeated for the next digitized value of the u-signal. This detection scheme is sensitive for large fluctuations about the short time average of the signal.

Blackwelder and Kaplan [1976] reported that their scheme is not very sensitive for the short averaging time T_m -they advised to use $T_m u_r^2 / \nu = 10$, but that the scheme is sensitive for the threshold parameter k . However they stated that the dependence on k does not affect the measured shape of the detected events, because conditionally averaged velocity profiles scale with the root of the threshold value.

Blackwelder and Kaplan measured the instantaneous profiles of the streamwise velocity during a burst with a rake of ten hot-wires in the wall region. The u-signal at $y^+ = 15$ was used for detection.

Fig. 6 shows the conditionally sampled velocity profiles. These profiles show the inflectional point near the wall just before detection as indicated by the visual results of Kim et al. [1971] and Corino and Brodkey [1969].

Willmarth and Lu [1972] used a detection scheme based upon the visual observation that fluid ejections near the wall are preceded by a region of fluid with low streamwise velocity. A single hot-wire, at $y^+ = 16.2$, was used for detection. A burst was deemed to occur when the low-pass filtered detector signal became lower than a trigger level. Again there appeared to be a dependency on this level.

With this scheme Willmarth and Lu and Lu and Willmarth [1973] studied the instantaneous Reynolds stress near the wall. They found very large values during the ejection and sweep, as observed by Corino and Brodkey [1969]. Lu and Willmarth measured also the downstream convection of bursts. The trajectory of the bursts in the x-y plane was in agreement with the results of Kline et al. [1967] (fig. 2).

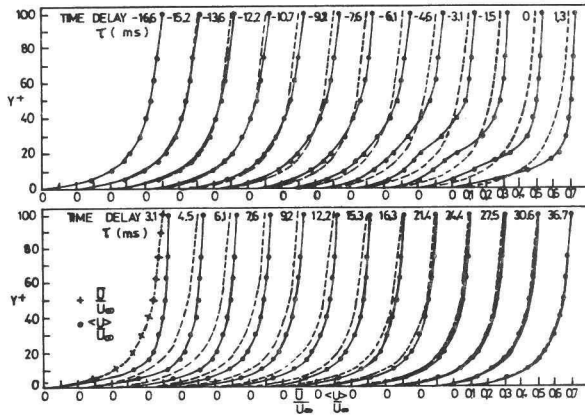


Figure 6: Conditionally sampled velocity profiles before, $\tau < 0$, and after, $\tau > 0$, burst detection: —; mean velocity profiles: ---. $Re_\theta = 2550$. From Blackwelder and Kaplan [1972].

In the first studies of bursts the process was considered to be an essential wall-bounded phenomenon with characteristic scales determined from the wall parameters u_τ and ν . Rao et al. [1971] changed this opinion. They showed that even in the wall layer over a fairly wide range of Reynolds numbers ($600 < Re_\theta < 9000$) the mean burst period scaled with outer (U_∞, δ) rather than with inner (u_τ, δ) variables. The mean dimensionless burst period was given by $U_\infty T_B / \delta = 5$ (fig. 7).

[T_B is the mean burst period.]

This range has been extended by Narayanan and Marvin [1978] to $600 < Re_\theta < 95000$.

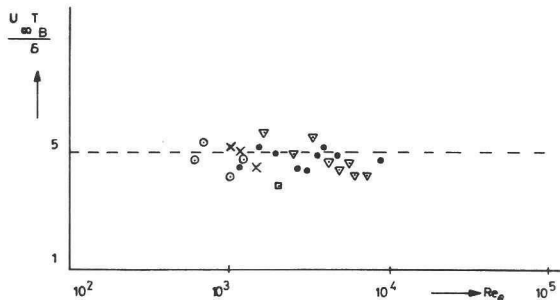


Figure 7: Dimensionless mean burst period. From Rao et al. [1971].

However Bandyopadhyay [1982] has disproved this scaling. He showed that the observed scatter in measurements of $U_\infty T_B / \delta$ is not entirely due to the uncertainties of measurement, but that the scatter is systematic. So $U_\infty T_B / \delta$ is not an universal constant, but its value depends on the flow.

Ueda and Hinze [1975] designed a detection scheme based on the intermittent character of the ejection and sweep process. They counted the burst rate using the high-frequency band-pass signal of $(\partial u / \partial t)^3$. According to Ueda and Hinze a burst occurred when the absolute value of $(\partial u / \partial t)^3$ exceeded a given threshold value.

They measured that the dimensionless mean burst period $U_\infty T_B / \delta$ was approximately 5 for $y^+ \leq 10$, which value decreased to 2.5 for $y^+ > 40$ (fig. 8).

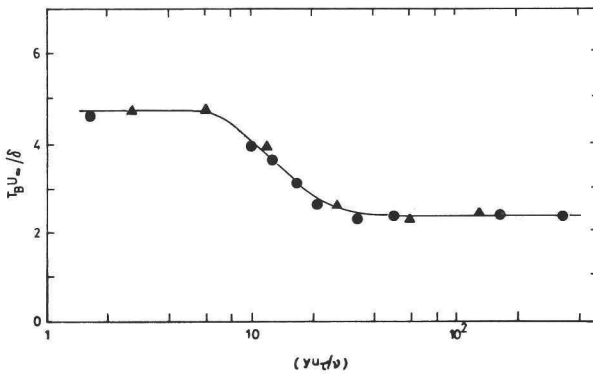


Figure 8: Distribution of burst period T_B of band-pass signal.
 Re_θ : \blacktriangle , 1244; \bullet , 4248. From Ueda and Hinze [1975].

Blackwelder and Eckelmann [1979] have made a rather detailed study of the structure of wall streaks using heated wall elements to measure the streamwise and spanwise vorticity.

They identified the low-speed streak observed by Kline et al. [1967] as the accumulation region between streamwise vortices. They measured the streamwise length of the vortices to be $\lambda_x^+ = 1000$.

[The superscript + indicates that the streamwise length λ_x of the vortices is made dimensionless with u_τ and ν ($\lambda_x^+ = \lambda_x u_\tau / \nu$).]

1.2.1.3 Comparison between methods of burst detection

Offen and Kline [1973] compared the burst detection schemes of Blackwelder and Kaplan [1972], Willmarth and Lu [1972] and three other schemes devised by Offen and Kline, based upon the normal velocity, the velocity-profile slope and the uv-signal, with their own visual observations. They concluded that

"none of the proposed detection schemes correlates very well with the visual indications of bursting or with any other scheme.

Hence, there remain serious questions about what events are measured by each technique. Despite the poor correlation, the various schemes rarely detect ejections that do not pass the probe in the plane parallel to the wall, they agree with each other to a certain extent in their relationship to visual data, they generally produce conditional averages and velocity signatures which are similar and agree qualitatively with the expected results (i.e., streamwise velocity defect, outward motion of the fluid, and Reynolds stresses greater than the mean), and many of them are as effective as the visual data at detecting periods of high uv."

1.2.2 Structure of the outer layer

1.2.2.1 Flow visualization in the outer layer

Nychas et al. [1973], using the same flow visualization technique as Corino and Brodkey [1969], studied the outer region of a turbulent boundary layer.

They observed that the single most important event in the outer region was a large-scale motion, called bulge, that appeared as a transverse vortex transported downstream with a velocity slightly less than the local mean. The observed large-scale motions appeared to be the result of an instability-producing interaction between accelerated and decelerated fluid that is believed to be closely associated with wall layer ejections. The flow phenomena associated with bulges extended all across the boundary layer and made substantial contributions to the Reynolds stress.

Falco [1977] combined visual (oil droplets) and hot-wire observations. Falco found two types of large-scale motion: one half of the motions had a zone average streamwise velocity less than the local mean (type T1) and one half had a streamwise velocity greater than U (type T2).

In the turbulent boundary layer Falco observed a repetitive family of highly coherent motions, called 'typical eddies'. These eddies appeared at the back of the large-scale motions as slightly flattened mushroom vortices (fig. 9).

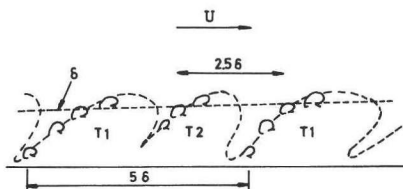


Figure 9: A model of the flow in the outer region of turbulent boundary layers, showing the relation between typical eddy scale to large-scale motion scale for moderate Reynolds numbers. From Falco [1977].

Hot-wire measurements showed that the Reynolds number dependent typical eddies produce most of the Reynolds stress in the outer half of the layer at $Re_\theta = 1200$. The lengths of the eddies scaled on the inner parameters and the frequency of occurrence of these eddies scaled on the outer parameters, suggesting that there exists a relation between the structures in the inner and the outer layer.

Head and Bandyopadhyay [1981], using flow visualization (smoke) and hot-wire measurements to study the zero-pressure gradient turbulent boundary layer over the Reynolds number range $500 < Re_\theta < 17500$, obtained a different picture of the turbulent boundary layer.

At high Reynolds numbers they observed many elongated hairpin vortices or vortex pairs, originating in the wall region and extended through a large part of the boundary layer thickness or beyond it. For the most part they are inclined to the wall at a characteristic angle in the range of 40° to 50° . Large scale features appear to consist mainly of random arrays of such hairpin vortices.

At low Reynolds numbers (which covers about two-third of the literature on this subject) the hairpin vortices are much less elongated and are better described as horseshoe vortices* or vortex loops. Large-scale features now consist simply of isolated or a few interacting vortex loops.

 * The horseshoe vortex is a vortex model postulated by Theodorsen [1955].

Head and Bandyopadhyay suggest that the typical eddies of Falco [1977] are in fact the tips of the hairpin vortices.

1.2.2.2 Quantitative measurements in the outer layer

Investigating the outer or intermittent region of a turbulent boundary layer a similar problem arises as in detecting structures in the wall layer: what property of the flow must be used to decide if the flow is turbulent or not.

The detection scheme of Kovaszny et al. [1970] was based on the presence of large-amplitude fluctuations of the derivative $\partial u/\partial y$, which is one term in the spanwise vorticity component.

They observed that vorticity appeared to exhibit a discontinuity across the turbulence interface of the bulge, whereas the velocity was continuous.

According to Kovaszny et al. the bulges in the outer flow are correlated over 3δ in the streamwise direction and over δ in the spanwise direction. They suggested that the bursts observed by Kline et al. [1967] in the near-wall layer are responsible for the bulges in the outer region.

They also reported that there was a difference between the upstream-facing (back) and the downstream-facing (front) portions of the bulges in the outer layer. The back of the turbulent non-turbulent interface showed intense turbulent activity*.

Blackwelder and Kovaszny [1972] have reported measurements that complement their previous results (Kovaszny et al. [1970]), using the same experimental set-up (turbulent boundary layer, $Re_\theta = 3000$) and the same detection technique. They found that intense fluctuations of u and v in the wall region remained strongly correlated out to $y/\delta = 0.5$, confirming other observations that the disturbance associated with a burst extends across the entire boundary layer.

Blackwelder and Kovaszny estimated that the large eddies contributed as much as 80% to the Reynolds stress in the outer layer.

*This phenomenon is not restricted to turbulent boundary layers alone. Intense turbulent activity along upstream-facing interfaces has been found in the turbulent slugs and puffs in pipe flow (Wynanski & Champagne [1973] and Wynanski et al. [1975]), in the turbulent spot (Wynanski et al. [1976]) and in the near wake of a cylinder (Cantwell [1975]).

Combining measured point averages of the streamwise and normal velocities at various locations relative to the detector probe they were able to construct an average flow pattern within and around a turbulent bulge (fig. 10). This picture, showing a circulatory flow within the bulge, agrees with Falco's observations [1977]. The outer flow is 'riding over' the turbulent fluid within the bulge having an average velocity U_c of $0.93U_\infty$.

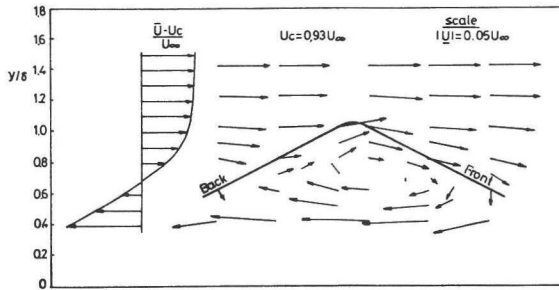


Figure 10: Composite velocity distribution in the outer region.
From Blackwelder and Kovaszny [1972].

Antonia [1972] used the fluctuations of the uv -signal to detect turbulence in the intermittent region. If $(\partial uv / \partial t)^2$ exceeds some arbitrary threshold level, turbulence is presumed to be present.

Except minor differences regarding the shape of the interface and the point-averaged streamwise velocities Antonia's results agree with those of Kovaszny et al. [1970].

In this study Antonia found that the averaged Reynolds stress in the bulges is of the order of half the wall shear stress, supporting the idea that the strength of the large eddy motion is closely related to the wall shear stress.

Hedley and Keffer [1974] performed investigations similar to those of Kovaszny et al. [1970], but at large values of Re_θ ($Re_\theta = 9700$), using the large amplitudes of $[(\partial u / \partial t)^2 + (\partial v / \partial t)^2]$ as detector.

In general their results agree with those of Kovaszny et al. Hedley and Keffer found that the Reynolds stress strongly increased across the back of the bulge, as observed by Falco [1977] at higher Reynolds numbers.

Brown and Thomas [1977] correlated the wall shear stress with the stream-wise velocity across a turbulent boundary layer. They found a line of maximum correlation which lay at an angle of 18° to the wall in downstream direction. They attributed this line to some organized structure at an oblique angle to the wall moving along the wall at about $0.8U_\infty$. For they found evidence that the large-scale motion in the organized structure produces a slowly varying component in the wall shear stress and also a high frequency large amplitude fluctuation occurring near the maximum in the slowly varying wall shear stress. Brown and Thomas stated that the high frequency part in the wall shear is associated with the bursting phenomenon.

1.2.3 Structure in the Reynolds stress

Independently Willmarth and Lu [1972] and Wallace et al. [1972] developed a method of sorting the contributions to the instantaneous Reynolds stress per unit density into the four quadrants of the u - v plane. The reason for this is to obtain quantitative measurements of the relative importance of the ejection and sweep.

Visual investigations indicate that during bursts, the ejection should occur in the second quadrant (in which $u < 0$ and $v > 0$) and that the sweep should occur in the fourth quadrant ($u > 0$, $v < 0$). In addition to these major events there occur interactions between these two events which cause a negative contribution to the Reynolds stress. The first quadrant is associated with a sweep being reflected back in the outer layer (outward interaction: $u > 0$, $v > 0$) and the third quadrant with an ejection deflected back to the wall (inward interaction: $u < 0$, $v < 0$). Fig. 11 shows the u - v plane.

Fig. 12, from Brodkey et al. [1974] shows the different contributions of each quadrant to the Reynolds stress. Close to the wall ($y^+ < 15$) the sweep contributes most to the Reynolds stress, whereas for the region further away from the wall it is the ejection that is most important for the Reynolds stress.

Lu and Willmarth [1973] extended the technique of sorting uv contributions into quadrants. They introduced a further classification of the uv contrib-

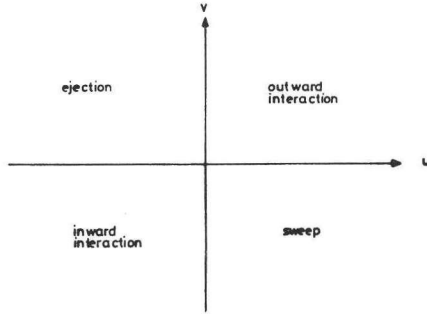


Figure 11: The u-v plane.

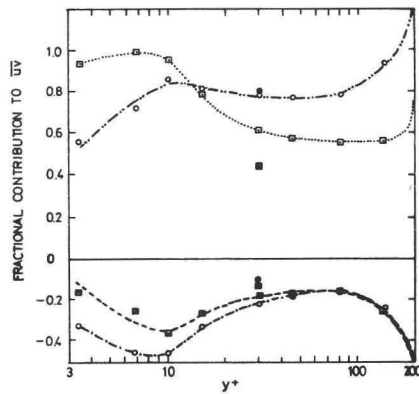


Figure 12: The sorted Reynolds stresses normalized with the local average Reynolds stress, (●, ■, results of Willmarth and Lu [1972]): , sweep, -·-·-·-·- , ejection, -·-·-·-·- , outward interaction, - - - - , inward interaction. From Brodkey et al. [1974].

utions to each quadrant depending upon the magnitude of the contribution by drawing a 'hole' in the u-v plane (fig. 13).

Now five regions can be distinguished. The hole is bounded by curves $|uv| = Hu'v'$.

[H is called the hole-size.

v' is the turbulence intensity in normal direction ($v' = \sqrt{v^2}$).]

The four quadrants excluding the hole are the other four regions. With this hole-technique or quadrant analysis technique large contributors to uv rela-

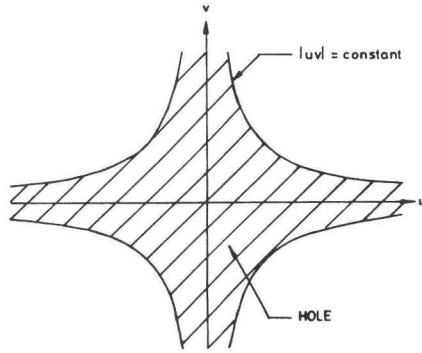


Figure 13: Sketch of the hole in the u - v plane.

tive to the local turbulence intensities u' and v' can be extracted leaving the smaller fluctuating $uv(t)$ -signal in the hole.

Fig. 14 is a typical result of the hole-technique. From this figure it can be deduced that for most of the time the uv -signal is small and that in a short time the ejection and sweep events make substantial contributions to the Reynolds stress.

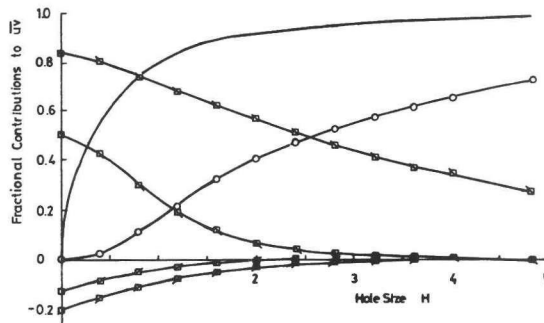


Figure 14: Fractional contributions to uv from different events at $y/\delta = 0.021$. Quadrant 1: \blacksquare ; quadrant 2: \blacktriangle ; quadrant 3: \blacklozenge ; quadrant 4: \blacklozenge ; hole: \circ . Fraction of time in hole: —. From Lu and Willmarth [1973].

Taking for instance a hole-size of 1 it follows from fig. 14 that the hole contributes in 80% of the time only 18% to the Reynolds stress. The ejection (72%) and the sweep (26%) account for the remaining positive Reynolds

stress, while the outward and inward interaction make small negative contributions to the Reynolds stress (4% respectively 10%).

1.2.4 Organized motion in a turbulent boundary layer

A lot of models have been suggested to describe the behaviour of the wall and outer layer and the connection between these two regions. In this context only the model of Hinze [1975] is described having much in common with the models of Offen and Kline [1973] and of Smith [1983]. Joining facts obtained from experimental investigations Hinze constructed the following qualitative description of the turbulence mechanism in the wall layer:

"It is striking that, notwithstanding the random nature of the turbulence, a repetition of similar processes may be distinguished, with a distinct and recognizable average spacing in both spanwise and streamwise directions. In time it corresponds with, on the average, some cyclic process, with many features similar to the laminar-turbulent transition process. When trying to give a description of this 'cyclic' process in the fully developed turbulent flow, it is immaterial where the beginning of the 'cycle' is fixed. Because of the similarity mentioned with the transition process we will begin the 'cycle' with the situation where, owing to a large-scale disturbance already present in the outer region and outer part of wall region, a horseshoe-shaped vortex is beginning to be formed locally at the wall. This vortex is deformed by the flow into a more and more elongated U-shaped loop in streamwise direction. Because of self-induction processes the tip of the loop moves away from the wall thereby coming into regions of ever-increasing velocities. Consequently the vorticity increases due to stretching processes. At the same time it gives rise to an outward flow between the legs of the U-loop, with a strong v-component near the tip. Between the vortex moving away from the wall and the wall a local deceleration of the fluid is effected. This process transports low-momentum fluid away from the the wall, thus producing a positive and marked contribution to the Reynolds stress. Moreover, at distances $y^+ = 5$ to 30, an intense horizontal shear-layer is formed, showing up in the instantaneous U-velocity as a dent with inflection points. The resultant local inflexional instability and breakdown of the flow surrounding the original tip

of the vortex produces a turbulence burst, similar to that observed during the laminar-turbulent transition process. The pressure waves associated with the turbulence burst are propagated throughout the whole boundary layer. At the same time the blob of fluid of high turbulence intensity produced during the burst is convected downstream and moves farther away from the wall, thereby increasing in scale, amongst others, by turbulent diffusion. Since at the same time high-momentum fluid is entering from upstream, the above blob of fluid is convected in an accelerated way or swept in downstream direction. The above pressure waves may add to the movement of fluid towards the wall, resulting in a sweep-inrush flow. The inrush process has already been preceded and initiated by a negative v -component downstream of the U-looped vortex before its breakdown. The sweep-inrush flow makes a very small angle (5° to 15°) with the wall, which at the wall also is observed as the entry of higher momentum fluid in almost horizontal direction. Both the ejection burst process, as well as the sweep-inrush flow contribute to the shear-stress, and consequently are responsible for the turbulent production, mainly in the region $y^+ = 10$ to 15 from the wall.

The horizontal movement during the sweep-inrush period will be strongly retarded near the wall. It may eventually, in conjunction with the action of overtaking faster moving fluid at a greater distance from the wall develop into another horseshoe-type vortex."

In fig. 15 an attempt is made to show the 'cyclic' process described above. Of course this model, showing only the ejection, is highly idealized.

Hinze and others (Rao et al. [1971], Kovasznay et al. [1970], Nychas et al. [1973]) consider the burst process to be a result of an instability of the sublayer produced by the pressure field associated with the the large-scale motion in the outer layer.

According to Offen and Kline [1973] the sweeping motions from the logarithmic region impress on the wall layer the temporary adverse pressure gradient required to cause the streak liftup that precedes an ejection. Smith [1983] suggests that during bursting not one but more (2 to 5) horseshoe-shaped vortices are formed creating a spanwise pressure gradient which rede-

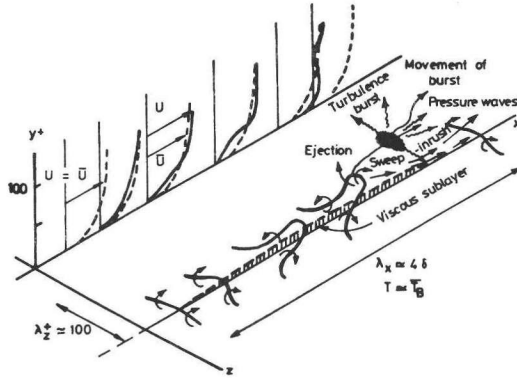


Figure 15: Conceptual model of turbulence near the wall during an 'cyclic' process with averaging spacings λ_x and λ_z . From Hinze [1975].

velops the streak region by further accumulation of low-momentum fluid between the legs.

Another aspect of the interaction problem regards the maintenance of the outer flow. The dominant view is that the outer flow is in some sense the wake formed by merging of successive bursts near the wall.

1.3 STRUCTURE OF FREE-TURBULENCE

Not only in wall-bounded shear layers organized structures have been observed, also in free shear layers organized motion has been found.

In appendix B the various regions of an axisymmetric jet are described.

1.3.1 Plane mixing layers

In a study of turbulent mixing layers, Brown and Roshko [1974] showed that the layer was dominated by large-scale spanwise vortices (fig. 16). Spark shadow pictures of the plane turbulent mixing layer between two streams of different gases (nitrogen and helium) with different speeds revealed these organized flow structures. These structures originate in the transitional part of the layer, they do not vanish when smaller-scale turbulence sets in and they appear to remain as a permanent feature of the flow at all higher Reynolds numbers.

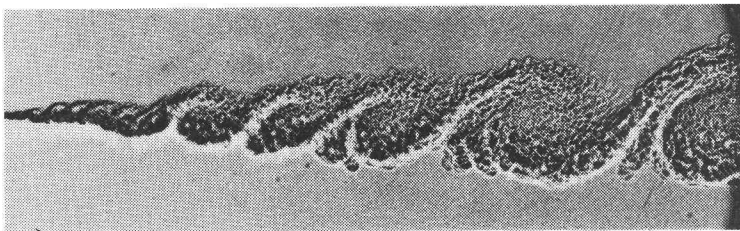


Figure 16: Shadowgraph of mixing layer in flow between helium (upper, $U \approx 10$ m/s) and nitrogen ($U \approx 4$ m/s).
From Brown and Roshko [1974].

In a mixing layer with a low Reynolds number, Winant and Browand [1974] carried out a detailed study of vortex pairing as observed by Freymuth [1966] in a separated laminar boundary layer. By injecting dye through the upper side of the splitter plate just before the two streams of water with different velocities were brought together the pairing process in the mixing layer could be observed (fig. 17). In pairing adjacent vortices rotated about each other under their mutual induced velocity field. And as rotation progressed they formed a single vortex of larger scale. This vortex pairing process was observed to occur repeatedly, controlling the growth of the mixing layer.

Brown and Roshko [1974] observed a similar pairing process at much higher Reynolds numbers.

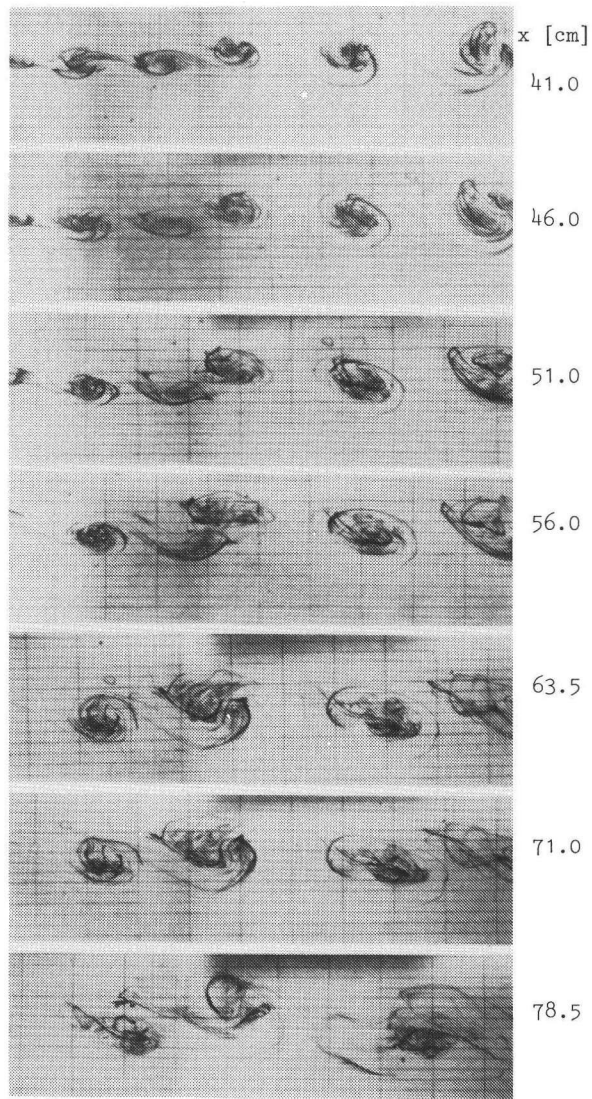


Figure 17: Sequence of photographs showing vortex pairing. Heavy dye lines marks the centre of the shear layer. Camera is moving with the mean speed \bar{U} . Downstream distance to the centre of each frame is indicated to the right. From Winant and Browand [1974].

1.3.2 Axisymmetric shear layers

As the first few diameters of jets can be regarded as a two-dimensional shear layer 'wrapped around' the axis, it was not surprising to find in this region a sequence of discrete vortex rings.

Fig. 18, from Wille [1963] using smoke-visualization, shows how ring vortices are formed out of the laminar shear layer shed from a nozzle. Tripping the boundary was shown to destroy much of this order (fig. 19).

[$Re_D = U_e D/\nu$, with U_e the nozzle exit velocity and D the nozzle diameter.]

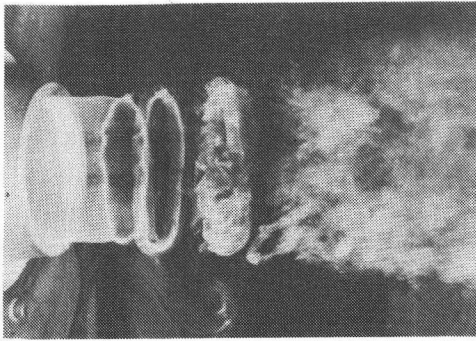


Figure 18: Smoke photograph of ring vortices in the initial region of a circular jet at $Re_D = 70000$. From Wille [1963].

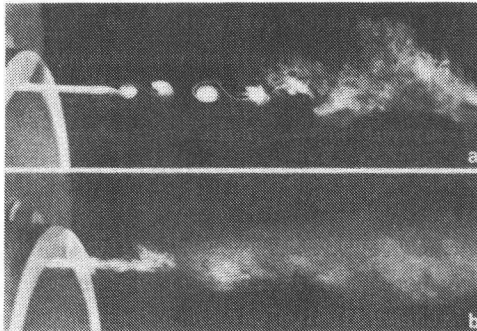


Figure 19: Effect of tripping the boundary layer at the nozzle exit on the rolling-up of the shear layer. (a) Separated laminar shear layer. (b) Separated turbulent shear layer. From Wille [1963].

However, conditional sampling techniques revealed the existence of large-scale flow structures -vortex rings- in jet flow irrespective of outflow conditions (laminar or turbulent outflow, low or high Reynolds number). A similar vortex pairing process as observed by Winant and Browand [1974] was found.

Lau et al. [1972] proposed a vortex model which accounts for the observed flow characteristics in the mixing layer region of a turbulent jet. This model consists of an axial array of discrete vortex rings spaced one and a quarter nozzle diameter apart and being convected downstream at about 0.6 times the nozzle exit velocity. Fluid is transported by each vortex in radial direction. The leading edge of a vortex induces an outflow of high velocity fluid from the potential core of the mixing layer region into the low velocity region. Low velocity fluid is transported by the trailing edge inwards into the potential core.

Using the same experimental facilities but slightly different conditional sampling techniques Lau and Fisher [1975] and Bruun [1977] investigated the structure in the first few diameters of a jet.

In both studies the spikes in the u -signal of a fixed hot-wire were used to trigger the conditional sampling of the u -signal of a moveable hot-wire. Lau and Fisher used a correlator for conditional averaging, so only positive time events could be evaluated. To study also negative time events Bruun used a digital computer.

Bruun was able to identify the vortex rings in a jet at a low Reynolds number ($Re_D = 10000$) and Lau and Fisher found large-scale flow structures at a higher Reynolds number ($Re_D = 200000$).

The results of Lau and Fisher and of Bruun are in accordance with the vortex model of Lau et al. [1972].

Because the large-scale structures, especially in the turbulent regions of a jet, are immersed in the superimposed, large-amplitude, random fluctuations, and because special averaging techniques are necessary to reveal those structures even in the developing regions of a jet, controlled excitation is used to study jet flows.

As demonstrated by Crow and Champagne [1971] periodically occurring vortices can be observed in a 'stimulated' jet. Periodic excitation was provided by a loudspeaker placed in the settling chamber.

Zaman and Hussain [1980] and Hussain and Zaman [1980] studied vortex pairing in a circular jet using a loudspeaker in the settling chamber to introduce the controlled excitation.

They used hot-wire and flow-visualization (smoke) techniques.

Zaman and Hussain discovered two possibilities for vortex pairing, viz. vortex pairing of the near-exit thin vortex rings occurring when the Strouhal number based on the initial shearlayer momentum thickness is about 0.012 and vortex pairing of thick vortex rings at $x/D = 1.75$ happening when the Strouhal number based on the jet diameter is about 0.85.

[x is the axial co-ordinate of a jet, originating at the exit.]

Hussain and Zaman found that the coherent structure Reynolds stress is much larger than the background turbulence Reynolds stress for $0 < x/D < 3$. From zone-averaging they deduced that the Reynolds stress over the cross-section of a merging vortex pair is much larger than that over a single vortex, either before or after vortex pairing.

Most of the investigations in jets have been performed in the first few diameters of a jet, because it is believed that the structures in this region play a dominant role in the entrainment, the mixing and the aerodynamic noise production.

Only a few investigations have been carried out in the regions of partial and complete self-preservation.

Chevray and Tutu [1978] measured at $x/D = 15$ in a slightly heated jet; the temperature could be treated as a passive scalar. The differentiated fluctuating axial velocity component indicated the presence of a turbulent/non-turbulent interface. Zone averaging showed that the turbulent fluid moves fast -compared with the mean velocity- and outwards, whereas the non-turbulent fluid moves slow and inwards. The turbulent fluid appeared to be responsible for most of the momentum and heat transport.

At $x/D = 59$ Sreenivasan et al. [1979] studied a slightly heated turbulent jet within a co-flowing jet (jet: $U_e = 32$ m/s, $D = 2.03$ cm; co-flowing jet: $U_e = 4.8$ m/s).

Using a temperature signal it became possible to identify a large-scale pattern. Sreenivasan et al. separated the mean shape of this pattern from fluctuations superimposed on it. The fluctuations -consistent with local isotropy- appear to make the dominant contribution to the turbulence intensities and, in regions of substantial turbulence production, to the Reynolds stress. As the distance from the jet-axis increases, however, an increasingly larger fraction of the local Reynolds stress is contributed by the large-scale pattern.

In a jet, Hussain and Clark [1981] measured the wavenumber-convection velocity spectrum $W(k,U)$ -the double Fourier-transformation of the space-time correlation of axial velocity fluctuations- at $x/D = 8$ and 30 ; $U_e = 30$ m/s and $D = 2.54$ cm.

[k is the wavenumber, defined as $k = 2\pi f/\bar{U}$.]

The spectra indicate that the jet is characterized by energetic large-scale structures, not only at $x/D = 8$, but also in the region of partial self-preservation ($x/D = 30$).

This method of analysis does not reveal the details of coherent structures, but provides statistics of the most energetic eddy and the range and distribution of its convection velocity. The convection velocity of the most energetic eddies decreases from about $0.73U_e$ to $0.25U_e$ between $x/D = 8$ and 30 . The smallest eddies are essentially transported passively with nearly the local time-mean velocity.

Tso et al. [1981] measured both long and short time-averaged space-time correlations of axial velocity fluctuations in a 2.54 cm axisymmetric jet at $Re_D = 6.8 \cdot 10^4$ for $x/D \geq 40$ in order to investigate if large-scale coherent structures exist in the region of partial self-preservation.

Long time-averaged space-time correlations with probe separations in axial direction by as much as $25D$ suggest the passage of large-scale coherent structures. The radial extent of these structures is about one local jet diameter and the azimuthal extent is about a quadrant of the local cross section.

Short time-averaged correlations with probe separations in axial direction exhibit reoccurring quasi-periodic patterns, providing evidence for the existence of large-scale structures.

Dimotakis et al. [1983] studied the development region and the fully developed region of a water jet, using laser-induced fluorescence and particle streak velocity measurements. These measurements indicated that large-scale vortical structures dominate the dynamics of turbulent jets, not only in the mixing layer region but also in the regions of partial and complete self-preservation.

The large-scale structures appear to be nearly axisymmetric or spiral, or in the transitional state between these forms. Entrainment is closely associated with the kinematics of these structures and does not appear appropriately describable as a gradient diffusion phenomena.

1.4 PRESENT INVESTIGATION

Flow visualization has revealed the existence of coherent structures in turbulent flows.

Unfortunately, the description of a coherent structure is too qualitative when based on flow visualization. Consequently efforts have been made to obtain quantitative data of coherent structures using point measurements.

To that purpose the conditional sampling technique was applied; this means that only the experimental results were taken into account when a coherent structure was present at the measuring station. However, the success of this approach depends on the imagination -hence the prejudice- of the investigator. In flow visualization a similar problem arises. As Hussain [1983] points out, here lies the dilemma:

"prejudices which are essential for the success of a coherent structure study, can also become liabilities as these can easily mislead one; one can usually see in flow visualization what one wants to see as one can find different structures in the same signal."

Therefore, attempts have been made in the past to develop objective methods for detecting coherent structures from measured signals. A detection method is called objective, when the detected flow structures and the results of conditional sampling based on the detected structures are independent of the parameters of the method.

The aim of this investigation is to examine the objectivity of some well-known detection methods and -if necessary- to improve detection.

Hereto experiments have been carried out in wall-bounded turbulent flows and in a free turbulent flow. In chapter II the experimental facilities used in this investigation are described. Also conventionally measured turbulence quantities of the flows in these set-ups are reported.

In chapter III the results of testing the objectivity of the detection methods of Ueda and Hinze [1975] and of Blackwelder and Kaplan [1972, 1976] are presented. Also the objectivity of a modified version of Blackwelder and Kaplan's method is examined.

Finally the autocorrelation technique is investigated.

To improve detection and to verify some results of the detection methods flow visualization and laser-Doppler measurements have been performed in a turbulent channel flow simultaneously. The results are given in chapter IV.

In chapter V the results of the application of the quadrant analysis technique to an axisymmetric jet flow are presented. This technique is used in order to detect structures not only in the mixing layer region but also in the region of partial self-preservation.

In chapter VI the results of this investigation are summarized and discussed.

Chapter II

DESCRIPTION OF EXPERIMENTS

In order to get a better insight in the problem of detecting coherent structures measurements have been performed in four different flow types, viz. a turbulent boundary layer, a turbulent pipe flow, a turbulent channel flow and an axisymmetric jet flow.

In this chapter the experimental facilities are described briefly and usually measured turbulence quantities are reported. More details concerning set-ups and experimental results are given by Boelsma [1981], Godefroy and Kunen [1984], Talmon [1984] and Vink [1984] respectively. Details about the jet are also reported by Fondse et al. [1983].

2.1 BOUNDARY LAYER

2.1.1 Experimental set-up

The first measurements concerning the detection of coherent structures were carried out in a low-turbulence windtunnel of the closed type. The working section is 4.5 m long and has a rectangular cross section of 0.9*0.7 m². The windtunnel has a 10:1 contraction. At the centerline of the working section a glass plate is placed vertically, in streamwise direction. By means of moveable opposite walls the streamwise static-pressure gradient was adjusted to a negligibly small value. The measurements were performed in a centre position of the boundary layer on one side of the glass wall at 4.18 m from the leading edge. Transition from laminar to turbulent flow of the boundary layer was fixed at 1.27 m from the leading edge using a tripping wire attached to the working surface. The turbulence level in the tunnel was less than 0.2% at a free stream velocity of 4 m/s.

In the boundary layer only measurements of the turbulent velocity component in streamwise direction were performed.

The mean velocity and the turbulence intensity were measured with a constant-temperature hot-wire anemometer. Platinum plated tungsten wires with a length of 1 mm and a diameter of 0.005 mm were employed. The distance between the prongs of the hot-wire probe was 16 mm.

The mean velocity was also measured with total pressure tubes.

The wall shear stress was measured using a Preston tube.

2.1.2 Experimental results

The measurements in the boundary layer were carried out at a free stream velocity of approximately 4 m/s.

In the viscous sublayer the hot-wire results were corrected for the conductivity effect to the plate with Wills' method (Wills [1962]).

From the distributions of the mean velocity -measured with hot-wire and total pressure tube- the boundary layer thickness $\delta_{0.99}$ was derived.

[$\delta_{0.99}$ is the y-position where the mean velocity equals $0.99U_\infty$.]

The displacement thickness δ^* and the momentum thickness θ were calculated by numerical integration of the distribution of $(1-\bar{U}/U_\infty)$ and $\bar{U}/U_\infty(1-\bar{U}/U_\infty)$, respectively.

[Displacement thickness δ^* is defined as $\delta^* = \int_0^\infty (1-\bar{U}/U_\infty) dy$.]

The wall friction velocity u_τ was calculated from Preston tube measurements, from the slope of the mean velocity near the wall and from a Clauser fit of the mean velocity data (Clauser [1956]). The values agree very well with these predicted by Ludwig and Tillmann's empirical relation (Ludwig & Tillmann [1949]).

In table 1 the measured boundary layer parameters are given.

Table 1.

Boundary layer parameters.

u_τ	$\delta_{0.99}$	δ^*	θ	Re_θ
[m/s]	[mm]	[mm]	[mm]	
0.177	54.1	9.0	6.5	1750

The mean velocity and the turbulence intensity distribution are shown in

fig. 20 and 21, respectively. These distributions agree well with those obtained in other investigations on boundary layers and pipe flows.

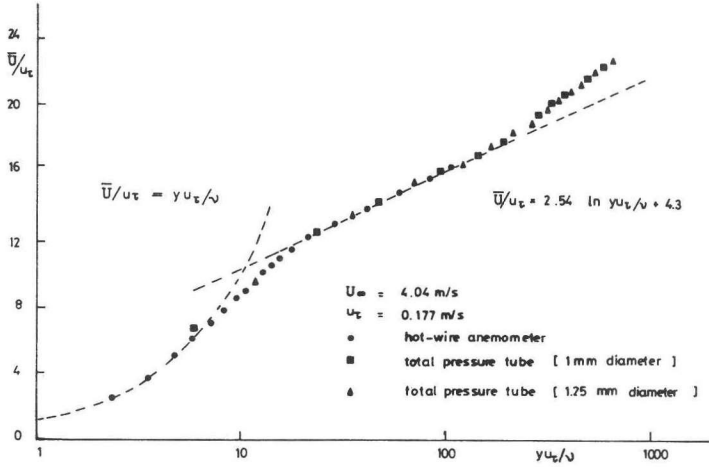


Figure 20: Time-mean velocity distribution in turbulent boundary layer.

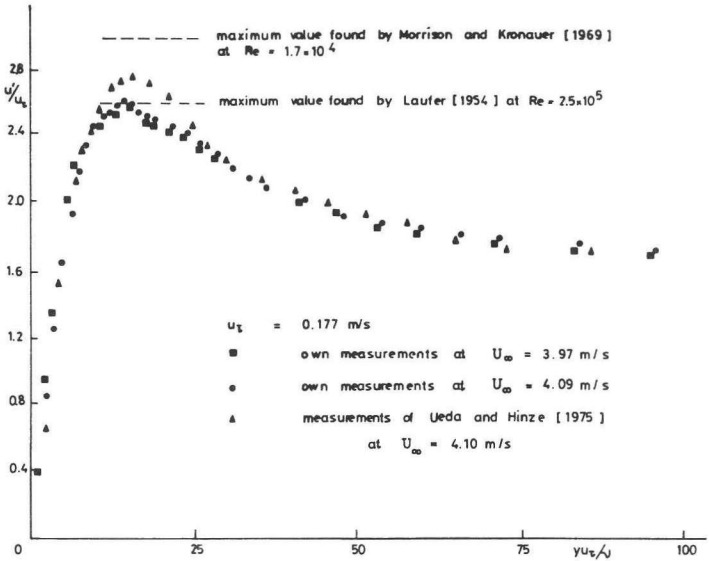


Figure 21: Turbulence intensity distribution in turbulent boundary layer flow and pipe flow. (Indicated Reynolds numbers are based on centerline velocity and tube radius.)

2.2 PIPE FLOW

2.2.1 Experimental set-up

In a pipe flow the measurements regarding the detection of coherent structures were continued. The flow system was of a recirculating type. The working fluid was water. Fig. 22 shows the flow system used in the experiments schematically.

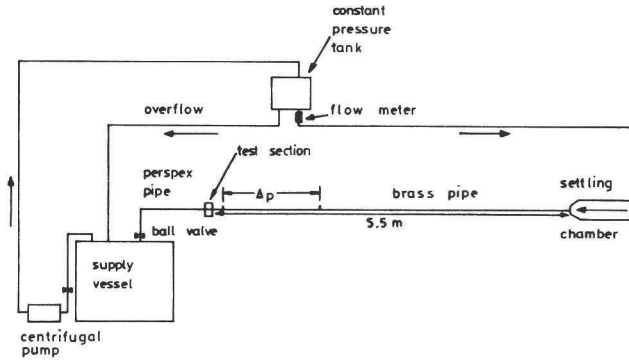


Figure 22: Flow system of turbulent pipe flow experiments.

Water from a 2 m^3 supply vessel was pumped by a centrifugal pump into a constant pressure tank which was also connected with the supply vessel by means of an overflow tube. Immediately downstream of the constant pressure tank an electromagnetic flowmeter was installed for measuring the flow rate. The settling chamber had a 58:1 contraction ratio.

The brass test tube had an inside diameter of 4.4 cm and a length of 5.5 m. Over 1.5 m of the test tube, beginning at 3.75 m downstream of the entrance, the pressure drop was measured with a differential pressure transducer and an inverted water precision manometer.

A detailed sketch of the test section is shown in fig 23. Inside the test section -a rectangular vessel made of perspex- the brass pipe was replaced by a thin acetate film (thickness 0.1 mm), so laser-Doppler anemometry could be used with an optimal orientation of the measuring volume. The test section was made so that the change from brass pipe to film and from film to perspex pipe, used downstream of the test section, were flush. On both sides of the central part of the film there was water with nearly the same static pressure. Therefore it was not necessary to glue the film on the supporting

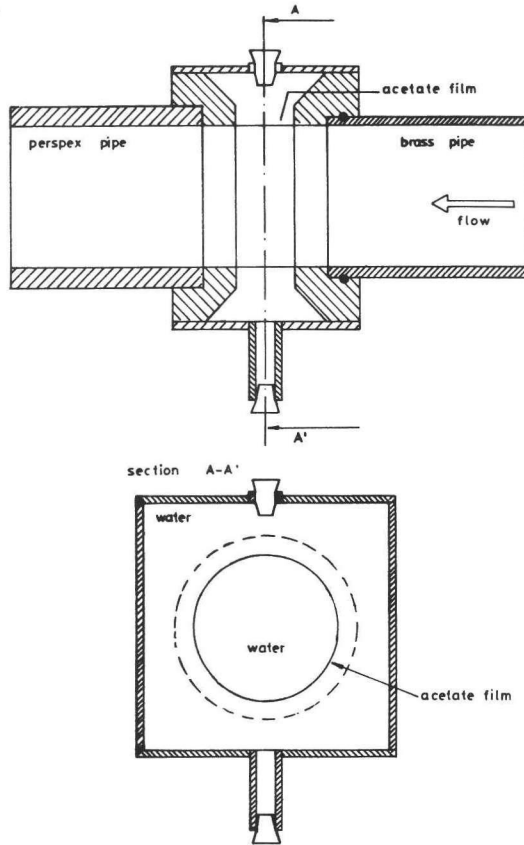


Figure 23: Test section of turbulent pipe flow experiments.

perspex, but the film was kept in its place by the fluid. Because an O-ring was applied in the connection between brass pipe and test section, it was possible to clean or to replace the film. Similar test sections were used by Mizushima and Usui [1977] and van Maanen and Fortuin [1983]. The flow rate in the circuit could be adjusted with a ball valve.

The measurements were performed with a laser-Doppler anemometer, operating in the reference beam mode (see Durst et al. [1976]). No additional seeding of the water was needed to carry out the measurements. Displacements of the laser-Doppler anemometer were accomplished by vertical and horizontal traversing devices.

A laser-Doppler anemometer capable of measuring the axial velocity component U was used for examining the pipe flow.

In the optical system a 15 mW HeNe-laser, two lenses for positioning the waist in the measuring volume, a beam splitter, two Bragg cells, a lens (focus length $f = 150$ mm) to create the measuring volume (dimensions: length 0.470 mm, width 0.055 mm), two lenses with a special diaphragm, a pinhole and a photodetector were incorporated (fig. 24).

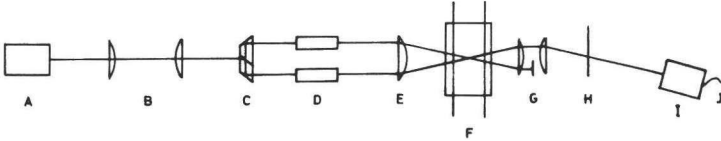


Figure 24: Optical system of one-component laser-Doppler anemometer.
 [A laser, B lenses, C beam splitter, D Bragg cells,
 E lens, F test section, G lenses with diaphragm,
 H pinhole, I photodetector, J laser-Doppler signal.]

The use of the Bragg cells resulted in a preshift frequency of 250 kHz in the photodetector output signal. So the problem of the high sensitivity to laser noise of an anemometer operating in the reference beam mode could be overcome by filtering the output signal of the photodetector.

To measure close to the wall it appeared necessary to image the measuring volume on a pinhole using two lenses with a special diaphragm that blocked the main beam (fig. 25). Otherwise laser light scattered by the film reached also the photodetector.

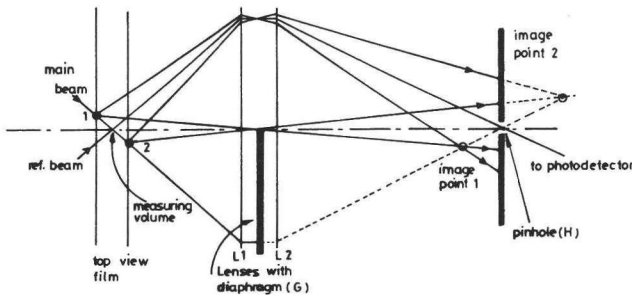


Figure 25: System of lenses and diaphragm to measure close to pipe wall.

The filtered photodetector signal was fed into a tracker (frequency-to-voltage converter).

The mean and rms value of the axial velocity were measured analogously.

The actual measurements were carried out with a laser-Doppler anemometer capable of measuring not only the axial velocity component U but also -simultaneously- the radial velocity component V . These velocity components were not measured directly by the anemometer, but the sum and the difference of the two components were measured at an angle of 45° .

There are three reasons for the choice of this measuring method. The optical system is easier to align. If measuring close to the wall introduces refractive deviations in the beams, these deviations are the same for the two laser-Doppler signals. The two tracker output signals are comparable in strength, so they can be processed in the same way.

To measure the sum and the difference of the two velocity components the optical system described above was modified. The beam splitter, the Bragg cells and the lenses with diaphragm were rotated over 90° and the system was extended with a beam displacer, a beam splitter to create two reference beams (fig. 26) and with a photodetector.

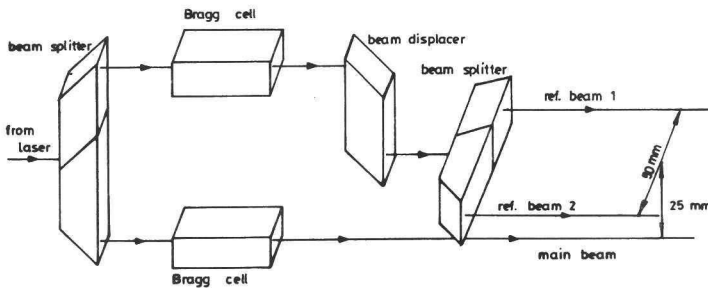


Figure 26: Extension of optical system to measure two velocity components.

The measuring volume had the following dimensions: length 0.70 mm and width 0.06 mm. The laser-Doppler anemometer operated now with a preshift frequency of 750 kHz.

To obtain the axial and the radial velocity component the tracker output signals were added and subtracted. The U - and V -signal were recorded on a

four channel FM recorder. But before recording the U-signal was decreased with approximately the mean voltage to keep enough resolution in the signal. Afterwards the signals were recorded with a PDP-11/34 minicomputer on magnetic disk using 10 V 12 bit analog-to-digital conversion and sampling rates of 0.5 and 1.25 kHz. (Signals measured with an average flow velocity higher than 75 cm/s, were digitized with the highest frequency.) The recorded signals had a duration of 8.5 min. With the minicomputer the distributions of the mean velocity component \bar{U} , the turbulence intensities u' and v' and the Reynolds stress $-\rho\bar{u'v'}$ were calculated.

2.2.2 Experimental results

In the pipe measurements were performed with average flow velocities in the range from 15 to 100 cm/s ($Re_D = 6600$ to 44000).

The pressure drop measurements agreed well with the relation of Blasius (fig. 27).

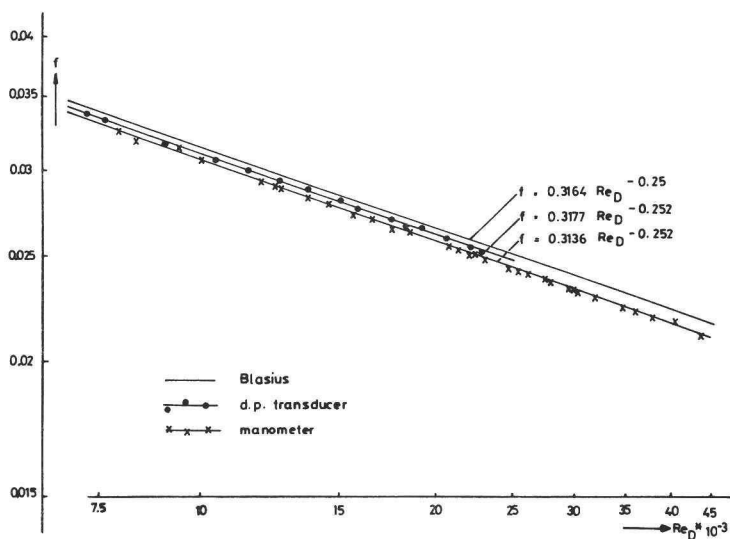


Figure 27: Friction factor.

The differential pressure transducer measurements yielded values for the friction factor f approximately 1.5% lower than indicated by Blasius' relation. The manometer measurements resulted in values for f some 3% too low.

[Friction factor f is defined as $f = 4\tau_w / (\frac{1}{2}\rho U_{av}^2)$.]

With the one-component laser-Doppler anemometer it was checked if the film did not disturb the flow and if the flow was fully developed. From fig. 28 and 29 it follows that the flow is axial symmetric at the measuring position.

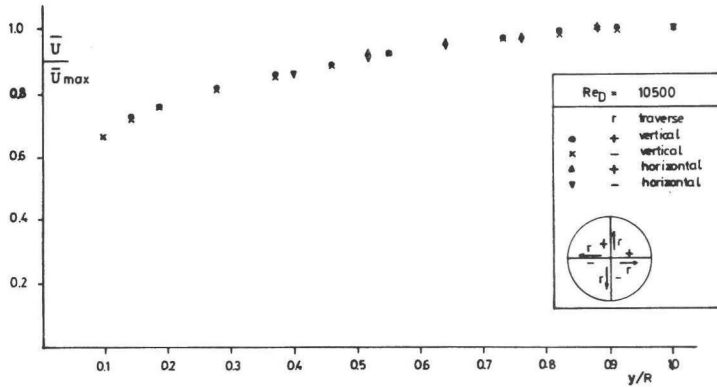


Figure 28: Time-mean axial velocity distribution in pipe cross section measured with one-component laser-Doppler anemometer.

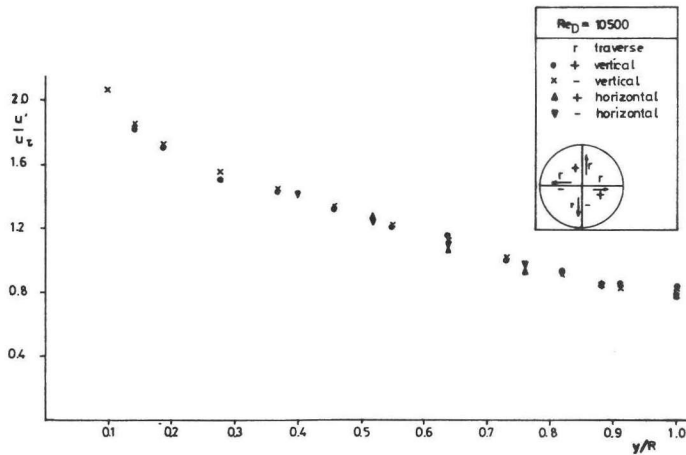


Figure 29: Axial turbulence intensity distribution in pipe cross section measured with one-component laser-Doppler anemometer.

From turbulence intensity measurements close to the wall no influence of the film can be found (fig. 30). Because the distribution of the turbulence intensity u' agrees very well with other measurements in pipe and channel flows (Laufer [1954], Lawn [1971], Eckelmann [1970]), it was concluded that the pipe flow was fully developed (see fig. 30 and 31).

With the two-component laser-Doppler anemometer measurements were carried out at three flow velocities. In table 2 the pipe flow parameters corresponding to these three velocities are given.

Table 2.

Pipe flow parameters.		
U_{av}	u_{τ}	Re_D
[cm/s]	[cm/s]	
23.3	1.45	10500
44.9	2.56	20800
90.2	4.75	38700

The measurements with the two-component laser-Doppler anemometer appeared to be in agreement with the results of the one-component anemometer (fig. 32 and 33). In fig. 34 up to and including 40 the distributions of the mean axial velocity \bar{U} , of the axial and radial turbulence intensity u' and v' , of the Reynolds stress $-\rho\bar{u}v$ and of the correlation factor R are shown.

[Correlation factor R is defined as $R = -\bar{u}v / (u'v')$.]

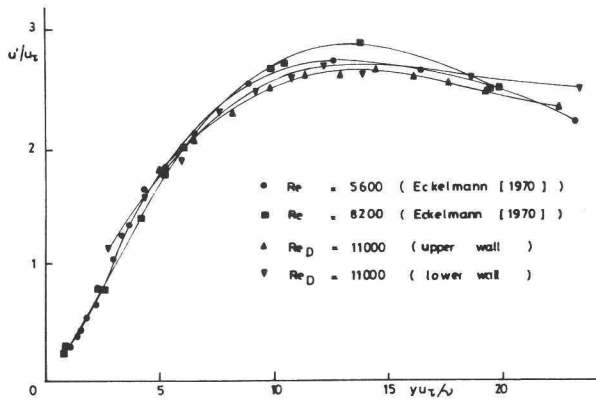


Figure 30: Comparison of Eckelmann's results with axial turbulence intensity, measured with one-component laser-Doppler anemometer. (Re is based on centerline velocity and channel width.)

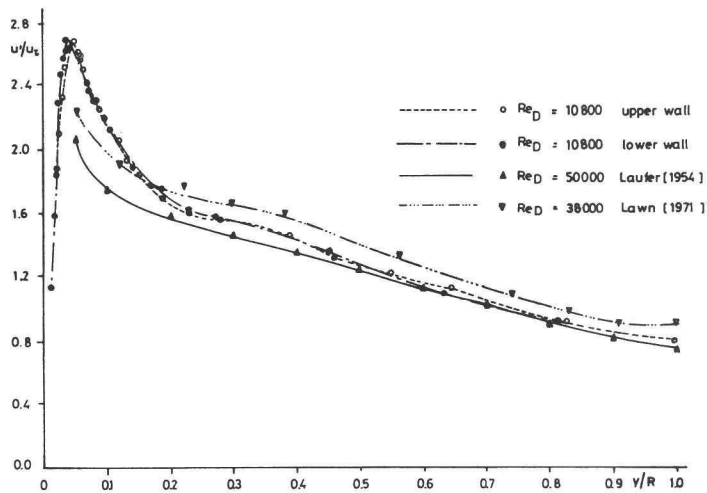


Figure 31: Axial turbulence intensity distribution in pipe cross section measured with one-component laser-Doppler anemometer.

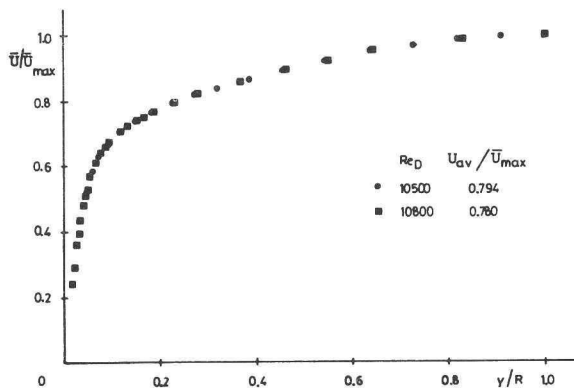


Figure 32: Time-mean axial velocity distribution in pipe cross section measured with one- and two- (circles) component laser-Doppler anemometer.

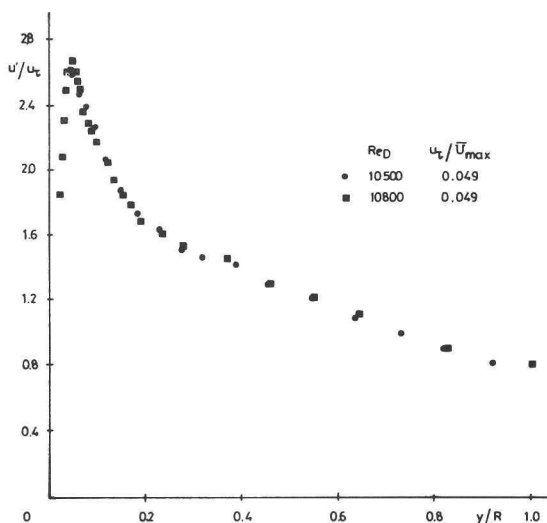


Figure 33: Turbulence intensity distribution in pipe cross section measured with one- and two- (circles) component laser-Doppler anemometer.

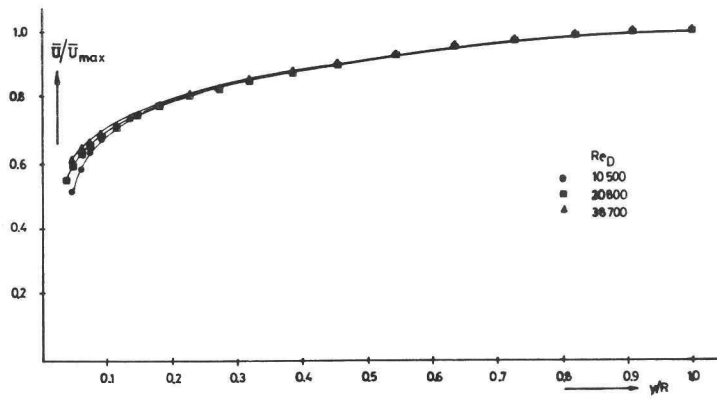


Figure 34: Time-mean axial velocity distribution in pipe cross section.

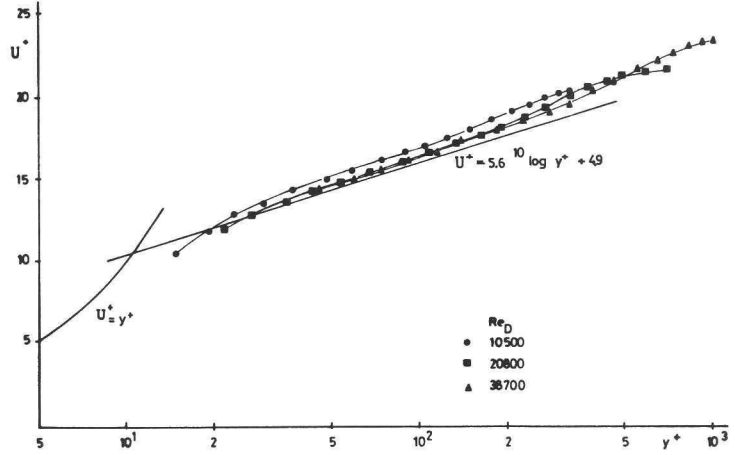


Figure 35: Logarithmic time-mean axial velocity distribution in pipe cross section.

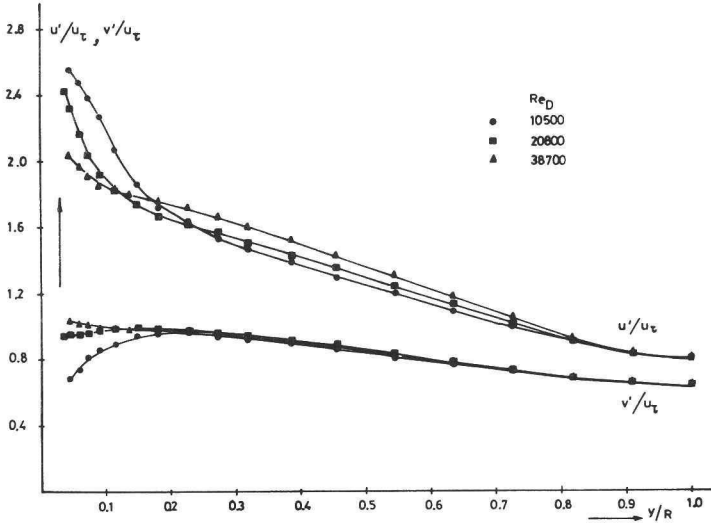


Figure 36: Axial and radial turbulence intensity distribution in pipe cross section.

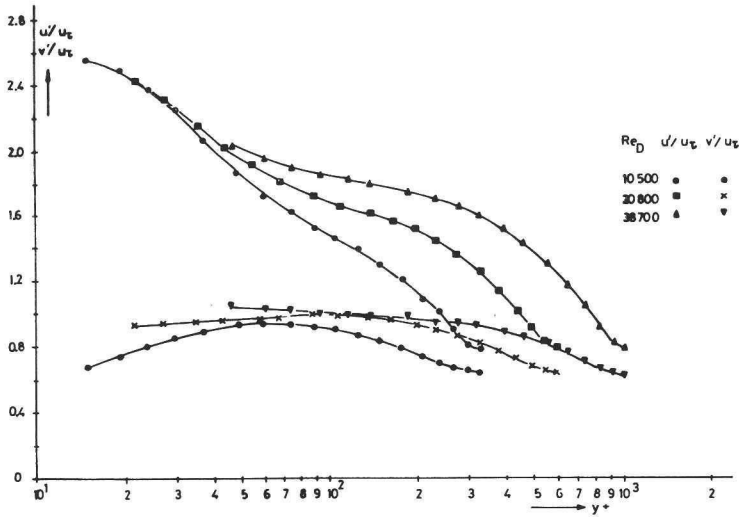


Figure 37: Logarithmic axial and radial turbulence intensity distribution in pipe cross section.

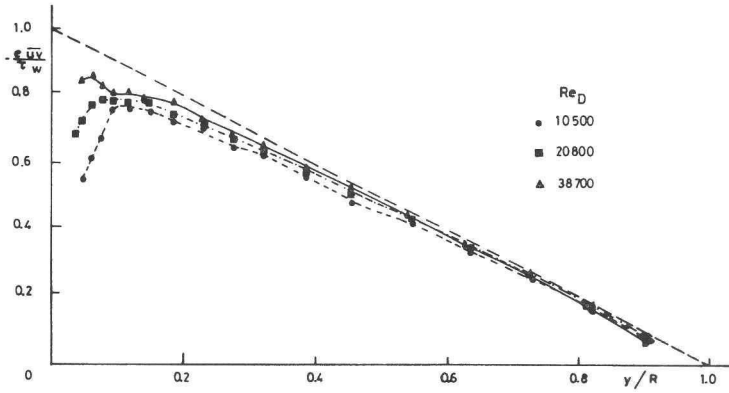


Figure 38: Reynolds stress distribution in pipe cross section.

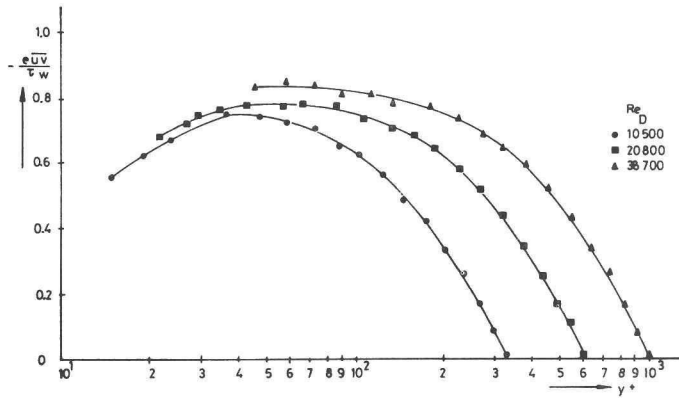


Figure 39: Logarithmic Reynolds stress distribution in pipe cross section.

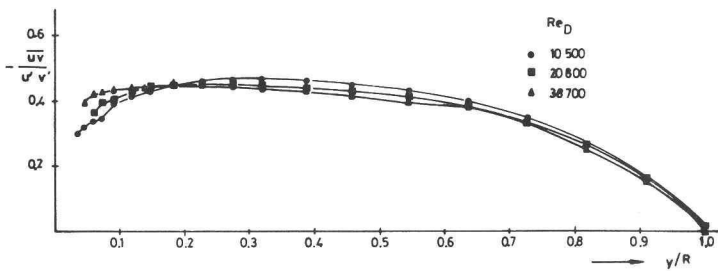


Figure 40: Correlation factor distribution in pipe cross section.

2.3 CHANNEL FLOW

2.3.1 Experimental set-up

In the study of coherent structures an open-recirculating water channel was employed to be able to compare detection methods using points measurements with visual detection.

Laser-Doppler anemometry was used to measure two velocity components of the flow and the hydrogen bubble technique was employed to visualize the flow.

The flow system was similar to that used for the pipe flow experiments. Again water from a supply vessel was pumped by a centrifugal pump into a constant pressure tank. By means of overflows the water could flow from there through an open settling chamber (with corner-vanes and flow straightener, contraction ratio of 5:1 at a water depth of 9 cm) and an open channel (dimensions: 280*150*12 cm³) back into the supply vessel or directly back into the vessel.

On the bottom of the channel a false floor (dimensions: 210*50*1.6 cm³) was placed at 8 cm from the left side wall of the channel (see fig. 41). That way visualization could be performed without disturbing the flow or damaging the channel bottom.

Transition from laminar to turbulent flow was fixed at 9 cm downstream of the channel entrance by means of a tripping wire with a diameter of 3 mm. To be sure of a certain water depth an adjustable threshold was installed 245 cm downstream of the entrance. With valves -between constant pressure tank and settling chamber and between channel and supply vessel- the water speed could be adjusted.

The channel bottom and the false floor were made of glass and the side-walls of perspex. The settling chamber and the channel were mounted vibration free from the rest of the system.

Laser-Doppler measurements were performed in the turbulent boundary layer along the false floor 158 cm downstream of the tripping wire and 13.4 cm from that side-wall where the laser was mounted (see fig. 41).

As in the pipe flow experiments turbulence measurements were carried out with a laser-Doppler anemometer operating in the reference beam mode and capable of measuring instantaneously two mutually perpendicular velocity components. The two velocity components U and V -respectively the main flow velocity component and the velocity component normal to the wall

(see fig. 41)- were not measured directly, but at an angle of 45° the sum and the difference of these components were measured.

The measurements were performed with a 15 mW HeNe laser. To create the main beam and the reference beams and to provide for the necessary preshift a rotating diffraction grating was used (rotation frequency: 49.7 Hz, preshift frequency: 815 kHz). With a lens ($f = 120$ mm) the three beams were focused into one point, the measuring volume (dimensions: 0.65×0.06 mm²).

Because the channel was too wide to pick up the reference beams at the other side of the channel (too much light was scattered), two small mirrors were placed in the channel at 43 cm from the side-wall which deflected down the two reference beams through false floor and channel floor (fig. 41). Beneath the channel two other mirrors deflected the beams to the photodetectors. The total measuring system could be translated vertically.

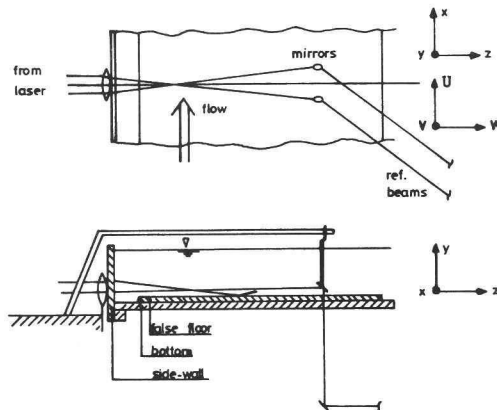


Figure 41: Laser-Doppler arrangement in channel.

Before recording on magnetic disk the fluctuating tracker output signals were low-pass filtered to remove the rotation frequency of the grating. The signals were also amplified before recording.

From the filter characteristic and some spectra, given in fig. 42, it follows that filtering was acceptable; the calculation of the spectra was performed at a free water speed of 13.4 cm/s with signals measured 2 mm above the false floor and recorded with a low-pass cut-off frequency of 20 Hz, a sampling rate of 100 Hz and a duration of 2 hours.

[E(f) is the one-dimensional energy spectrum,

E_∞ is the one-dimensional turbulence kinetic energy ($E_\infty = \int_0^\infty E(f)df$.)

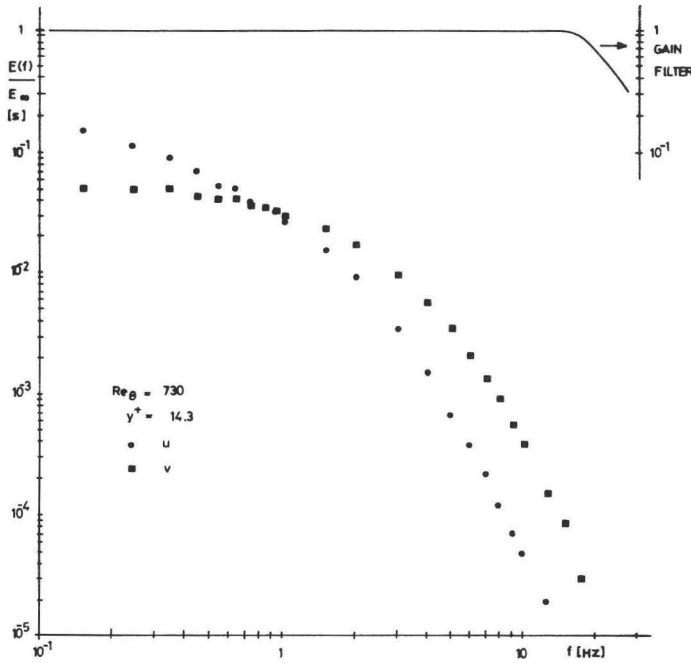


Figure 42: Energy spectra measured in channel flow.

The measurements in the turbulent boundary layer were performed with a cut-off frequency of 20 Hz, with sampling rates of 50 and 100 Hz (to avoid aliasing in spectrum calculations) and with a duration of 30 min.

With the minicomputer the turbulence intensities u' and v' , the skewness and flatness of u - and v -fluctuations (S_u , S_v , F_u and F_v) and the Reynolds stress $-\rho\overline{u'v'}$ were computed.

[F_u and F_v are the flatness factors of u and v respectively.

Flatness factor F of a turbulence quantity $q(t)$ is defined as $F = \overline{q^4}/(\overline{q'})^4$.

S_u and S_v are the skewness factors of u and v respectively.

Skewness factor S of turbulence quantity $q(t)$ is defined as $S = \overline{q^3}/(\overline{q'})^3$.]

The mean velocity U was calculated from the directly measured VCO-frequency (Voltage Controlled Oscillator) of the tracker, which equals the sum of Doppler, preshift and intermediate frequency.

The hydrogen bubble technique was adopted to visualize the flow. In this technique a fine platinum wire is stretched in the water. This wire is the negative electrode of a dc circuit. At this wire hydrogen bubbles are generated. These bubbles are the markers for flow visualization. By pulsing the voltage at regular time intervals bubble lines are produced.

In the channel wires were placed in normal (y) and transverse (z) direction to visualize x-y and x-z planes of the flow (see fig. 43 and 44).

The wires used were 0.07 mm in diameter. The normal wire was 9 cm in length and the total transverse wire 28.5 cm from which 11.5 cm was not insulated. The normal wire was jammed in a small hole drilled in the false floor at a distance of 38 mm upstream of the measuring station of the laser-Doppler anemometer. The transverse wire was soldered to supports which could be translated vertically at 9.3 mm upstream of the measuring station.

The voltage applied to the wires was pulsed with a frequency of 20 Hz.

Simultaneously flow visualization with hydrogen bubbles and measurements with laser-Doppler anemometry were performed. The measured fluctuating tracker output signals were recorded on magnetic disk and the visualized flow was filmed with a 16 mm camera.

In fig. 43 and 44 the arrangements are shown for filming the flow in side and plan view respectively.

To film in side view a periscope-like construction was made with one mirror in the water and one beneath the channel. In the first mirror two notches were made to let through the two reference beams.

Illumination of the x-y plane was accomplished using three film-lights, two above and one beneath the channel. The light made an angle of approximately 60° with the camera line of sight.

Between channel bottom and second mirror a green filter was placed to reduce the light intensity of the laser beams on the exposed film. The camera field of view was 143 mm in length (streamwise direction) and 68 mm in width (normal direction).

In the plan view was filmed using a mirror and a film-light beneath the channel. The light now made an angle of approximately 80° with the camera line of sight.

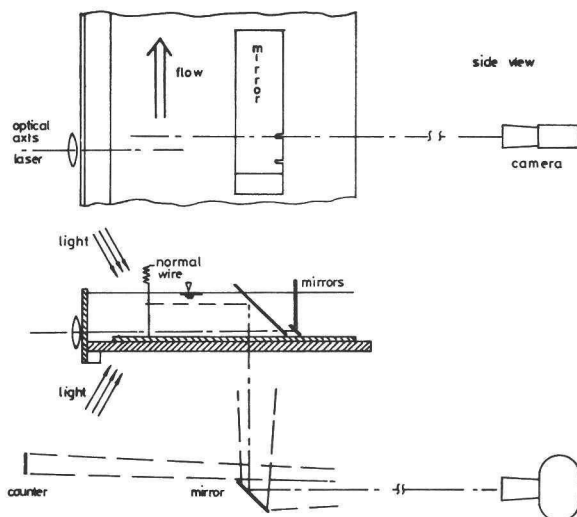


Figure 43: Arrangement for filming the channel flow in side view.

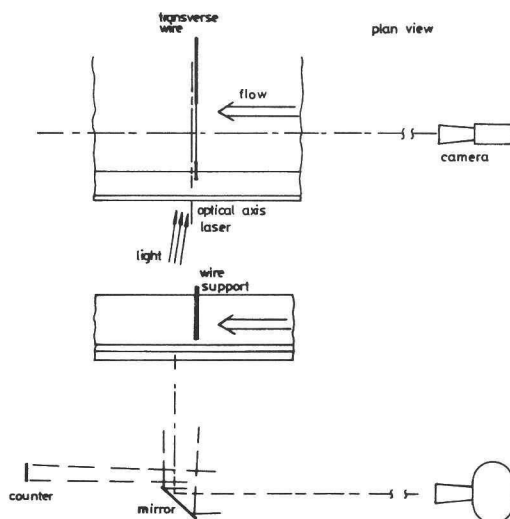


Figure 44: Arrangement for filming the channel flow in plan view.

In the plan view it was impossible to film and measure at the same distance from the wall, because too much laser light was scattered by the hydrogen bubble 'plane'. It appeared necessary to separate measuring point and platinum wire over 2 mm in normal direction. In the plan view all films were exposed measuring 2 mm beneath the visualized 'plane'.

Now the dimensions of the camera field of view were $70 \times 110 \text{ mm}^2$ (in stream-wise and transverse direction respectively).

The clock pulse the minicomputer used for sampling, was also used to link up the recorded velocity components with the corresponding film frames. The clock pulse actuated a counter which appeared at the top of each frame. So the numbers on the frames correspond to the time series of the recorded signals.

As in the boundary layer measurements the fluctuating tracker output signals were low-pass filtered with a cut-off frequency of 20 Hz and recorded on magnetic disk with a digitizing rate of 50 Hz and a duration of 30 min. Because the camera magazine could contain films of maximally 30 m length and because filming was performed with about 45 frames/s, only the flow could be filmed during approximately the first 90 s of sampling.

An exposure time of $1/125 \text{ s}$ was used, so relatively sharp photographs could be made.

2.3.2 Experimental results

With the laser-Doppler anemometer traverses were made through the turbulent boundary layer developed over the false floor. The free stream water speed was 14.1 and 13.4 cm/s and the water depth was about 9 cm. Sampling rates of 50 and 100 Hz respectively were used.

In fig. 45 and 46 the measured mean velocity distributions are shown.

As in the boundary layer experiments the displacement thickness δ^* and the momentum thickness θ were calculated by numerical integration.

Using the empirical velocity distribution $\bar{U}/U_\infty = (y/\delta)^{-11}$ the boundary layer thickness δ was computed (Hinze [1975]).

The wall friction velocity u_τ was derived by fitting the velocity data to Clauser's form of the logarithmic law (Clauser [1956]).

In table 3 the channel flow parameters are summarized.

In fig. 47 the distributions of the turbulence intensities u' and v' and of the Reynolds stress -in dimensionless form- and of the correlation factor are shown. Also indicated are the maximum and minimum values of the 30 min. signals measured during and after filming; see the next paragraph.

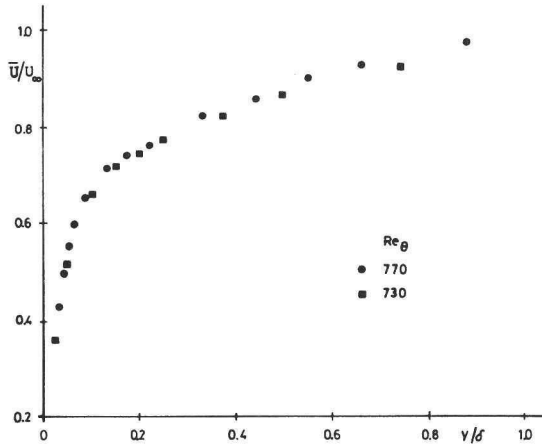


Figure 45: Time-mean velocity distribution in channel flow.

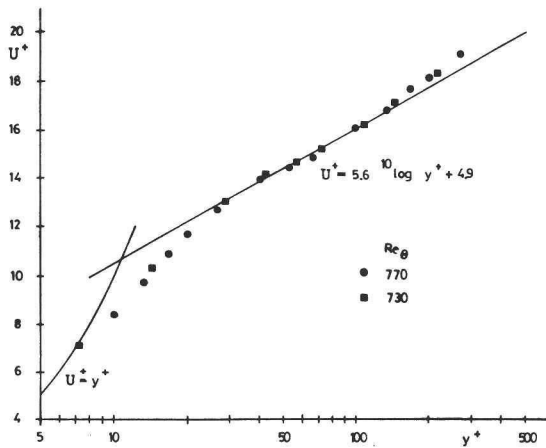


Figure 46: Logarithmic time-mean velocity distribution in channel flow.

At logarithmic scale the distribution of u'/u_τ , S_u and F_u and of v'/u_τ , S_v and F_v are given in fig. 48 and 49 respectively. Comparison with measurements of Gupta and Kaplan [1972] in a turbulent boundary layer and with measurements of Kreplin and Eckelmann [1979] in a turbulent channel flow yields a good agreement for the inner layer. In the outer layer of the turbulent boundary layer the agreement with these measurements is less, but the results show the same tendency.

Table 3.

Channel flow parameters.

U_∞	u_τ	δ	δ^*	θ	Re_θ
[cm/s]	[mm/s]	[mm]	[mm]	[mm]	
14.1	7.2	45.6	8.9	5.9	770
13.4	6.8	40.6	7.5	5.2	730

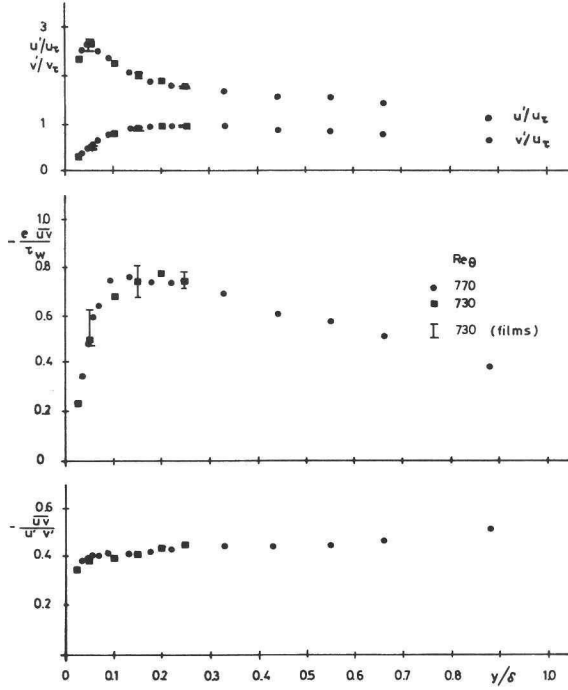


Figure 47: Distribution of turbulence quantities in channel flow.

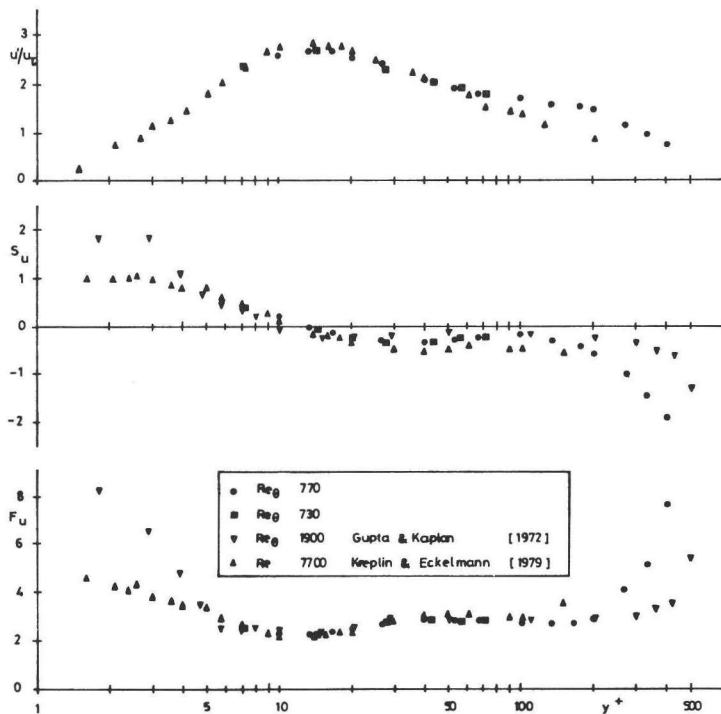


Figure 48: Logarithmic distribution of dimensionless moments of u -fluctuations in channel flow. (Kreplin and Eckelmann based Re on centerline velocity and channel width.)

In total 12 times recordings of measured signals and films of the water flow were made simultaneously, 8 times in side view and 4 times in plan view. The flow conditions were approximately the same as in the second traverse (table 3, $U_\infty = 13.4$ cm/s). In table 4 the measuring positions and filming conditions are given.

[y_w^+ denotes the nondimensional y -position of the platinum wire and y_1^+ the position of the measuring point.]

The calculated maximum and minimum turbulence quantities of the measured 30 min. signals are indicated in fig. 47. The scatter in these results can be caused by the hydrogen bubbles which are rising slowly due to buoyancy.

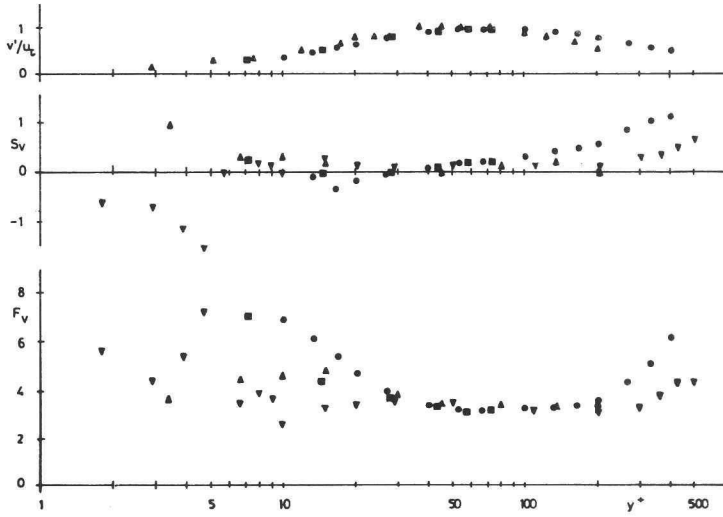


Figure 49: Logarithmic distribution of dimensionless moments of v -fluctuations in channel flow (see fig. 48 for symbols).

Table 4.
Information about films.

film no.	view	y_w^+	y_1^+	duration [s]
1	side	---	14	97
2	,,	---	14	93
3	,,	---	43	99
4	,,	---	43	99
5	,,	---	43	95
6	,,	---	72	93
7	,,	---	72	88
8	,,	---	72	93
9	plan	29	14	78
10	,,	29	14	94
11	,,	57	43	95
12	,,	57	43	95

To be able to compare flow patterns and measured signals the position of the measuring point has to be visible on the frames.
In case of filming in side view the laser beams show that position.

Because in the plan view the measurements were performed at approximately 2 mm below the visualized 'plane', the position of the measuring point has to be indicated on the frames after filming. Therefore the first meter of each film was exposed with the platinum wire at the same distance from the wall as the reference beams. Now hydrogen bubbles were generated continuously. That way the position of the intersection of the laser beams -the measuring point- was marked on each film.

2.4 AXISYMMETRIC JET FLOW

2.4.1 Experimental set-up

In order to detect also coherent structures in free-turbulence hot-wire measurements were performed in an axisymmetric jet, discharging air into ambient air at rest.

Fig. 50 shows the jet facility schematically.

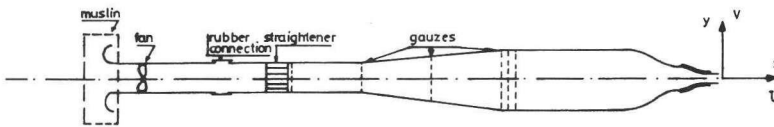


Figure 50: Sketch of jet facility.

A fan, mounted vibration free from the rest of the set-up, supplied the air. The entrance of the flow system was covered with muslin to remove the dust from the incoming flow. The air flowed through a pipe with flow straightener and a diffuser with gauzes into a settling chamber. Via two contractions, with ratios of 7:1 and 18:1, and a small pipe, with a length-diameter ratio of 1, the air left the facility.

The total length of the facility is 7.7 m and the exit diameter is 7 cm. The centerline of the set-up is found 1.2 m above the ground.

Precautions were taken to avoid possible influences of the neighbourhood on the jet.

With platinum plated tungsten hot-wires measurements were performed in the jet flow. The constant temperature method was applied. The wires had a length of 1 mm and a diameter of 0.005 mm.

To establish the exit boundary layer conditions the time-mean velocity \bar{U} and the turbulence intensity u' were measured with a single hot-wire.

In the development region of the jet the axial and radial velocity component U and V were measured by means of X-wires.

The velocity calibration of the X-wires was carried out with the wires placed in the centre of the exit cross section and perpendicular to the axial velocity. A third degree polynomial was calculated by a least square fit.

The direction-sensitivity was also determined at the centre of the exit cross section. Hereto the X-wires were placed at angles in the range from 0° to 135° with the constant axial velocity. With the third degree polynomials the effective velocities -the normal components of the velocity- were calculated. The following relation appeared to be the best approximation for the direction sensitivity of the X-wires:

$$U_{\text{eff}} = c |\underline{U}| \sin\phi,$$

in which U_{eff} is the effective velocity, c a constant and ϕ the angle between wire and instantaneous velocity vector \underline{U} .

During the measurements fluctuating output signals of the two anemometers with a duration of 320 s were recorded on magnetic disk. The signals were low-pass filtered and digitized with the same frequency, viz. 5 kHz, because no Fourier transformation was applied to these signals. Simultaneously the mean voltage of the anemometer output signals was measured. To calculate turbulence quantities the joint probability distribution of the two fluctuating signals was determined. Using this distribution and the mean voltages the time-mean axial velocity \bar{U} , the turbulence intensities u' and v' , the Reynolds stress $-\rho\overline{uv}$ and the skewness and flatness of the axial velocity fluctuations were computed with the equations mentioned above.

2.4.2 Experimental results

The boundary layer experiments were performed 3 mm upstream of the jet exit at a Reynolds number of $1.10 \cdot 10^5$.

The measured dimensionless mean velocity \bar{U}/U_e and turbulence intensity u'/U_e are plotted in fig. 51 versus the dimensionless wall distance y^*/δ^* . The displacement thickness δ^* has been derived from the measured velocity profile.

[y^* is the wall distance (see fig. 50), $y^* = R-y$]

(y is the radial distance and R the exit radius).]

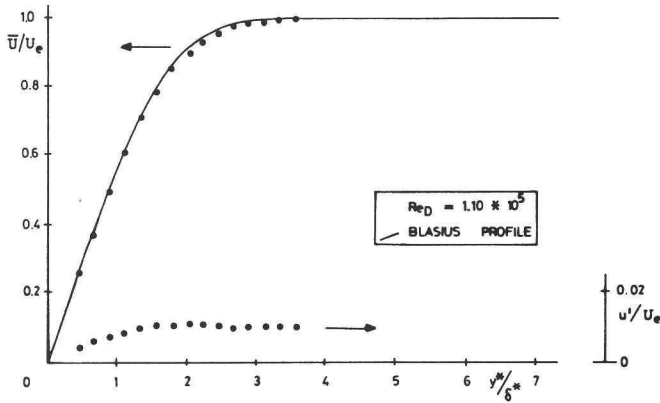


Figure 51: Velocity and turbulence intensity profile in exit boundary layer.

Also the Blasius profile is shown in fig. 51 As can be seen the measured velocity profile agrees well with Blasius profile, indicating that the exit boundary layer is laminar. Using the shape factor of the Blasius profile the momentum thickness θ has been derived.

The measured exit boundary layer parameters are summarized in table 5. The maximum value and the value at the centerline of the dimensionless turbulence intensity, u_{max}'/U_e and u_e'/U_e , are also indicated.

Table 5.
Results for jet exit boundary layer.

Re_D	δ [mm]	θ [mm]	u_{max}'/U_e	u_e'/U_e
$1.10 \cdot 10^5$	0.45	0.17	0.011	0.010

At a Reynolds number of $1.17 \cdot 10^5$ measurements were carried out in the development region of the jet. \bar{U} , u' , v' , $-\rho \bar{u}v$, S_u and F_u were measured at a few radial positions at $x/D = 1.5, 3, 4.5, 6, 7.5, 9$ and 20 .

In fig. 52 up to and including 57 the dimensionless mean velocity \bar{U}/U_e , the dimensionless axial and radial turbulence intensities u'/U_e and v'/U_e , the dimensionless Reynolds stress $\bar{u}v/U_e^2$ and the skewness and flatness of u are plotted as function of the dimensionless radial distance y/D .

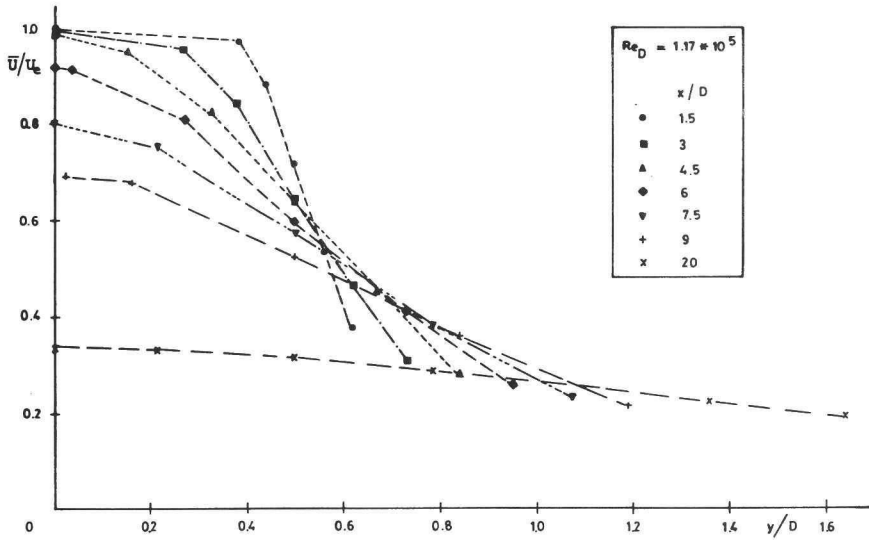


Figure 52: Velocity profiles in jet cross sections.

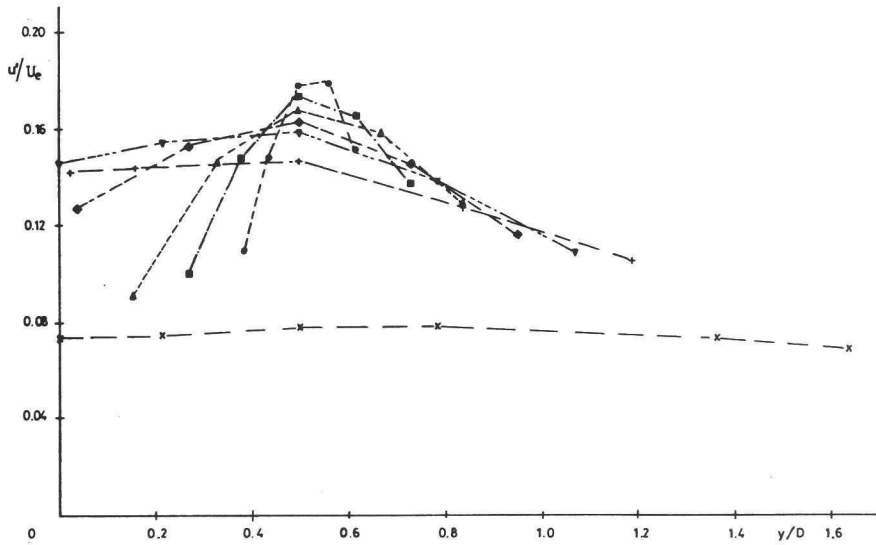


Figure 53: Axial turbulence intensity profiles in jet cross sections.
(See fig. 52 for symbols.)

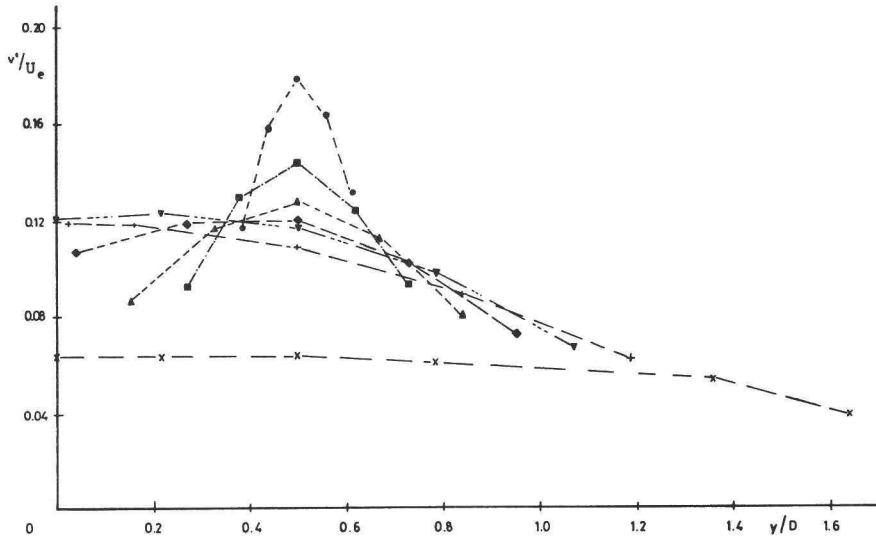


Figure 54: Radial turbulence intensity profiles in jet cross sections.
 (See fig. 52 for symbols.)

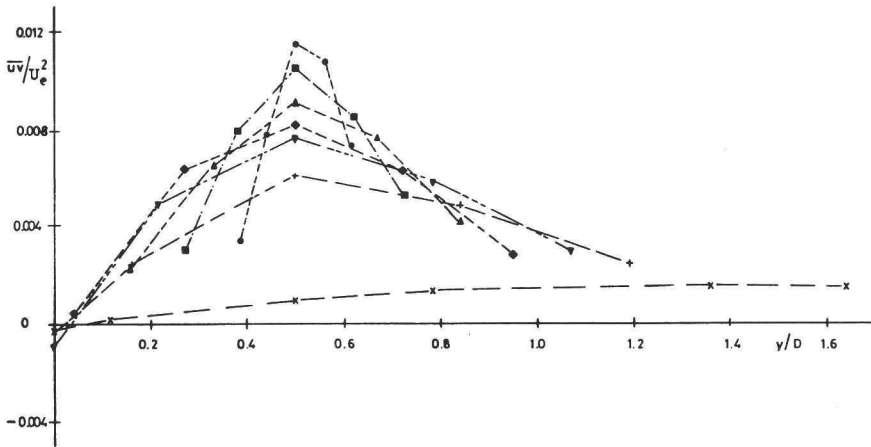


Figure 55: Reynolds stress profiles in jet cross sections.
 (See fig. 52 for symbols.)

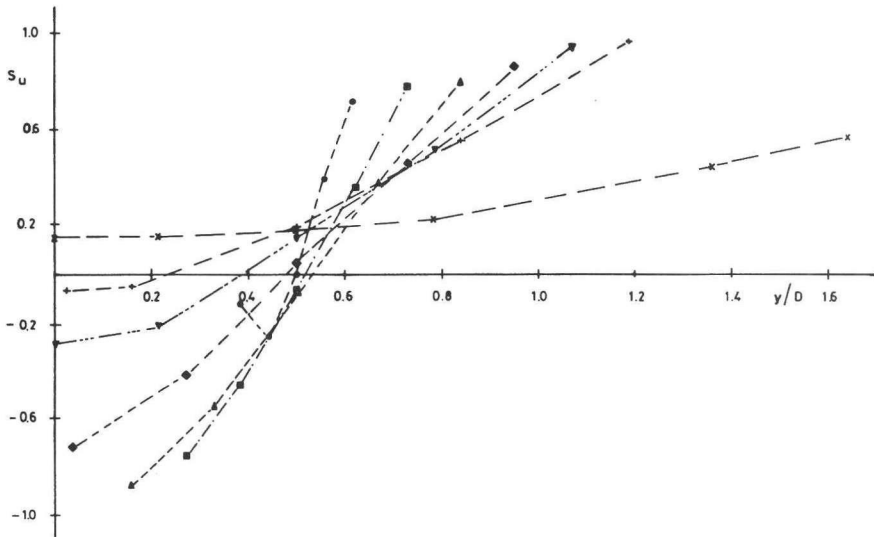


Figure 56: Skewness profiles of axial velocity fluctuations in jet cross sections. (See fig. 52 for symbols.)

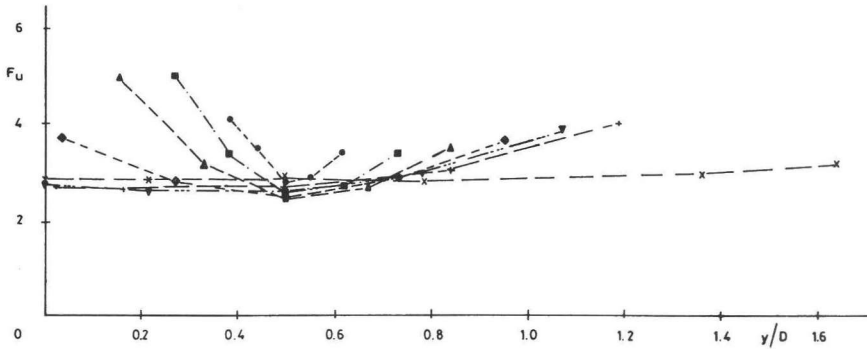


Figure 57: Flatness profiles of axial velocity fluctuations in jet cross sections. (See fig. 52 for symbols.)

Chapter III

DETECTION SCHEMES

As mentioned in chapter I it is difficult to design a detection scheme for coherent structures using only velocity information in one, or more, directions from one position in the flow.

In the past a lot of schemes have been developed making use of one velocity component only. However, it has not been proved whether these methods are objective (see section 1.4 for a definition of an objective detection method). So it is not clear whether results from these schemes can be attributed to coherent structures.

In the following sections the objectivity of three detection schemes will be studied. The scheme of Ueda and Hinze (see Vink [1981]), the scheme of Blackwelder and Kaplan (see Boelsma [1981] and Vink [1982]) and a modified version of Blackwelder and Kaplan's scheme (see Vink [1982]) are examined. Also results of the autocorrelation technique will be presented (see Vink [1981]).

3.1 SCHEME OF UEDA AND HINZE

3.1.1 Description of the scheme

According to Ueda and Hinze [1975] high frequency parts of a differentiated u -signal indicate the presence of bursts. Therefore in their detection scheme narrow-band signals of $(\partial u / \partial t)^3$ were used for counting the burst rate.

In the scheme a linearized u -signal is differentiated, raised to the third power, band-pass filtered (mid-frequency equaled half the Kolmogorov frequency, relative bandwidth equaled 0.24) and compared with a threshold level.

So the parameters of this detection method are the mid-frequency, the relative bandwidth and the threshold level.

3.1.2 Test results

From the paper of Ueda and Hinze the influence of the parameters on the scheme is not clear. Further investigations were made therefore to ascertain the dependency on the parameters.

In section 2.1 the experimental arrangement used in this investigation is described. In fact, it is the same windtunnel Ueda and Hinze used. Only the boundary layer conditions, see table 1, were slightly different because of an other position of the tripping wire.

The same electronic equipment was used too. In this investigation also a fourteen channel FM magnetic tape recorder was employed for recording the linearized u-signals, recording speed 120 in/s. So for testing the scheme the same signals were used.

At two wall distances -at $y^+ = 15$ and $y^+ = 50$ - signals were recorded with a duration of 12 min. Additional information about the signals can be found in table 6.

Table 6.
Turbulence quantities of recorded signals.

y^+	λ [mm]	ϵ [m ² /s ³]	η [mm]	f_K [kHz]
15	4.3	2.43	0.19	1.6
50	3.9	1.66	0.21	2.0

[λ is the dissipation length scale, defined by $1/\lambda^2 = \overline{(\partial u / \partial x)^2} / u^2$;

ϵ is the dissipation per unit mass and time, deduced from the following relation $\epsilon = 15 \nu u^2 / \lambda^2$;

η is the Kolmogorov length scale, defined as $\eta = (\nu^3 / \epsilon)^{0.25}$;

f_K is the Kolmogorov frequency, defined as $f_K = \bar{U} / 2\pi\eta$.]

The detection scheme was applied to these two signals. The mean time T_d between successive detections was determined as function of the threshold level. Fig. 58 shows the results; the mean time between successive detections is given in the dimensionless form of $T_d U_\infty / \delta_{0.99}$.

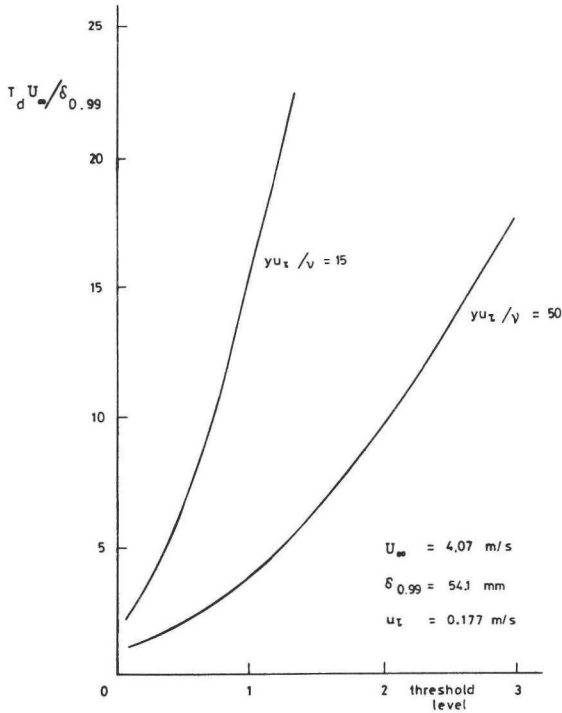


Figure 58: Dimensionless mean time between successive detections according to Ueda and Hinze's scheme. (Threshold level in arbitrary units.)

There appears to be a great dependency on this threshold level. Although the dependency on the two remaining parameters, viz. the mid-frequency and the relative bandwidth, has not been tested, the detection scheme of Ueda and Hinze can not be called objective. So results of the scheme as reported by Ueda and Hinze become questionable (see fig. 8).

3.2 SCHEME OF BLACKWELDER AND KAPLAN

3.2.1 Description of the scheme

Since the results of the visualization studies indicated that the bursts were associated with a high degree of velocity fluctuation (Corino and Brodkey [1969], Kim et al. [1971] and Grass [1971]), Blackwelder and Kaplan [1972,1976] designed a detection scheme which searches this condition. The guiding philosophy was to try to keep the scheme as simple as possible while

yet retaining the essential features of the burst. This resulted in a scheme using only the u-fluctuations and keeping the number of conditions, which have to be fulfilled, to a minimum.

In order to concentrate on a localized region in space -or better time, using Taylor's hypothesis- the Variable-Interval Time Averaging (VITA) method was employed. The variable-interval time average of a fluctuating quantity $q(x,y,z,t)$ is defined by:

$$\hat{q}(x,y,z,t,T_m) = T_m^{-1} \int_{t-T_m/2}^{t+T_m/2} q(x,y,z,s)ds,$$

in which x, y and z are the Cartesian co-ordinates and T_m is the averaging time.

To obtain a local average of some phenomenon, the averaging time T_m must be chosen of the order of the time scale of the phenomenon under study, thus of the order of the time scale of a coherent structure.

A measure of the intensity of velocity fluctuations of short duration is obtained by computing the VITA-variance of the streamwise velocity component, defined as:

$$\hat{v}ar(x,y,z,t,T_m) = \hat{u}^2(x,y,z,t,T_m) - [\hat{u}(x,y,z,t,T_m)]^2.$$

If the VITA-variance is larger than a certain threshold level ku'^2 a coherent structure is supposed to be present. k is the threshold parameter and u' is the usual r.m.s. value of u when an infinite large averaging time is used. Blackwelder and Kaplan introduced as detection function $D(t)$:

$$D(t) = \begin{cases} 1 & \text{if } \hat{v}ar > ku'^2 \\ 0 & \text{otherwise} \end{cases}$$

Fig. 59 shows a schematic representation of Blackwelder and Kaplan's scheme. Blackwelder and Kaplan used a computer for the application of the detection scheme.

To answer the question whether the detection can yield information about coherent structures, a 'pseudo-turbulence' signal was generated from a doubly exponentially filtered digital random-number generator.

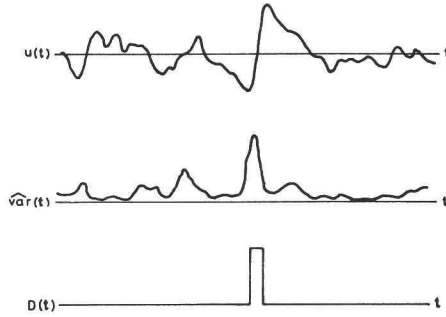


Figure 59: Detection scheme of Blackwelder and Kaplan.

This signal had almost the same spectral distribution as the streamwise velocity at $y^+ = 15$.

When the detection scheme was applied to the pseudo-turbulence and conditional averages* were computed, there was hardly a noticeable deviation from zero. So Blackwelder and Kaplan concluded that any conditionally averaged results for real turbulence were closely related to the turbulence structure and not to the detection scheme.

In Blackwelder and Kaplan's scheme two parameters are involved, viz. the averaging time T_m and the threshold parameter k . According to Blackwelder and Kaplan the scheme is not very sensitive for varying T_m , but the dependency on k is greater. But because the conditional average of the streamwise velocity component scaled with the square root of the threshold level, Blackwelder and Kaplan believed that variation of the threshold level only affected the magnitude of the detected events and not its structure.

In their study Blackwelder and Kaplan used a threshold parameter of 1.2 and an averaging time of $T_m u_\tau^2 / \nu = 10$.

*The conditional average of a turbulence quantity q is defined by

$$\langle q(x, y, z, \tau) \rangle_{y^+} = N^{-1} \sum_{n=1}^N q(x, y, z, t_n + \tau).$$

The subscript y^+ denotes the position at which detection occurred. N is the number of samples added in the ensemble average. The quantities t_n are those positions in time when detection occurred. The times t_n were taken to be midway between beginning and end of the period during which detection occurred. With a negative and a positive time delay τ the temporal behaviour of q was determined before and after detection.

3.2.2 Test results

The detection scheme of Blackwelder and Kaplan was investigated more extensively with the aid of a PDP-11/34 minicomputer. Blackwelder and Kaplan's scheme was translated into a Fortran program.

To that purpose signals were used from a turbulent boundary layer in the windtunnel, described in section 2.1, and from a white noise generator. In table 1 the turbulence quantities of the boundary layer are summarized.

Two u-signals were recorded on magnetic disks of the minicomputer. The first u-signal was measured at $y^+ = 17$ and had a duration of 76.8 s, the second at $y^+ = 15$ with a duration of 1310.7 s. Before digitizing -sampling frequencies 20 and 10 kHz, respectively- the signals were low-pass filtered with cut-off frequencies of 8 and 4 kHz. In the following the two signals are denoted as signal A and signal B, respectively.

As third signal a 'pseudo-turbulence' signal was recorded from a doubly exponentially filtered white noise generator (signal C, duration 524.3 s, sampling frequency 10 kHz, cut-off frequency 4 kHz).

Signal C had a similar spectral distribution as signal B (fig. 60).

The tests which Blackwelder and Kaplan performed, were repeated. Firstly, the mean time T_d between successive detections was determined as function of the parameters T_m and k using signal A. The averaging time T_m was varied in the range from 6 to 20 ms and the threshold parameter k in the range from 0.8 to 1.8. The small dependency on T_m (fig. 61) and the great influence of k (fig. 62) are in agreement with the results of Blackwelder and Kaplan.

Secondly, the conditionally averaged streamwise velocity component was calculated. Signal B was used and the parameters had the following values: $T_m = 12$ ms ($T_m u_r^2 / \nu = 25$) and $k = 1.0, 1.4$ and 1.8 respectively. The conditionally averaged streamwise velocity component had the same form as reported by Blackwelder and Kaplan (fig. 63). The calculation of the conditional average was done slightly different. The point midway between beginning and end of the detection was not taken as time t_n in the averaging process, but the first point of detection. This is probably the reason why the conditional averages do not scale well with the square root of the threshold level.

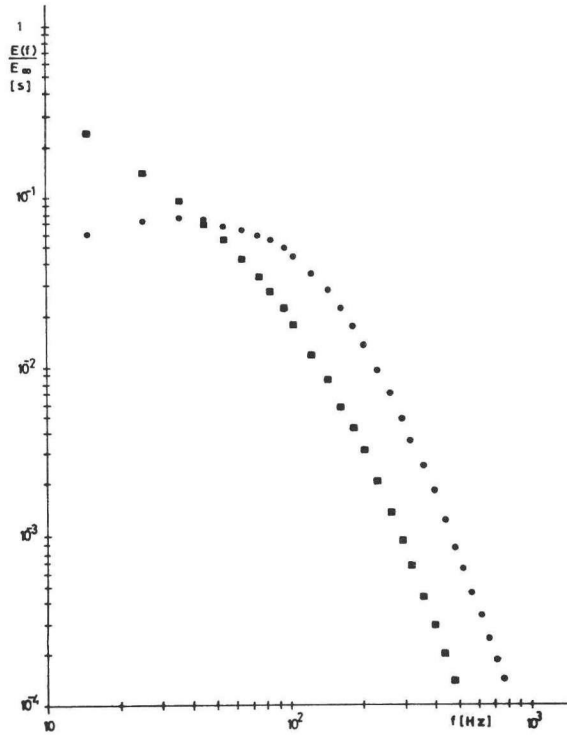


Figure 60: Spectrum of pseudo-turbulence (circles) and boundary layer turbulence (signal B).

The conditional average of signal C, the pseudo-turbulence signal, is shown in fig. 64. As found by Blackwelder and Kaplan there is scarcely a deviation from zero.

The results mentioned above indicate that also Blackwelder and Kaplan's scheme does not seem to be an objective detection method.

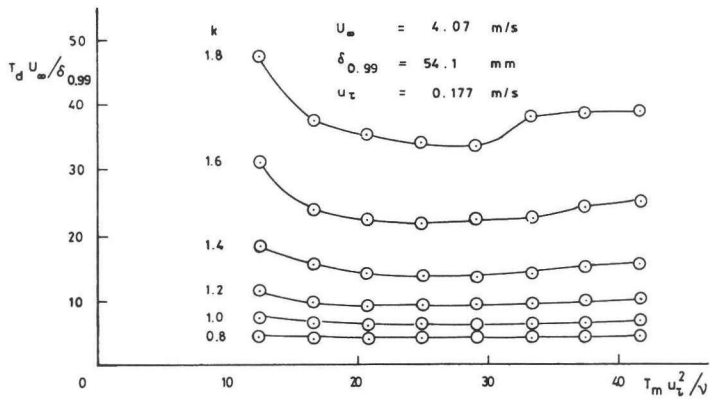


Figure 61: Dimensionless mean time between successive detections according to Blackwelder and Kaplan's scheme.

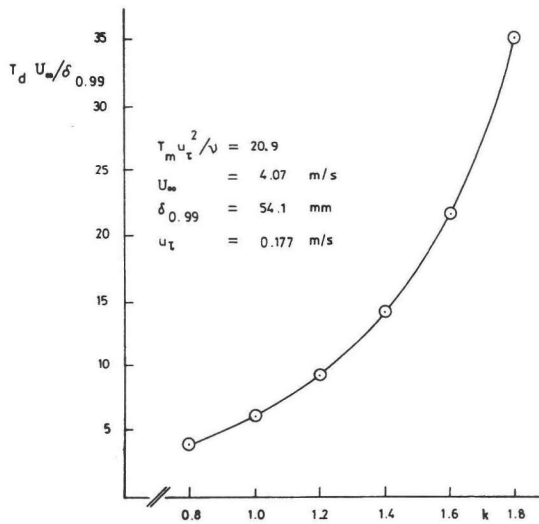


Figure 62: Dimensionless mean time between successive detections according to Blackwelder and Kaplan's scheme.

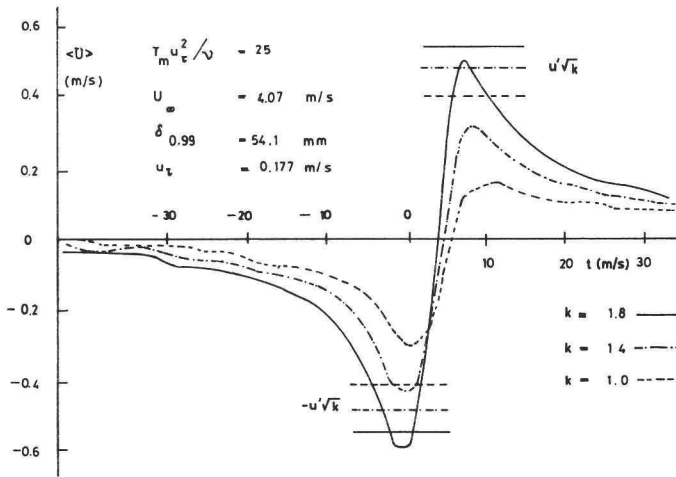


Figure 63: Conditionally averaged streamwise velocity component according to Blackwelder and Kaplan's scheme.

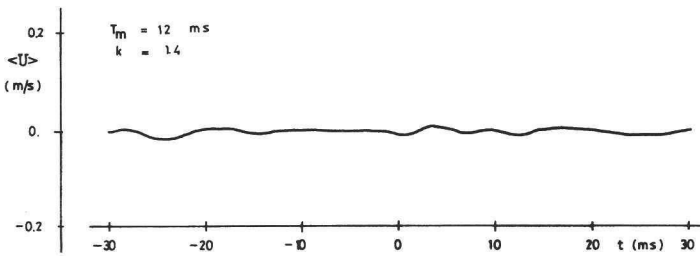


Figure 64: Conditional averaged pseudo-turbulence signal according to Blackwelder and Kaplan's scheme.

3.2.3 Further tests

Because Blackwelder and Kaplan's scheme has been adopted by many investigators, it was decided to examine whether some properties of the detected structures are the same as observed in visualization studies.

From visual data Kim et al. [1971] found a broad distribution of time intervals t_d between successive structures (fig. 65).

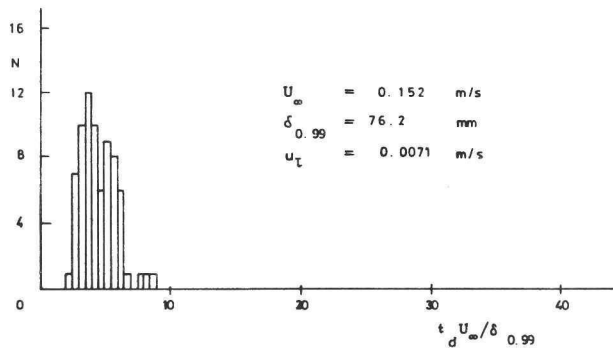


Figure 65: Distribution of time intervals between successive detections according to visualization studies of Kim et al.

The same distribution was calculated from the detection data of Blackwelder and Kaplan's scheme to the neglect of time intervals smaller than the averaging time. The time interval between two successive detections was defined as the time passed between the end of the first detection and the beginning of the second, as indicated by the detection function $D(t)$ (fig. 59). It was assumed that detections with time intervals smaller than averaging time T_m are reactions on the same structure and therefore these detections were treated as one detection.

In fig. 66 the time interval distributions are shown for 78.6 s of signal B with threshold parameters of 0.8, 1.2 and 1.6 and an averaging time of 12 ms ($T_m u_\tau^2 / \nu = 25$).

Again it can be concluded that the calculated distribution is very dependent on the threshold parameter k .

The time interval distribution of pseudo-turbulence has the same form as the distributions of the turbulence signals for low values of k (fig. 67). Moreover, the calculated distribution differs from the distribution found during the visualization studies of Kim et al. According to Blackwelder and Kaplan's scheme for low values of k the highest probability for a new detection to occur is immediately after the previous one. A similar conclusion was drawn by van Maanen and Fortuin [1983]. According to the visualization study of Kim et al. a new coherent structure occurs most likely after a finite time. With Blackwelder and Kaplan's scheme this is only found for large values of k , for instance for $k = 1.6$ in fig. 66.

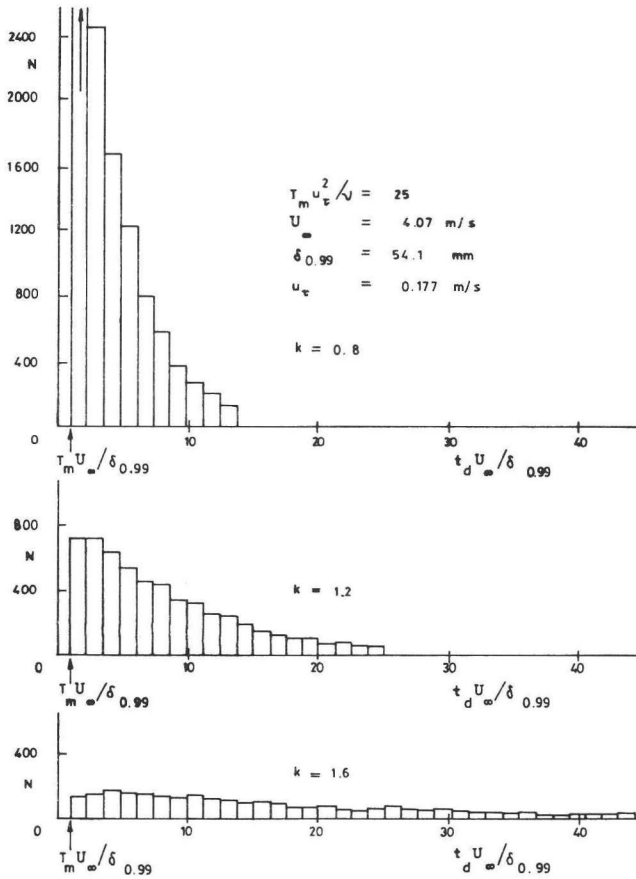


Figure 66: Distribution of time intervals between successive detections according to Blackwelder and Kaplan's scheme.

Researches were made into another feature of coherent structures. As reported in visualization studies (Corino and Brodkey [1969], Kim et al. [1971]) the major part of the Reynolds stress is produced by coherent structures.

Therefore the contribution of the detections of Blackwelder and Kaplan's scheme to the Reynolds stress was calculated, when the scheme was applied to the u -signal. As in the case of the time interval distributions two detections with a time interval smaller than the averaging time were treated as one detection in this calculation.

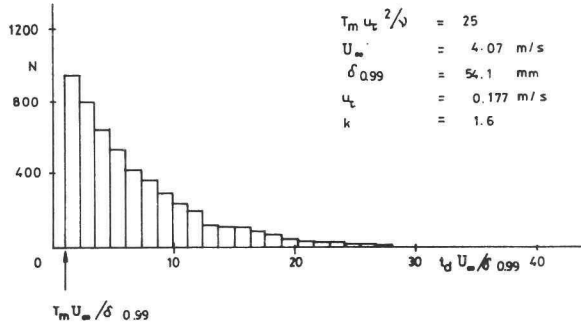


Figure 67: Distribution of time intervals between successive detections in pseudo-turbulence according to Blackwelder and Kaplan's scheme.

Hereto signals from the turbulent pipe flow, described in section 2.2, were used. At a Reynolds number of 10150 u - and v -signals from two measuring points were recorded on magnetic disk. The dimensionless distances from the wall were 15 and 33, the sampling frequency was 500 Hz, the cut-off frequency of the low-pass filters was 250 Hz and the duration of the signals was 5222 s.

The calculation was based on detection function $D(t)$. As it is not known if a period of high Reynolds stress falls within a detection period, the calculation was performed in three ways.

In the first approach the duration of the uv -parts used for the computation was enlarged.

As a first step the parts of the uv -signal indicated by the original detection function $D(t)$ were used in the calculation. Next the uv -parts were enlarged. The detection function $D(t)$ was changed in such a way, that the beginning of each detection was assumed to have taken place $n\Delta\tau$ s earlier than in the original detection function and the end $n\Delta\tau$ s later, where n is the number of times each detection was enlarged. Pieces of the uv -signal that would be counted twice so (overlapping detection periods), were only counted once.

In fig. 68 and 69 the results of the computation are shown. In Blackwelder and Kaplan's scheme the following parameter values were used: $T_m = 5$ and 15 ms ($T_m u_\tau^2 / \nu = 9.8$ and 29.4), $k = 0.8, 1.2$ and 1.6.

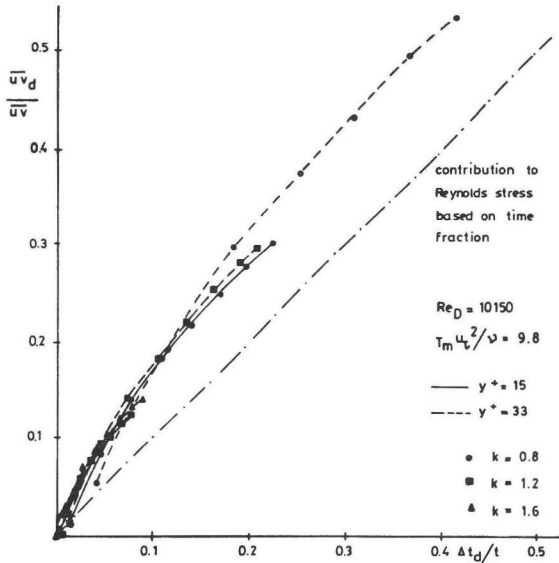


Figure 68: Contribution to Reynolds stress due to detections according to Blackwelder and Kaplan's scheme.

The absciss in these figures gives the time fraction $\Delta t_d/t$ of the measured signal due to detections. The ordinate gives the fraction $\overline{uv}_d/\overline{uv}$ of the Reynolds stress due to detections.

[t is the duration of the total signal.

Δt_d represents the total time that detections occurred or were assumed

to occur ($\Delta t_d = \int_0^t D(s) ds$).

$-\rho \overline{uv}$ is the Reynolds stress ($\overline{uv} = t^{-1} \int_0^t uv(s) ds$).

$-\rho \overline{uv}_d$ is the Reynolds stress due to detections

($\overline{uv}_d = t^{-1} \int_0^t uv(s) D(s) ds$.)

The first points in fig. 68 and 69 were calculated using the original detection functions of Blackwelder and Kaplan's method. The next points apply to the changed detections functions with enlarged detection periods; $\Delta \tau$ equaled $T_m/2$ and $T_m/4$ respectively, which means that each detection was enlarged nT_m and $nT_m/2$ respectively, when no overlap was present.

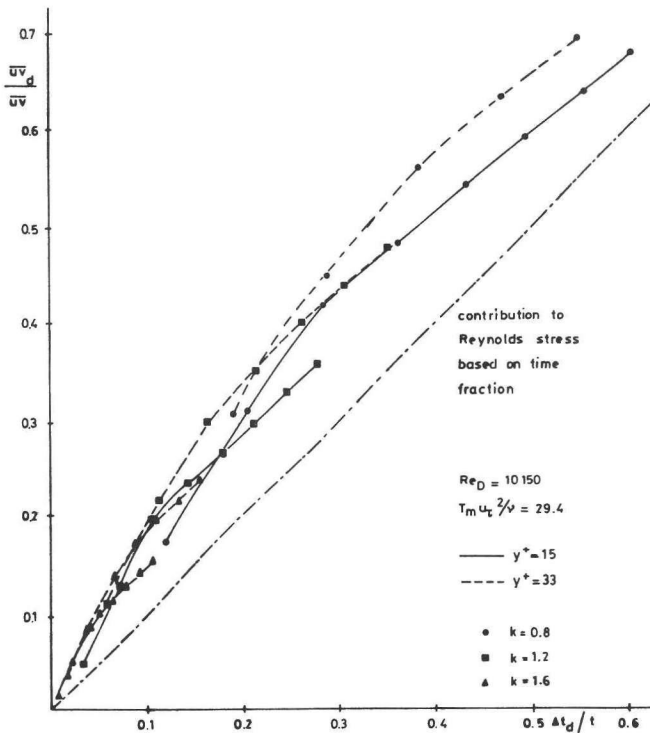


Figure 69: Contribution to Reynolds stress due to detections according to Blackwelder and Kaplan's scheme.

In the second approach the original detection function $D(t)$ was delayed with respect to the uv -signal. Now only the detections found with the averaging time of 15 ms were used and the delay time τ was varied in the range from -0.5 to $+0.5$ s.

For the dimensionless distance $y^+ = 15$ there appear to be two peaks -one just before and one just after detection- in the contribution to the Reynolds stress (fig. 70). For the dimensionless distance $y^+ = 33$ the peak just after detection has disappeared almost completely (fig. 71). Comparing fig. 63 and 70 it seems that on the whole ejection events cause the first peak and sweep events the second. In that case the disappearance of the second peak for $y^+ = 33$ agrees with the measurements of Brodkey et al. [1974] concerning the relative importance of ejection and sweep contributions to the Reynolds stress (see fig. 12).

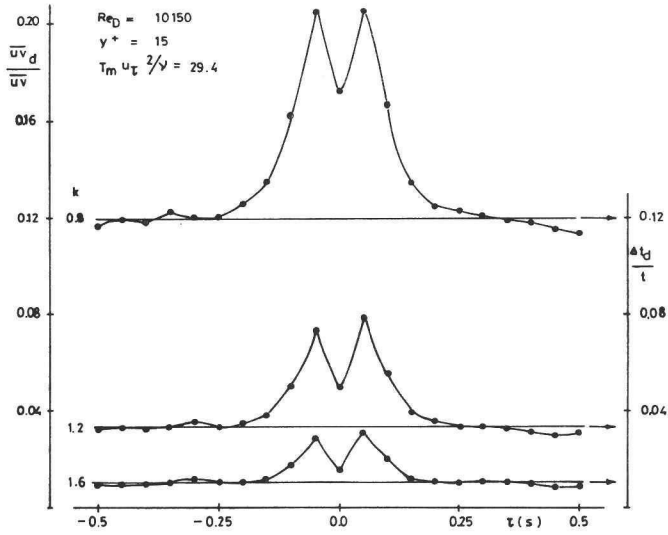


Figure 70: Contribution to Reynolds stress due to delayed detections according to Blackwelder and Kaplan's scheme.

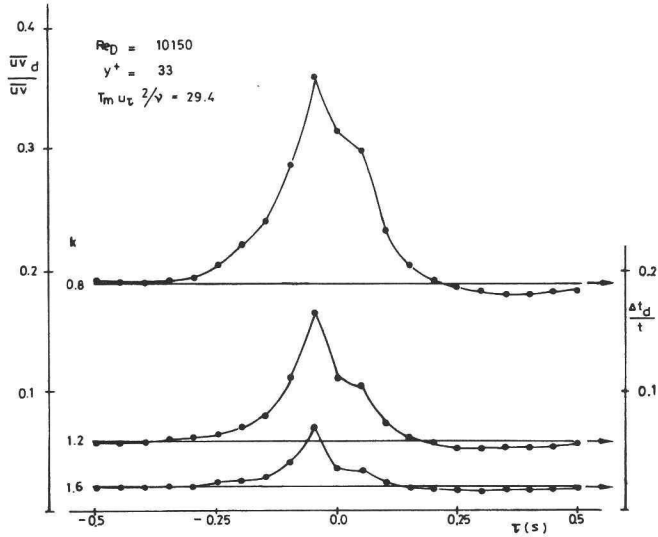


Figure 71: Contribution to Reynolds stress due to delayed detections according to Blackwelder and Kaplan's scheme.

In the third approach the quadrant analysis technique was used (see section 1.2.3). Here the hole was defined by the curves $|uv| = K|\overline{uv}|$.

$$[K = Hu'v' / |\overline{uv}|]$$

The quadrant analysis technique was firstly applied to the complete signals. As function of hole-size K the fractional contribution $\overline{uv}_i / \overline{uv}$ to the Reynolds stress of the four quadrants excluding the hole, and of the hole was computed; also the fraction t_i/t of the time the uv-signal spent in these quadrants excluding the hole, and in the hole, was calculated as function of K.

$[-\rho\overline{uv}_i$ is the Reynolds stress due to quadrant i excluding the hole

$$(i = 1, 2, 3 \text{ or } 4) \text{ and due to the hole } (i = 5) (\overline{uv}_i = t^{-1} \int_0^t uv_i(s) ds).$$

t_i is the total time the uv-signal spent in quadrant i excluding the hole, and in the hole.

(See fig. 13)]

In fig. 72 and 73 the results of the quadrant analysis technique are shown. These distributions agree with the results of Lu and Willmarth [1973] and of Brodkey et al. [1974].

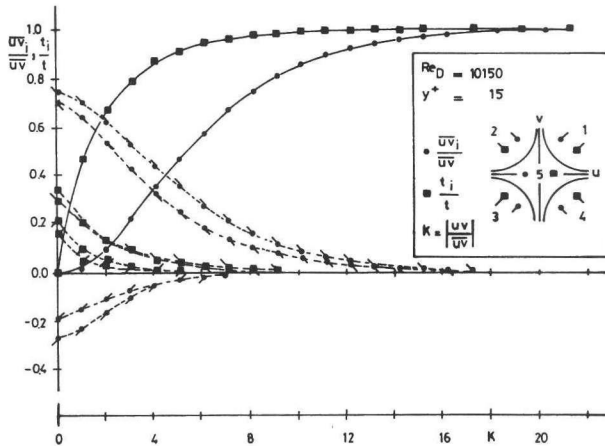


Figure 72: Fractional contribution to Reynolds stress and time fraction as function of hole-size K (quadrant analysis technique).

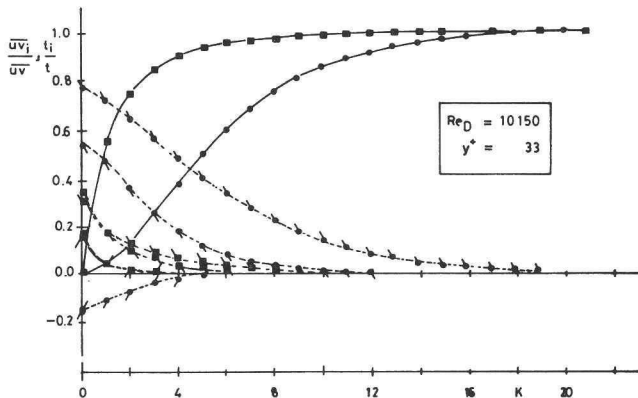


Figure 73: Fractional contribution to Reynolds stress and time fraction as function of hole-size K (quadrant analysis technique).

The quadrant analysis technique was then applied to the detected uv -parts of the signal recorded at $y^+ = 15$ and found with averaging time $T_m = 15$ ms. Without a hole and with a hole of size 2 ($K = 2$) the contributions of quadrant 2 and 4 due to detections were calculated (fig. 74 and 75).

$[-\rho \overline{uv}_{i,d}]$ is the Reynolds stress of quadrant 2 or 4 ($i = 2$ or 4),

excluding the hole, due to detections $(\overline{uv}_{i,d} = t^{-1} \int_0^t uv_i(s)D(s)ds)$.

$\Delta t_{i,d}$ is the total time the uv -signal spent in quadrant 2 or 4, excluding the hole, due to detections.]

Again the first points in these figures were calculated using the original detection function $D(t)$. The other points were computed with enlarged detection periods; $\Delta \tau$ equaled $T_m/4$.

The two dotted lines drawn in these figures indicate the contribution of quadrant 2 and 4 of the total signal to the Reynolds stress without hole (fig. 74) and with a hole of size 2 (fig. 75).

However, from all these results (fig. 68 up to and including 71 and fig. 74 and 75) it has to be concluded that the contribution of the detections to the Reynolds stress is not much greater than could be expected on the basis of the time fraction. So the major part of the Reynolds stress is not due to the detections of Blackwelder and Kaplan's scheme. This is contradictory to the results of the visualization studies.

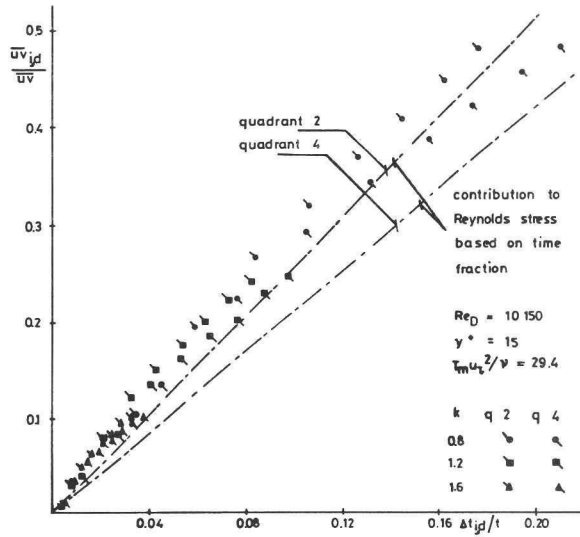


Figure 74: Contribution to Reynolds stress of quadrant 2 and 4 without hole due to detections according to Blackwelder and Kaplan's scheme.

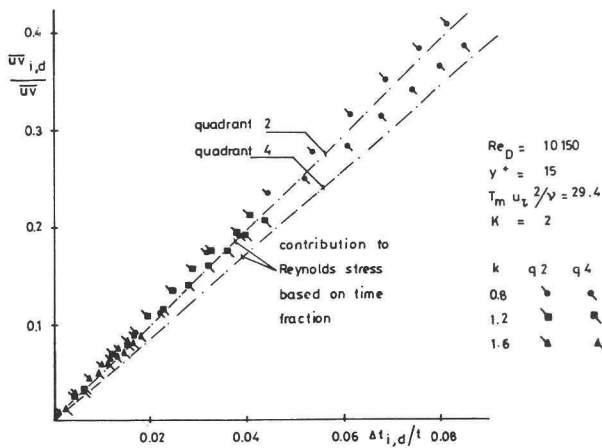


Figure 75: Contribution to Reynolds stress of quadrant 2 and 4 with hole due to detections according to Blackwelder and Kaplan's scheme.

The comparison between the results found with the aid of the detection

method of Blackwelder and Kaplan and the results from the visualization studies give rise to doubt, whether the method detects the same flow structures as observed during visualization studies.

In section 4.4 this point will be discussed further.

3.3 MODIFIED SCHEME OF BLACKWELDER AND KAPLAN

3.3.1 Description of the scheme

It was speculated that the detection scheme of Blackwelder and Kaplan did not work well, because the visual detection process was not imitated well enough.

Visually a coherent structure is perceived, because the structure distinguishes itself from the direct neighbourhood in the turbulent flow field. But in Blackwelder and Kaplan's scheme the VITA-variance is, however, compared with the variance of the total turbulent flow.

Therefore the scheme was changed so that a localized VITA variance of the u -signal is compared with the VITA variance of the u -signal in the direct surroundings. The detection function $DM(t)$ of the modified version of Blackwelder and Kaplan's scheme got the following form:

$$DM(t) = \begin{cases} 1 & \text{if } \hat{u}^2 - \hat{u}^2 > k(u^2 - \bar{u}^2) \\ 0 & \text{otherwise} \end{cases}$$

where $\hat{}$ denotes averaging over time T_m and $\bar{}$ averaging over time T_{mg} . T_m has to be chosen of the order of the time-scale of a coherent structure and T_{mg} of the order of the time between two successive structures.

In the modified scheme three parameters are involved, viz. the threshold parameter k and the averaging times T_m and T_{mg} .

3.3.2 Test results

The dependency on the parameters was examined using the turbulent boundary layer signals A and B and the pseudo-turbulence signal C (see section 3.2).

In fig. 76 and 77 the results for signal A for the mean time between successive detections are given as function of the parameter values.

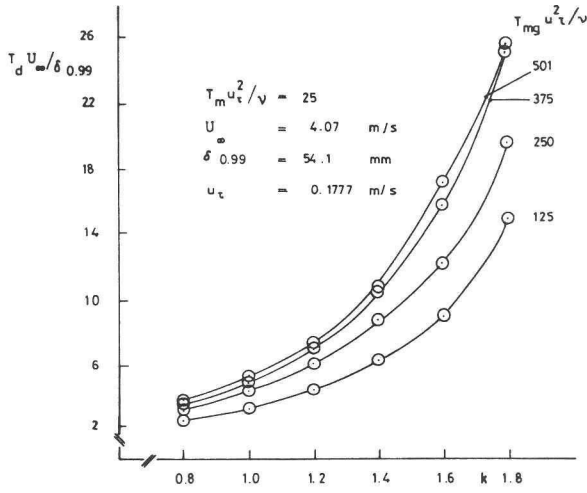


Figure 76: Dimensionless mean time between successive detections according to the modified scheme.

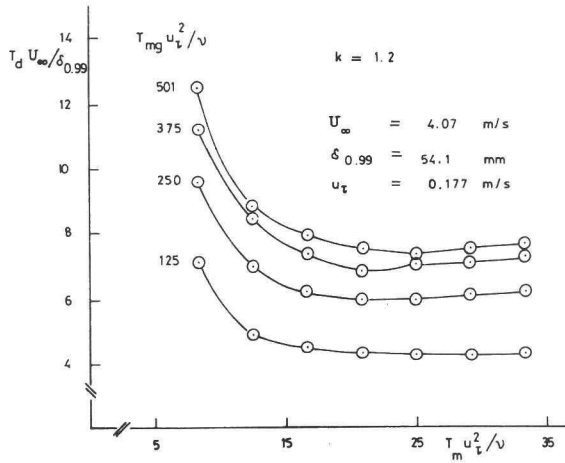


Figure 77: Dimensionless mean time between successive detections according to the modified scheme.

As can be seen the dependency on T_m is again negligible (when T_m is large enough, $T_m u_\tau^2 / \nu > 15$), the influence of T_{mg} decreases with increasing values for T_{mg} and the dependency on k is again large.

The modified scheme reacts more often than Blackwelder and Kaplan's scheme for the range of parameter values investigated.

Also the conditionally averaged streamwise velocity component has been calculated. In fig. 78 the results are shown for signal B with threshold parameters of 0.8, 1.2 and 1.6 and averaging times of 12 and 240 ms

($T_m u_\tau^2 / \nu = 25$, $T_{mg} u_\tau^2 / \nu = 500$).

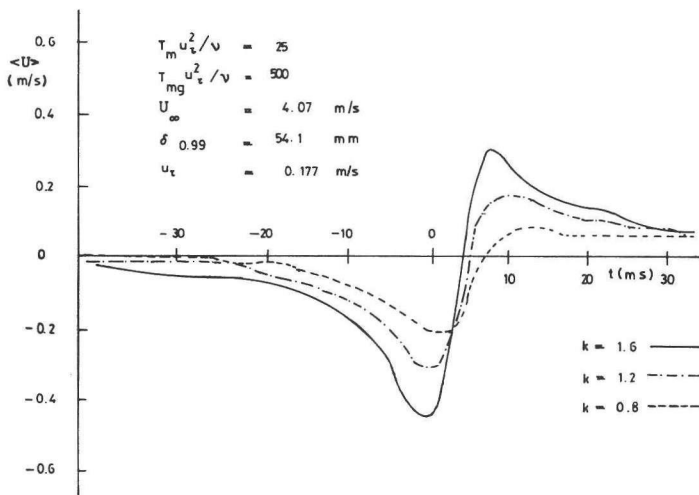


Figure 78: Conditionally averaged streamwise velocity component according to the modified scheme.

The modified scheme yields conditional averages of the streamwise velocity component with the same shape as Blackwelder and Kaplan's scheme did. The maximum and minimum of the average are again very dependent on the value of k . The conditional average of the pseudo-turbulence again deviates scarcely from zero (fig. 79).

Finally the distribution of time intervals between successive detections was calculated for different values of k . Successive detections with time intervals smaller than T_m are again treated as one detection.

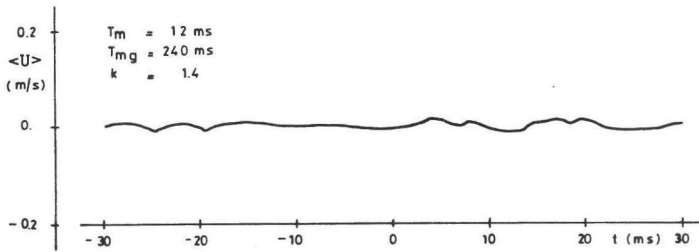


Figure 79: Conditional average of pseudo-turbulence signal according to the modified detection scheme.

For signal B the results are shown in fig. 80 for the following parameter values: $k = 1.0, 1.4$ and 1.8 , $T_m = 12\text{ ms}$, $T_{mg} = 240\text{ ms}$.

Again there is a considerable influence of k . The conclusions for these distributions are the same as for those found with the original scheme of Blackwelder and Kaplan. However, with the modified detection method a second peak appears in the distribution if the threshold parameter is large enough. But, in that case the distribution of the pseudo-turbulence shows such a peak (fig. 81) also. The position of the second peak appears not to be constant; it depends on the value of T_{mg} (compare fig. 80 and 82). So very likely the second peak is due to the modified scheme and not to turbulence structures.

In conclusion it can be stated that the modified scheme of Blackwelder and Kaplan is not an improvement over the original detection scheme of Blackwelder and Kaplan.

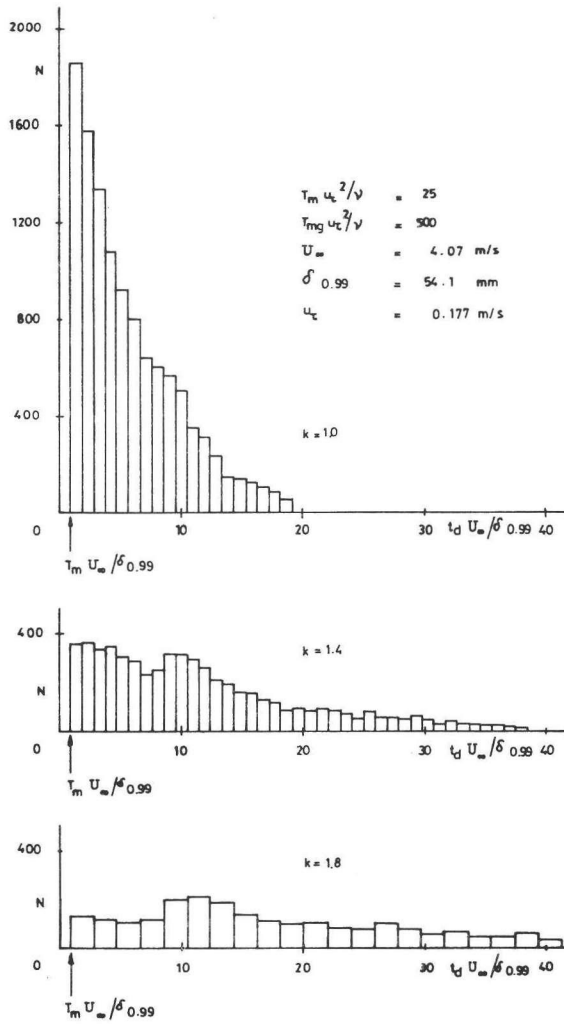


Figure 80: Distribution of time intervals between successive detections according to the modified scheme.

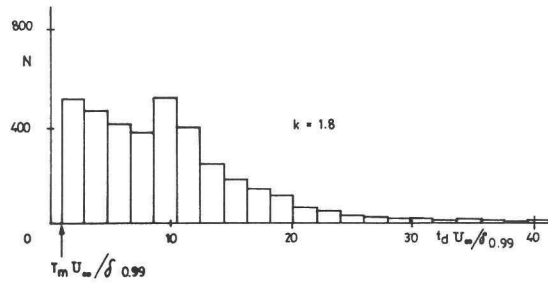
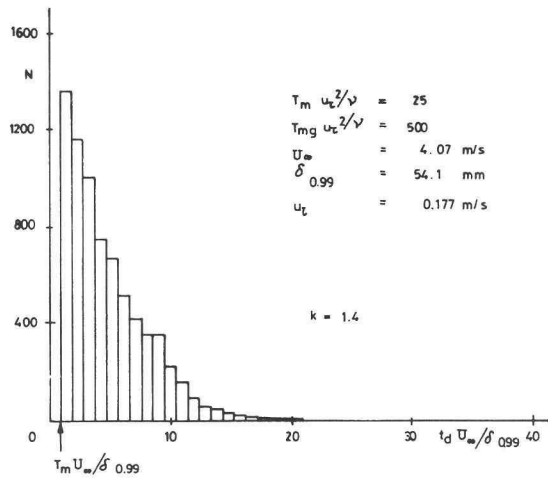


Figure 81: Distribution of time intervals between successive detections in pseudo-turbulence according the modified scheme.

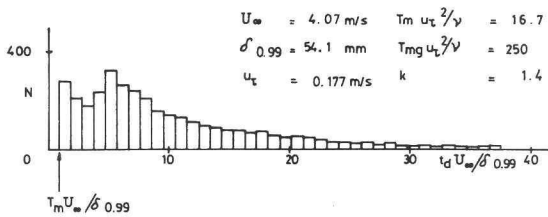


Figure 82: Distribution of time intervals between successive detections according to the modified scheme.

3.4 AUTOCORRELATION METHOD

Following Kim et al. [1971] Suzuki and Kawaguchi [1980] measured the burst period with the autocorrelation method.

In the autocorrelation method it is assumed that the second maximum in a short-time averaged autocorrelation of an u-signal indicates the burst period.

The bursting period measured by Suzuki and Kawaguchi scattered over a wide range and the distribution of the period obeyed a log-normal law.

With a correlation and probability analyzer the autocorrelation method was tested.

The u-signal, recorded at $y^+ = 15$ from a turbulent boundary layer for testing Ueda and Hinze's scheme (see section 3.1), was used. The autocorrelations were calculated over 1 s with a maximum delay time of 0.2 s.

At random 60 autocorrelation functions were computed.

In 30 of the autocorrelations a second maximum was perceptible, yielding a dimensionless mean burst period ($U_\infty T_B / \delta_{0.99}$) of 4.5. But in the other 30 autocorrelation functions no second peak was visible.

If the second maximum in an autocorrelation really indicates a burst period, the autocorrelation method appears not to be an adequate method of determining the mean burst period, because half of the time there is not enough periodicity to produce a second peak in the autocorrelation.

A similar conclusion is drawn in a later paper of Kawaguchi et al. [1983].

Chapter IV

HYDROGEN BUBBLE VISUALIZATION COMBINED WITH LASER-DOPPLER ANEMOMETRY

As the detection methods tested in chapter III appeared not to be objective, it was attempted to design a better detection method based on combined flow visualization and point measurements (see Talmon [1984]).

In a water channel a turbulent boundary layer visualized with hydrogen bubbles was filmed for that purpose, respectively in plan and side view. Simultaneously the fluctuating streamwise and normal velocity components measured at one position in the flow with laser-Doppler anemometry were recorded on magnetic disk.

In section 2.3 the set-up employed in this investigation is described. The turbulent boundary layer experiments performed in this channel are reported in this section.

In the first section of this chapter the structures observed in the films are described briefly. The structures perceived in the wall region of the turbulent boundary layer are compared in the second section with the simultaneously measured signals. A detection method based on the quadrant analysis technique is tested in the next section. In the last section the detection method of Blackwelder and Kaplan is studied once more to see on which flow phenomena the method reacts.

4.1 OBSERVED FLOW STRUCTURES

Studying the films made in plan and side view a similar flow picture arises as observed in the visualization studies of Kline and his colleagues at Stanford University (Runstadler et al. [1963], Kline et al. [1967], Kim et al. [1971], Offen & Kline [1973]). Flow phenomena observed by others appear to be also visible on the frames (Corino & Brodkey [1969]: ejection; Falco [1977]: bulge and typical eddy; Head & Bandyopadhyay [1981]: horseshoe vortex).

4.1.1 Plan view

The most remarkable structures observed in the plan view at $y^+ = 29$ (film 9 and 10, table 4) are the low-speed streaks, visible on the frames as accumulation areas of hydrogen bubbles - areas long in streamwise direction and small in lateral direction (fig. 83).

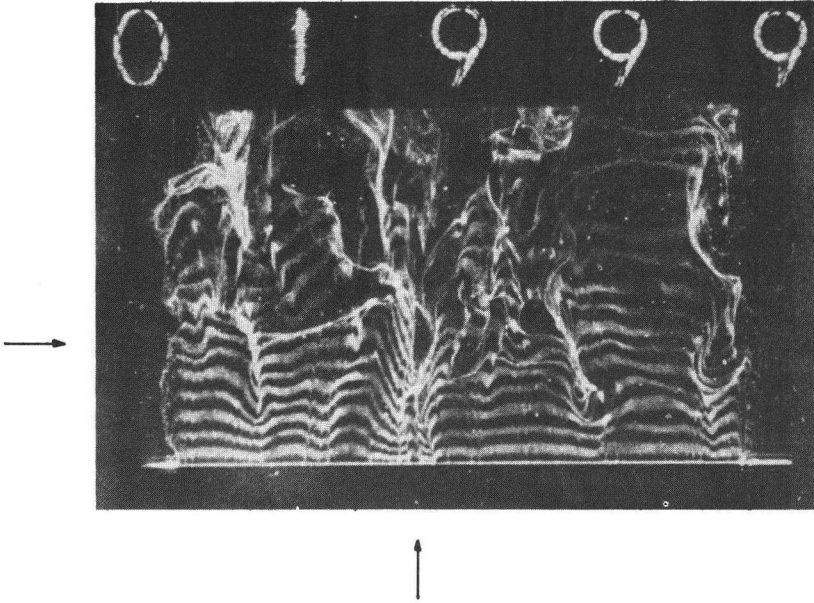


Figure 83: Low-speed and high-speed streaks in plan view.
(Flow direction is from bottom to top.
Intersection of arrows indicates dark spot.)

These low-speed streaks possess a tremendous persistence. Streaks are repeatedly longer than $490 x^+$, the maximum distance visible on the frames in streamwise direction. The width of the streaks ranges from 20 to $40 z^+$. The intermittency process of the low-speed streaks - their apparent disappearance and reappearance (Smith & Schwartz [1983]) - is observed also. The disappearance of a low-speed streak is frequently accompanied by a so-called dark spot. Just before disappearance there appears a dark spot at centerline of a streak; a dark spot is a small area within a streak from which the hydrogen bubbles have disappeared (fig. 83).

It is believed that these dark spots are closely related to the ejection described by Corino and Brodkey [1969].

In other hydrogen bubble visualization studies dark spots are not visible. This is probably due to a wrong combination of hydrogen bubble concentration and film technique.

The low-speed streaks are alternated by high-speed streaks (fig. 83). In high-speed streaks the hydrogen bubble concentration is low. The width of these streaks is two to four times the width of low-speed streaks and the high-speed streaks can also be longer than $490 x^+$.

The strongly vortical nature of a turbulent boundary layer is not revealed by the films made in plan view, only oscillation in lateral direction is visible.

On the films made with the platinum wire placed at $y^+ = 57$ (film 11 and 12, table 4) the phenomena described above are also visible, but -as expected- not so clear.

4.1.2 Side view

Looking at the films made in the side view (film 1 to 8, table 4) the attention is drawn by the intermittency in the outer layer. Large-scale motions, bulges (Falco [1977], most probably type T1), are followed by large, nearly undisturbed regions. These regions can reach the wall layer. The upstream interface between bulge and nearly undisturbed region is often quite sharp, making an angle of 15 to 30° in streamwise direction with the wall. At this interface -the back of the bulge- transverse eddies are visible. Their diameter is of the order of magnitude of $100 y^+$. These eddies are called typical eddies by Falco [1977], see fig. 84.

The presence of the laser beams makes it more difficult to study the motions in the wall layer.

As mentioned nearly undisturbed regions can reach the wall layer. Then small oscillations or even a solitary typical eddy can be found in the wall layer. Close to the wall small longitudinal eddies are seen sometimes making an angle of 0 to 10° in streamwise direction with the wall. These eddies can be accompanied by a movement of hydrogen bubbles away from the wall, but

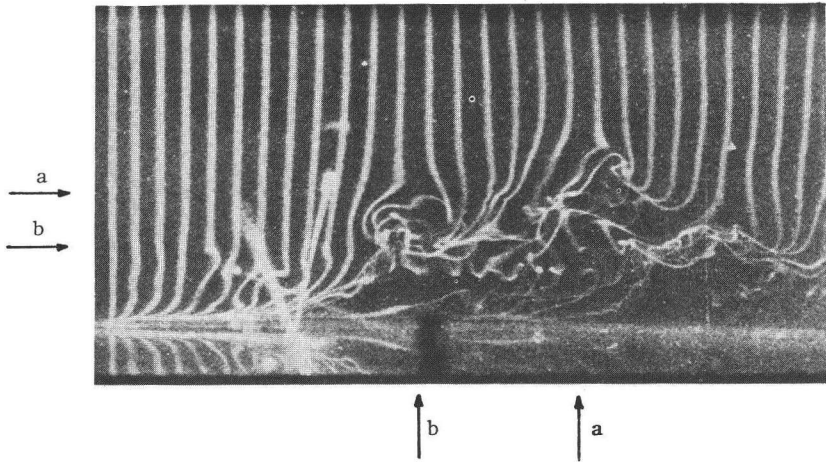


Figure 84: Side view of turbulent channel flow. (Flow direction is from left to right. Intersections of arrows indicate typical eddies.)

this movement can also be perceived without the presence of such eddies. The movement of eddies away from the wall takes place beneath the back of the bulge. Kim et al. [1971] associated this bubble movement or the appearance of longitudinal eddies in the wall layer with the ejection of a low-speed streak.

Not only in the wall layer but throughout the whole boundary layer longitudinal eddies can be observed. These eddies make an angle of 0 to 45° with the wall in downstream direction. The diameter of these eddies ranges from 10 to $50 y^+$. Sometimes such an arrangement of eddies is present on the frames, that these eddies can be part of a horseshoe eddy (fig. 85).

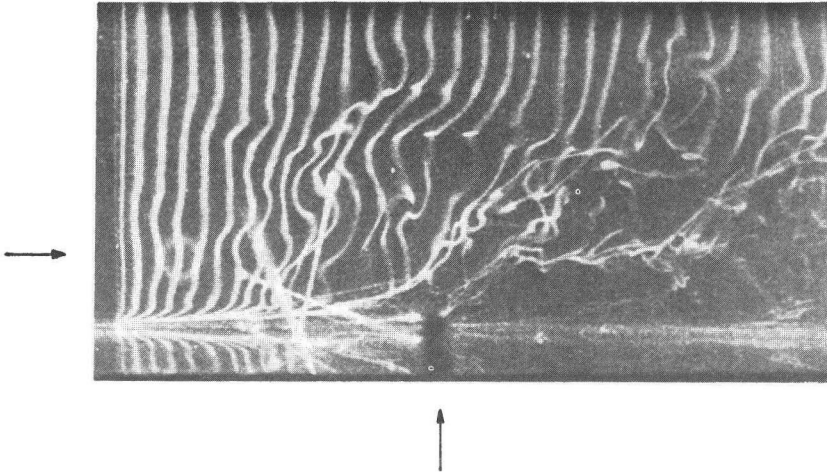


Figure 85: Side view of turbulent channel flow. (Intersection of arrows indicates horseshoe vortex.)

4.2 CHARACTERISTIC SIGNALS OF FLOW STRUCTURES IN THE WALL LAYER

Using a film viewer and a graphic terminal it is possible to study the filmed structures in the neighbourhood of the measuring point together with the simultaneously measured signals. In spite of interpretation problems there seem to be signals characteristic for low- and high-speed streaks.

The fact that in the plan view visualization and measurement were not performed at the same wall distance, is detrimental to the correlation of observed structures and measured signals. In case of a structure present at the measuring point as well as in the visualized area above that point there is no interpretation problem. But, if a structure is so small, i.e. due to intermittency of a low-speed streak, or if a structure is found in such an oblique position in the flow that it is present either in the visualized area or the measuring point, there will be no correlation between image and signals.

In the side view visualized area and measuring point have not to take up the same lateral position necessarily, because the hydrogen bubbles are also moving in lateral direction. This causes interpretation problems too.

In the following interpretation problems will be attributed to this spatial separation between visualized area and measuring point.

4.2.1 Low-speed streaks

When in plan view a low-speed streak is perceived above the measuring position, the measured velocity component in streamwise direction correlates well -the instantaneous streamwise velocity component is lower than its time averaged value- and the normal velocity is positive. So a low-speed streak is moving away from the wall and slower than the average flow in streamwise direction.

This implies a positive contribution to the Reynolds stress. This contribution is not constant, but very intermittent due to oscillation and disappearance and reappearance of the streaks. If the measuring point is found for some time in a low-speed streak, the streak contributes continuously to the Reynolds stress. In dark spots larger contributions to the Reynolds stress are measured, but such contributions can also be measured when no striking flow phenomena are observed. Spatial separation can explain the phenomenon.

The characteristic signals of a low-speed streak (negative u-component and positive v-component) are also observed in the signals measured during filming in side view. But the correlation between image and signals is quite poor. Low-speed streaks are not often marked by the hydrogen bubbles, because the streaks are not wide. As these streaks move also in lateral direction, the chance measurement takes places within a marked low-speed streak, is not high.

Sometimes it is observed that a low-speed streak is moving away from the wall. If measurement is performed in such a streak, the streak makes a substantial contribution to the Reynolds stress.

It is believed that significant contributions to the Reynolds stress which take place in the second quadrant of the u-v plane (see fig. 11, section 1.2.3) are associated with bursts and ejections in low-speed streaks. Bogard [1982] draws a similar conclusion, based on an investigation of dye motions and simultaneously measured uv-signals.

Originally a burst is defined as the gradual outflow, liftup, oscillation and breakup of dye injected in a water flow, which occurs in a low-speed

streak (Kline et al. [1967]). A burst is followed by a return to a more quiescent flow (Kim et al. [1971]). This is most probably the sweep, which on the average is preceded by the ejection (the eruption of low-speed fluid) as observed by Corino and Brodkey [1969]. According to Offen and Kline [1973] a burst can consist of a few ejections in the breakup phase. Dye ejections and high contributions to the Reynolds stress appear to coincide (Offen & Kline [1973]).

4.2.2 High-speed streaks

Observation and measurement of high-speed streaks correlate well in both plan and side view. Perceiving a high-speed streak the measured streamwise velocity is greater than the mean velocity and frequently the normal velocity is slightly negative. This negative v -component is measured especially in high-speed streaks appearing immediately after bulges. So a high-speed streak is moving faster in streamwise direction than the mean flow and the streak is often moving slowly towards the wall.

Not only in low-speed streaks but also in high-speed streaks high contributions to the Reynolds stress are measured. But contrary to the low-speed streaks, in high-speed streaks no phenomena are observed which can account for these contributions. This can be caused by the stationary position of the camera. Probably films made with a moving camera would reveal more details in high-speed streaks.

Contributions to the Reynolds stress by high-speed streaks take place in the fourth quadrant of the u - v plane. Contributions in this quadrant are usually attributed to the sweep (Lu & Willmarth [1973], Brodkey et al. [1974]), but from this investigation it is not clear which part of the sweep is responsible.

4.2.3 Eddies

Longitudinal and transverse (typical?) eddies are observed in the wall layer. Both types are attended by high contributions to the Reynolds stress. Regarding the typical eddies this is in agreement with Falco's measurements (Falco [1977]).

But no characteristic signals are observed during the passage of longitudinal or typical eddies. The contributions to the Reynolds stress do not take

place in a particular quadrant, most probably because the measurements are not performed at the same point in these eddies. Due to different spatial separation between eddies and measuring point the measurements will be carried out each time in different parts of the eddies.

4.2.4 Some illustrations

In fig. 86 and 87 examples are given on which the above has been based. Some pictures of film 9, made in the plan view (table 4), and the corresponding u -, v - and uv -parts are shown in fig. 86. The frames are not reproduced entirely, but only the area around the measuring point (dimensions: $380 x^+ * 190 z^+$). The flow direction on the pictures is from bottom to top. At the bottom of the pictures the platinum wire is visible generating hydrogen bubbles. The measuring position is marked on each picture with a plus sign. The non-dimensional signals are plotted against a time-axis from which the origin has been translated. The origin of the axis corresponds with framenummer 1420 of film 9. Beneath each picture the corresponding time is given. On the pictures indicated with $t = -0.9$ to -0.2 s a low-speed streak is moving towards the measuring point replacing a high-speed streak. During this time interval a decrease is observed in the u -signal and an increase in the v -signal. At $t = -0.1$ s the appearance of a dark spot is perceived. In the corresponding uv -signal a peak is observed (second quadrant; $uv/\overline{uv} = 7$). Immediately afterwards the low-speed streak is pushed away by a high-speed streak. At $t = 0.5$ s again a low-speed streak is perceived. On the following pictures the flow is quite disorderly, while the signals indicate that measurement is still performed in a low-speed streak which makes a high contribution to the Reynolds stress. This is probably caused by intermittency of the streak.

In fig. 87 some pictures of film 4, made in side view (table 4), and the corresponding parts of the measured signals are shown. Again the frames are not reproduced entirely; the dimensions of a picture are $580 x^+ * 250 y^+$. The flow direction is from left to right. On the left of the pictures the platinum wire is visible. The intersecting laser beams mark the measuring position. The origin of the time-axis of the plotted signals corresponds now with framenummer 12205 of film 4. Left of each picture the corresponding time is given.

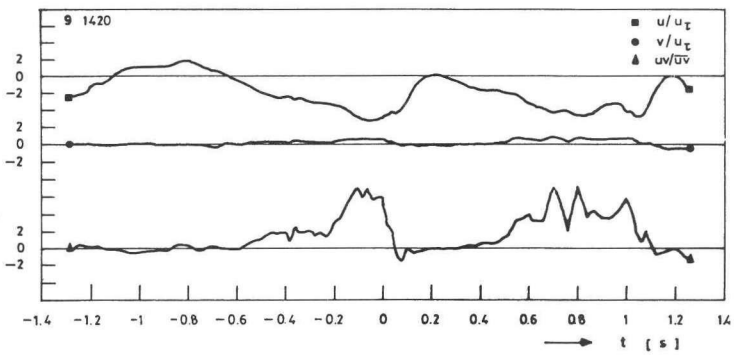
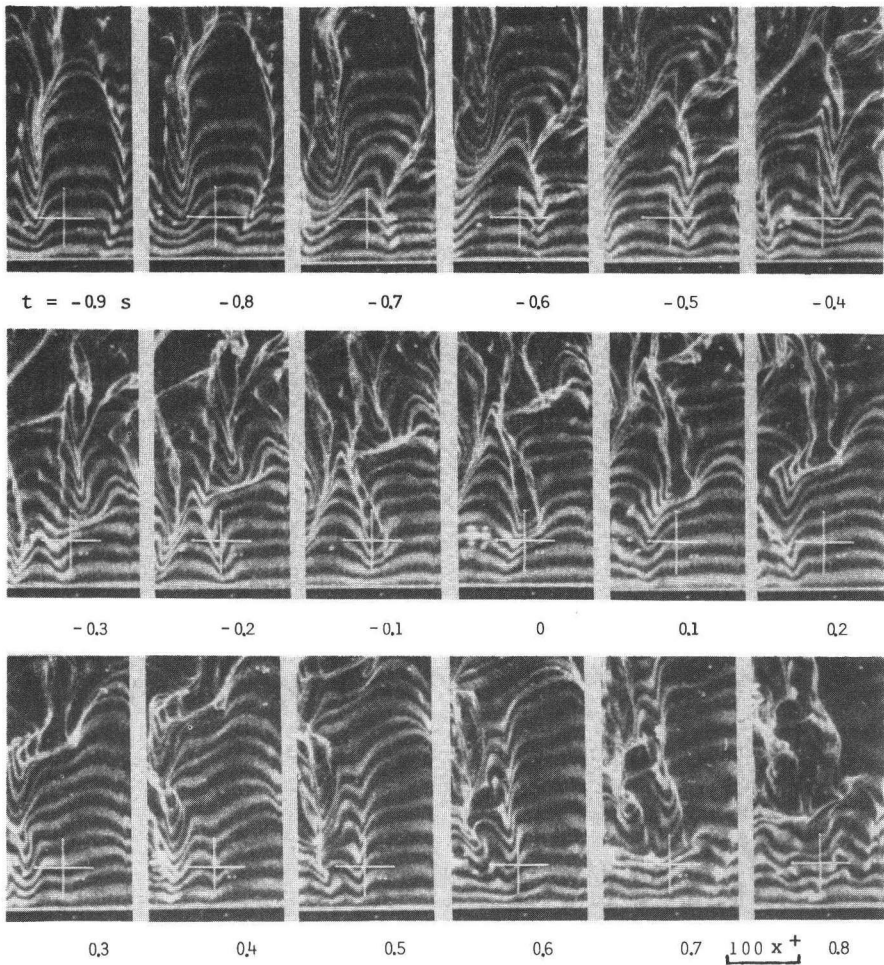


Figure 86: Measurement and visualization in plan view.

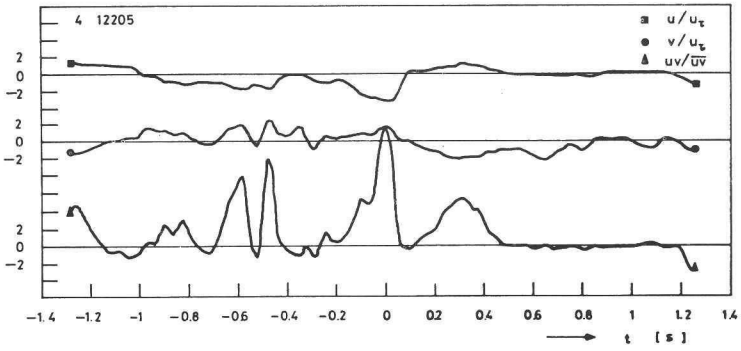
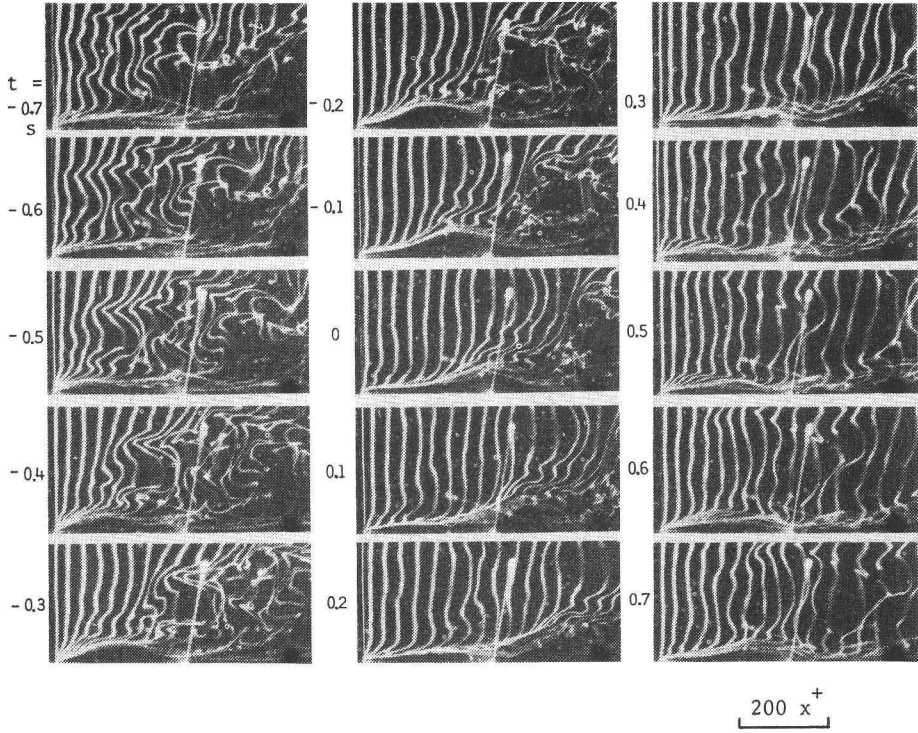


Figure 87: Measurement and visualization in side view.

On the pictures marked with $t = -0.7$ to 0 s the formation of a typical eddy is visible above and downstream of the measuring point. At $y^+ = 43$ a low-speed streak is measured contributing to the Reynolds stress in the second quadrant. The contributions at about $t = -0.6$ and -0.5 s can not be connected to some visible flow structure. At $t = 0$ s the movement away from the wall causes the contribution. Upstream of the measuring point there appears a high-speed streak which sweeps away the low-speed streak. Due to the high-speed streak a contribution to the Reynolds stress is measured at $t = 0.3$ s in the fourth quadrant. On the following pictures not much turbulence activity is observed and simultaneously almost the mean velocity components are measured.

4.3 SECOND QUADRANT DETECTION METHOD

4.3.1 Description and results

In section 4.2.1 a connection is found between observed low-speed streaks and measured high contributions to the Reynolds stress taking place in the second quadrant of the u - v plane. Especially in plan view the perception of low-speed streaks is attended by contributions to the Reynolds stress in quadrant 2. In side view this connection is not so obvious due to spatial separation.

Applying the quadrant analysis technique to signals measured in a turbulent wall layer the second and fourth quadrant of the u - v plane provide in short time the major part of the Reynolds stress (see section 3.2.3; Lu & Willmarth [1973] and Brodkey et al. [1974]).

As can be seen in fig. 88 this applies also to signals measured during and after filming in the turbulent channel flow.

In fig. 88 $\overline{uv}_i/\overline{uv}$ and t_i/t ($i = 2, 4$ or 5) calculated for the 78 s and 30 min. signal of film 9 (measured at $y^+ = 14$, table 4) are plotted as function of hole-size K ($|uv| = K|\overline{uv}|$). In case of the 78 s signal the Reynolds stress averaged over 30 min. is used in the calculation of the hole-magnitude. The differences between the 78 s and 30 min. signal will be due to the short measuring time of the 78 s signal.

Studying the individual contributions in the second quadrant of film 9 it appears that almost every contribution of magnitude $K|\overline{uv}|$ with $K \geq 2$ is caused by a low-speed streak. (\overline{uv} is again averaged over 30 min.) Due to

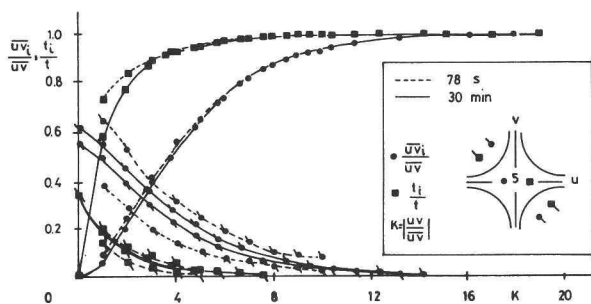


Figure 88: Fractional contribution to Reynolds stress and time fraction as function of hole-size K of signals measured during and after filming (quadrant analysis technique).

spatial separation -measuring at $y^+ = 14$ and filming at $y^+ = 29$ - a single contribution can be found without a visible low-speed streak. With $K = 2$ also not every visible streak is detected; a few streaks are not strong enough to cause a detection.

Intermittency and oscillation of low-speed streaks is observed. Hence more than one contribution can be found originating from the same low-speed streak. On the average two contributions with an absolute magnitude greater than or equal to $2|\overline{uv}|$ are measured for low-speed streaks in film 9.

Assuming that these contributions -frequently coinciding with dark spots- are closely related to ejections and bursts, see section 4.2.1, coherent structures can be detected in the second quadrant of the u - v plane with $|uv| \geq 2|\overline{uv}|$.

The distribution of time intervals t_d between successive detections of this method is calculated. Time interval t_d between two successive detections is defined as the time passed between the middle of the first and the middle of the second detection. For film 2 and 9 (total duration signals: 171 s, table 4) this distribution is shown in fig. 89). The mean time T_d between successive detections is 0.82 s for these films.

For film 9 is observed that on the average two contributions are made to the Reynolds stress in quadrant 2 by each low-speed streak. Offen and Kline [1973] perceived two ejections per burst. They assumed that dye activities (ejections) with time intervals smaller than a threshold level τ_d belong to the same burst.

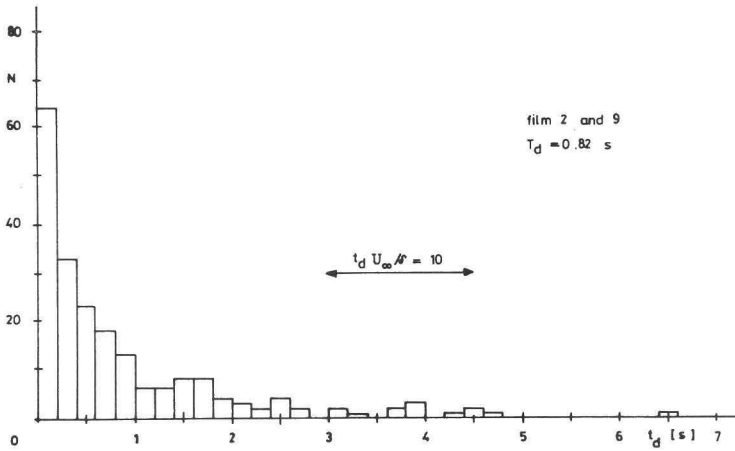


Figure 89: Distribution of time intervals between successive detections according to the second quadrant method.

Here a similar assumption is made. Based on hydrogen bubble observations it is assumed that detections at $y^+ = 14$ with time intervals smaller than 0.42 s are detections on the same structure. Most probably this structure is a burst, but for the time being this structure is called a coherent uv-group.

The visual classification of detections arising from the same low-speed streak agrees very well with the numerical classification of detections belonging to one coherent uv-group.

In fig. 90 the distribution of time intervals t_g between successive coherent uv-groups is shown. Time interval t_g is defined in the same way as time interval t_d . To calculate the distribution the signals measured during making film 1, 2 and 9 (total duration signal: 268 s; table 4) are used. The mean time T_g between successive coherent uv-groups is 2.1 s.

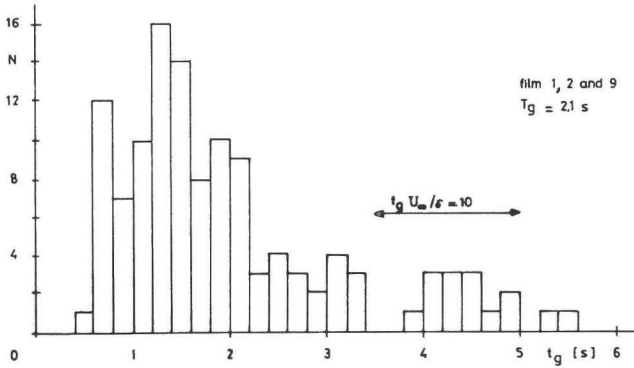


Figure 90: Distribution of time intervals between successive coherent uv-groups.

4.3.2 Comparison with other visualization studies

This study was carried out independently of the study of Bogard [1982]. Based on dye observations and hot-film measurements Bogard designed a similar detection method. With this method detection of ejections was assumed to occur when the instantaneous uv-signal is found in the second quadrant and when the following relation holds: $|uv| \geq Hu'v'$.

In a water flow ($U_\infty = 14.6$ cm/s, $\theta = 0.27$ cm, $u_r = 0.79$ cm/s) Bogard measured a value of 1.1 s for the mean time between successive detections ($y^+ = 15$; signal duration: 200 s; $H = 1.07$) Bogard assumed that two successive ejections, detected with $H = 1.07$, belong to one burst if the time interval is smaller than 0.8 s. He found a mean time between successive bursts of 2.2 s. These bursts were responsible for 80% of the contribution of the complete second quadrant to the Reynolds stress.

Bogard used for hole-size H the value 1.07, the ratio of the Reynolds stress of the second quadrant, averaged over the time the uv-signal spent in the second quadrant, and the Reynolds stress of the complete signal, because Comte-Bellot et al. [1979] measured that that ratio was nearly constant in the core region of a fully developed turbulent pipe flow.

The hole-size Bogard used is in the second quadrant detection method for film 9 comparable with $K = 3$. In table 7 quantities calculated for coherent uv-groups detected with K-values ranging from 2 to 5, are given for film 9.

$[-\rho\overline{uv}_g]$ is the Reynolds stress due to the coherent uv-groups.

Δt_g represents the total time coherent uv-groups are detected.]

If K equals 3, 47% of the Reynolds stress is contributed by coherent uv-groups. This corresponds with 75% of the Reynolds stress due to the second quadrant.

Table 7.

Some results of second quadrant analysis technique, $K = 2$ to 5.

K	N	T_g [s]	$\overline{uv}_g/\overline{uv}$ [%]	$\Delta t_g/t$ [%]
2	33	2.4	55	19
3	26	3.0	47	13
4	20	3.9	35	7
5	14	5.6	29	5

In spite of the the good agreement one should keep in mind that both studies are based on short signals, so the uncertainty in the results is quite large.

In fig. 91 the mean time T_g between successive coherent uv-groups ($K = 2$, $\tau_d = 0.42$ s) and the mean time T_B between successive bursts detected visually are compared in dimensional form, $T_B (T_g)$ versus u_τ , resulting in a very good agreement.

The distribution of time intervals between successive detections ($|uv| \geq 2|\overline{uv}|$) does not resemble the distribution found by Kim et al. [1971] (compare fig. 89 and 65), because the detections are probably ejections and the structures observed by Kim et al. bursts. Introducing the coherent uv-groups the distribution of time intervals (fig. 90) gets the same form as the distribution of Kim et al.

As the results of the second quadrant detection method agree very well with other visual results, the detected coherent uv-groups will be the visual bursts as defined by the Stanford group.

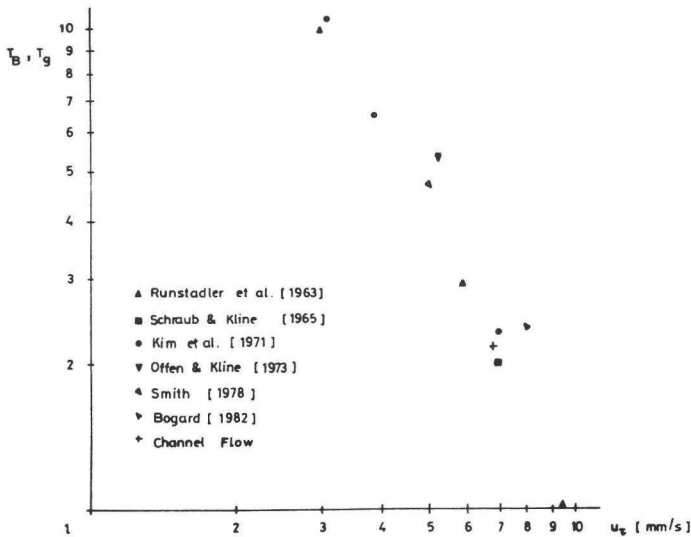


Figure 91: Mean period of bursts and coherent uv-groups.

4.4 DETECTIONS OF BLACKWELDER AND KAPLAN'S METHOD

Using the films made in plan view of the turbulent channel flow (table 4) and the simultaneously measured signals it is possible to see on which flow phenomena the detection of Blackwelder and Kaplan [1972, 1976] reacts. A description of this method is already given in section 3.2.

The method is applied to the u-signals measured at $y^+ = 14$ during making film 9 and 10. These signals have a total duration of 172 s. With an averaging time T_m of 0.6 s ($T_m u_\tau^2 / \nu = 26$) and a threshold parameter k of 0.9 37 detections are found in the u-signal.

These detections can be divided into detections of three flow situations:

- (1) detection of an oscillating low-speed streak (60% of detections),
- (2) detection of a disappearing low-speed streak, sometimes a dark spot is visible, followed by a high speed streak (30%),
- (3) detection of a high-speed streak followed by a disorderly low-speed streak (10%).

Blackwelder and Kaplan expect their method to react on bursts, but detection type 2 is the flow situation which closely approximates a burst. In spite of spatial separation effects and the short duration of the investigated signals it is not likely that bursts constitute the majority of detections of Blackwelder and Kaplan's method.

Results of Blackwelder and Kaplan's detection method have to be interpreted therefore based on oscillating low-speed streaks.

Using Blackwelder and Kaplan's method Blackwelder and Eckelmann [1979] measured on both sides of the detection point streamwise and spanwise vorticity. Based on these measurements Blackwelder and Eckelmann developed a model of the wall layer of a turbulent boundary layer consisting of pairs of counter-rotating streamwise vortices with low-speed streaks between them. The conditional averaged velocity profiles of Blackwelder and Kaplan [1976] (fig. 6) were associated with the low-speed streak. According to Blackwelder and Eckelmann the successive profiles were measured when a low-speed streak was passing the measuring point.

But regarding the above only the profiles measured directly before and after detection will be measured within a low-speed streak. The other profiles will be either measured when a low-speed streak is moving towards the measuring point (before detection) or when a low-speed streak is replaced by a high-speed region (after detection).

When streak oscillation is incorporated in Blackwelder and Eckelmann's model, then the sign change of streamwise vorticity measured on both sides of the measuring point just after detection becomes explainable. Just after detection vorticity measurement takes place in counter-rotating streamwise vortices of opposite sign with a high-speed streak between them.

Chapter V
APPLICATION OF QUADRANT ANALYSIS TECHNIQUE TO JET FLOW

Not only in the development region but also in the fully developed region of an axisymmetric jet coherent structures have been observed (see section 1.3.2).

In this investigation point measurements have been used trying to gather more information about these structures. Because the quadrant analysis technique appeared to be a very useful tool in studying coherent structures in wall-bounded turbulence (see section 4.3), this technique has also been applied to uv-signals from the development region of a round jet (see Vink [1984]).

Contrary to the pipe and channel flow experiments the quadrant analysis technique was applied as defined by Lu and Willmarth [1973]. So, when a hole was used, it was bounded by curves $|uv| = Hu'v'$.

Signals from the jet facility described in section 2.4, were used. The quadrant analysis technique was applied to most of the fluctuating hot-wire signals recorded on magnetic disk for calculating turbulence quantities of the jet flow. Therefore the u- and v-signals used in this computation were low-pass filtered and digitized with 5 kHz. The signals had a duration of 320 s. The recordings were performed in the development region of the jet at a Reynolds number of $1.17 \cdot 10^5$.

Starting with the computed joint probability distributions of the recorded signals the contributions of each quadrant -with hole-sizes equal or greater than zero- to the Reynolds stress were calculated.

In the following section the results of the quadrant analysis technique applied without hole to the uv-signals are presented.

In the last section of this chapter the results of the quadrant analysis applied with hole to the turbulence uv-signals are reported. These results are compared with quadrant analysis results of pseudo uv-signals having a normal probability distribution.

5.1 QUADRANT ANALYSIS WITHOUT HOLE

In fig. 92 the results are shown of the quadrant analysis technique applied without hole to uv-signals measured in the development region of the jet.

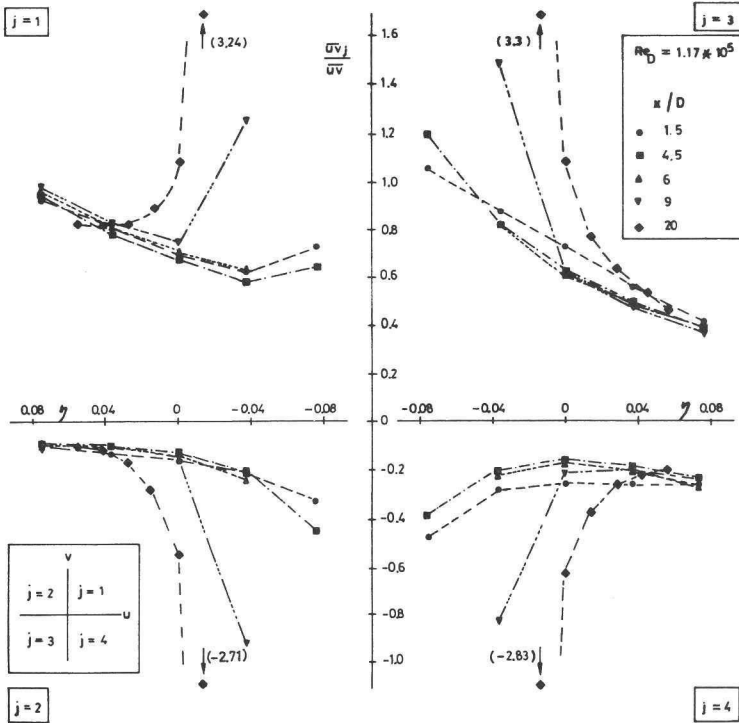


Figure 92: Fractional contribution of the four quadrants to the Reynolds stress in jet cross sections.

The measurements were performed at a few radial positions at $x/D = 1.5, 3, 4.5, 6, 9$ and 20 . Per quadrant the fractional contribution to the Reynolds stress is given.

[η is a dimensionless radial distance ($\eta = (y-R)/x$).

$-\rho \overline{u v}_j$ is the Reynolds stress due to quadrant j ($j = 1, 2, 3$ or 4 ;

$$\overline{u v}_j = t^{-1} \int_0^t u v_j(s) ds.]$$

In the mixing layer region ($x/D < 6$) the distribution per quadrant appears to be nearly independent of axial distance. In the inner part of the jet ($\eta < 0$) the contribution of quadrant 3 is most important, whereas in the outer part of the jet ($\eta > 0$) quadrant 1 contributes most to the Reynolds stress. Throughout the jet quadrant 2 and 4 do not make very substantial contributions to the Reynolds stress.

For $x/D > 6$ this picture changes only notably with respect to the inner part of the jet. There, all quadrants begin to contribute substantially to the Reynolds stress, most probably resulting in equally important contributions in the fully developed region. The contribution of each quadrant measured at the centerline of the jet support this statement, see fig. 93. In this figure the contributions of quadrant 2, 3 and 4 are made dimensionless with the contribution of quadrant 1.

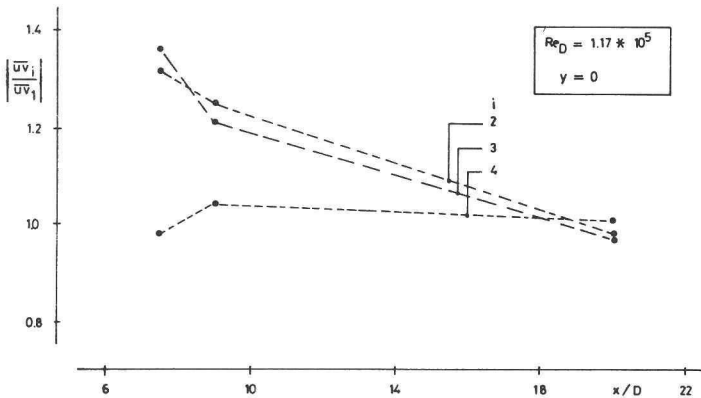


Figure 93: Importance of the contributions to the Reynolds stress of quadrant 2, 3 and 4, related to quadrant 1, at the jet axis.

In the mixing layer region the model of Lau et al. [1972] elucidates the contributions of each quadrant to the Reynolds stress. In this model the flow in the mixing layer region is described as an array of discrete vortex rings. The leading edge of a vortex transports high velocity fluid outwards, which explains the high contribution of quadrant 1 to the Reynolds stress in the outer part of the mixing layer region. The trailing edge transports low velocity fluid inwards, accounting for the high contribution of quadrant 3 in the inner part.

Dimotakis et al. [1983] observed that vortical structures exist also in the region of partial and complete self-preservation. The same mechanism as in the mixing layer region can explain therefore the high contribution of quadrant 1 to the Reynolds stress in the outer part of a jet for $x/D > 6$. In the inner part the vortical structures will transport low and high velocity fluid in- and outwards, because now vortical structures with different origin and orientation reach the inner part (Dimotakis et al.). Because the quadrant analysis technique does not distinguish between origin or orientation of structures, the four quadrants will contribute almost equally to the Reynolds stress for $x/D > 6$.

The quadrant analysis applied without hole appears to be only suitable for studying coherent structures in the mixing layer region and in the outer part of the remainder of the jet.

5.2 QUADRANT ANALYSIS WITH HOLE

The quadrant analysis was applied with hole to some of the recorded uv -signals to investigate whether this technique is able to detect structures in the inner part of a jet.

For two points in the mixing layer region -one in the outer part and one in the inner part at $x/D = 3$ - the fractional contribution of the four quadrants excluding the hole, to the Reynolds stress is plotted versus hole-size H (fig. 94 and 95 respectively). Also the fractional contribution of the hole and the time fraction the uv -signal spent in the hole (t_h/t), are shown. As in wall-bounded turbulence most of the Reynolds stress is produced in short time ($H < 2$) outside the hole. Quadrant 1 produces most in the outer part (fig. 94) and quadrant 3 in the inner part (fig. 95), as expected (see section 5.1).

At $x/D = 1.5$ this technique was also applied to two uv -signals -one recorded in the inner part and one at the centerline of the mixing layer ($\eta = 0$). For different hole-sizes the contribution of each quadrant excluding the hole (\overline{uv}_i) and normalized with the contribution of the particular quadrant

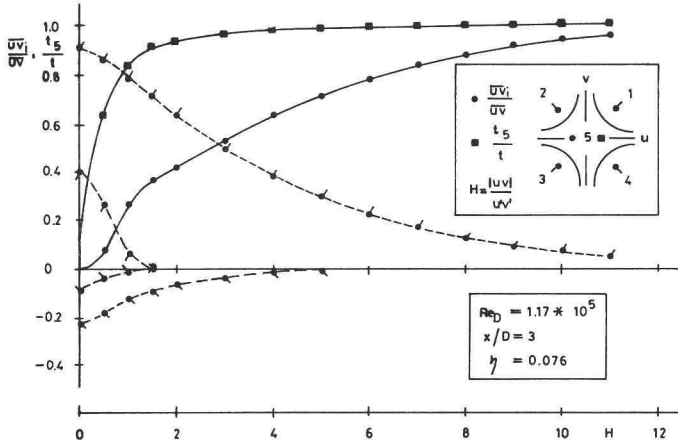


Figure 94: Fractional contributions to Reynolds stress and fraction of time spent in hole in outer part of mixing layer region.

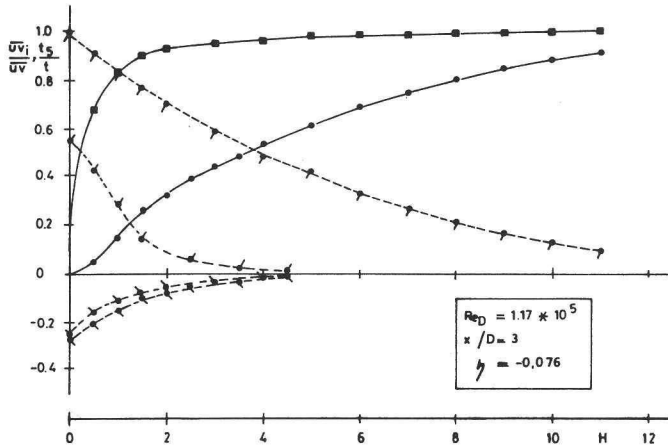


Figure 95: Fractional contributions to Reynolds stress and fraction of time spent in hole in inner part of mixing layer region.

without hole (\overline{uv}_j) is shown as function of the time fraction t_i/t_j (fig. 96 and 97 respectively).

[t_j is the total time the uv -signal spent in quadrant j without hole ($j = 1, 2, 3$ or 4)].

Also plotted is the fractional contribution $\overline{uv}_0/\overline{uv}$ to the Reynolds stress of the total area outside the hole as function of the time fraction t_0/t the uv -signal spent outside the hole.

[t_0 is the total time the uv-signal spent outside the hole.

$-\rho \overline{uv}_0$ is the Reynolds stress due to the total area outside the hole

$$(\overline{uv}_0 = \sum_{i=1}^4 \overline{uv}_i).$$

The quadrant analysis technique was also applied to a pseudo uv-signal having a normal probability distribution. For one quadrant the results are given in fig. 96 and 97 too.

The differences between the results of the turbulence uv-signals and the pseudo uv-signal will be caused by the structures present in the jet.

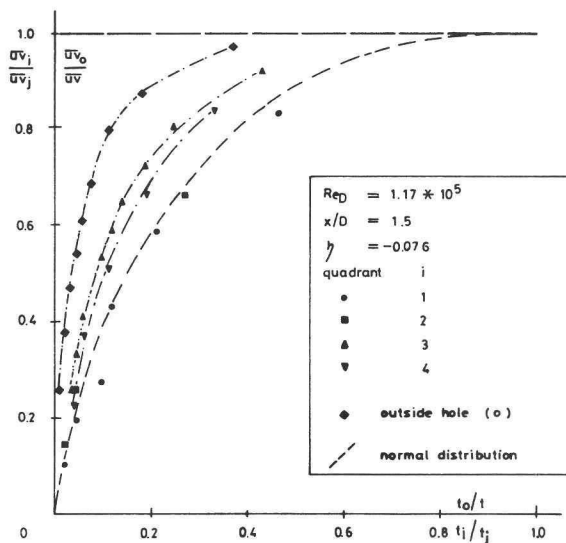


Figure 96: Relative contributions to Reynolds stress in inner part of mixing layer region. (Successive points indicate increasing hole-size.)

The same calculations were performed for two signals recorded in the region of partial self-preservation -one in the outer part and one at the centerline of the jet at $x/D = 20$. As can be seen there is still a substantial difference between the contributions of the uv-signal from the outer part and of the pseudo uv-signal (fig. 98). At the centerline there appears to be no difference anymore (fig. 99).

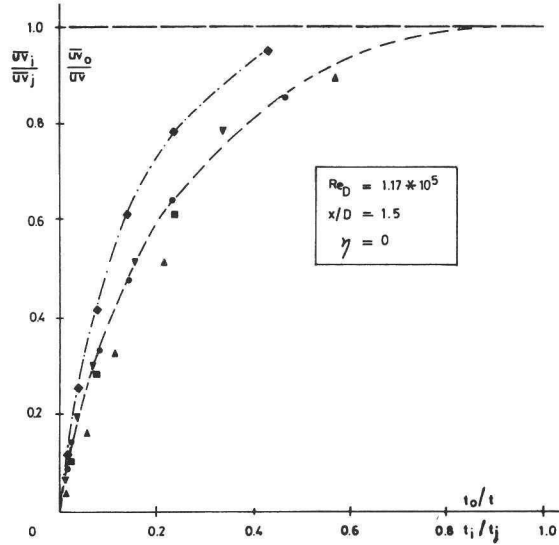


Figure 97: Relative contributions to Reynolds stress at centerline of mixing layer region. (Successive points indicate increasing hole-size.)

The differences between the quadrant analysis results of the turbulence uv -signals in the inner part of the mixing layer region and of the pseudo uv -signal indicate the existence of coherent structures in a turbulent jet. In the inner part of the region of partial self-preservation the quadrant analysis technique yields no information about coherent structures, probably because this technique does not distinguish between structures with different origin and orientation.

In the mixing layer region of a jet the quadrant analysis technique applied with or without hole appears to be an useful technique for studying coherent structures. In the development region this technique gives only information about structures in the outer part, but in the inner part this technique has to be combined with visualization in order to increase the knowledge of coherent structures.

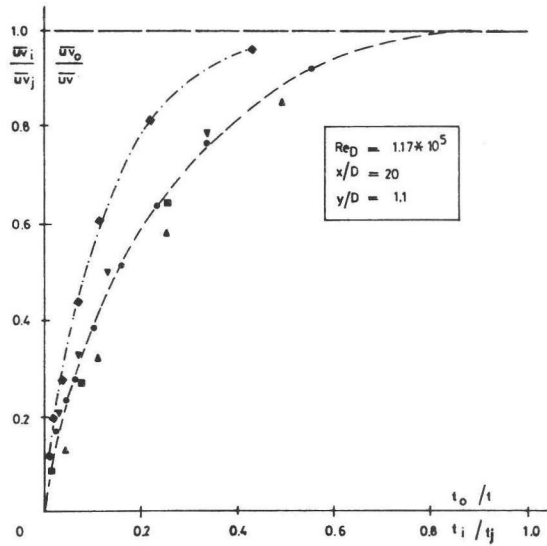


Figure 98: Relative contributions to Reynolds stress in outer part of region of partial self-preservation. (Successive points indicate increasing hole-size.)

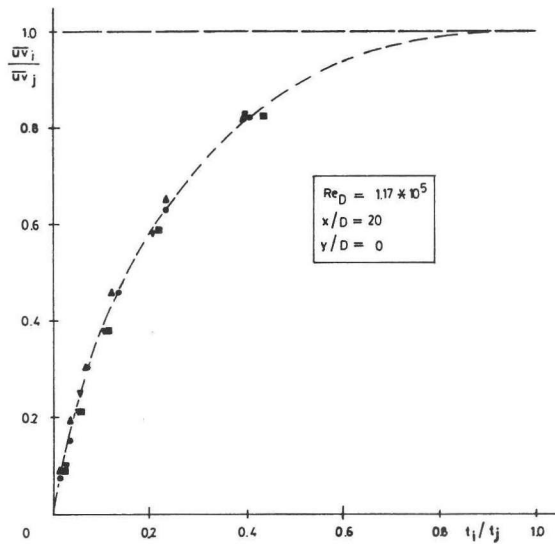


Figure 99: Relative contributions to Reynolds stress at centerline in region of partial self-preservation. (Successive points indicate increasing hole-size.)

Chapter VI

RECAPITULATION AND DISCUSSION

During the last few decades experimental research in turbulence has been focused on coherent structures. Coherent structures are responsible for a significant part of the transport of mass, heat and momentum. With increased knowledge about coherent structures it is believed that modelling of turbulent flows can be improved.

The existence of coherent structures has been revealed in visualization studies. As these studies only provide very qualitative descriptions of coherent structures, Eulerian detection methods have been developed to gather quantitative information about coherent structures.

In the preceding chapters of this thesis results of studying the detection of coherent structures in turbulent flows were presented.

After a review of research carried out in this field, chapter I, experiments were described in chapter II to examine detection in wall bounded and free turbulent flows. Measurements were performed in a turbulent boundary layer, a turbulent pipe flow, a turbulent channel flow and a jet flow.

In chapter III it was shown that the Eulerian detection methods investigated in the wall layer of wall bounded turbulent flows, viz. the method of Ueda and Hinze [1975], the method of Blackwelder and Kaplan [1972, 1976] and a modified version of Blackwelder and Kaplan's method are not objective; results of these detection methods -the mean time between successive detections, the distribution of time intervals between successive detections and the conditional averaged streamwise velocity of the detections- appear to depend on the parameter values used in the methods. Furthermore, the distribution of time intervals between successive detections and the contribution of detections to the Reynolds stress are not in agreement with results from visualization studies.

Therefore these detection methods are not most suitable for collecting quantitative data about coherent structures.

Although only three Eulerian detection methods are examined, it seems reasonable to expect that other Eulerian detection methods show deficiencies as well; especially those methods which approach the problem of detecting coherent structures in a similar way: some property, which is attributed to coherent structures, is used for detection without examining on a one-to-one basis whether Eulerian detection coincides with visual detection. Interpretation of results of Eulerian detection methods is difficult then, because it is not known which part of the results is caused by coherent structures and which part by detections on background turbulence. It may not be assumed that the influence of the 'wrong' detections is averaged out in the results, if it not is established to which extent coherent structures are detected. Results of the autocorrelation method (Kim et al. [1971], Suzuki and Kawaguchi [1980]) are questionable, because with this method only part of the measuring time data can be collected.

In order to improve the detection techniques Eulerian measurement and visualization were combined in a turbulent channel flow, see chapter IV. Hydrogen bubbles were used for visualization of the water flow. Not only the same flow phenomena as observed by Runstadler et al. [1963], Kline et al. [1967], Kim et al. [1971] and Offen and Kline [1973] were perceived on the films made of the water flow, but also other phenomena appear to be visible, viz. the ejection (Corino & Brodkey [1969]), the bulge and the typical eddy (Falco [1977]) and the horseshoe vortex (Head & Bandyopadhyay [1981]). The quadrant analysis technique was adopted for the detection of structures in the wall layer, using only the uv-parts of the second quadrant with an absolute magnitude greater than or equal to $2|\overline{uv}|$. In this way a high correlation was achieved between visual and Eulerian detection of ejections. Assuming that Eulerian detections with time intervals smaller than 0.42 s are detections on the same structure -this assumption is based on visual observations- the visual observed burst is detected. Results of this Eulerian detection method are not quite free from subjectivity, but so it is certain that coherent structures are detected. In contrast, the detections of Blackwelder and Kaplan's method appear not to coincide with bursts in general. Mostly low-speed streaks are detected which pass the measuring point.

With the second quadrant detection method it will be possible to measure the properties of coherent structures. The information about coherent structures can then be used for modelling turbulent flows. But first the same experiments should be carried out at higher Reynolds numbers, because the properties of coherent structures may change with Reynolds number; see for instance the publication of Head and Bandyopadhyay [1981].

In chapter V the quadrant analysis technique was applied to a jet flow. The technique appears to give only information about structures in those regions where much order is present, viz. the mixing layer region and the outer part of the development region. In the inner part of the development region the quadrant analysis technique is not very suitable for studying structures, because this technique does not distinguish structures with respect to origin and orientation. Simultaneously performed flow visualization could provide for this lacking information. With this additional information the quadrant analysis technique could be used to study coherent structures in a jet flow.

Another approach could be quite useful in studying coherent structures. The transition process of a laminar flow into a turbulent one is simulated by introducing small disturbances in a laminar flow near the wall at regular time intervals. So the origin of turbulent spots is fixed and the development of the spots can be measured.

Perhaps it is possible to introduce also small disturbances in wall bounded turbulent flows at regular time intervals, using for instance sparks to generate the disturbances. With flow visualization it can be examined whether these disturbances develop in the same way coherent structures do. If this is the case, fixed coherent structures can be studied.

LIST OF SYMBOLS

		definition or first occurrence on page:
c	coefficient of X-wire characteristic	60
D	nozzle diameter	28
	tube diameter	7
D(t)	detection function of Blackwelder and Kaplan's method	68
DM(t)	detection function of modified version of Blackwelder and Kaplan's method	83
E(f)	one-dimensional energy spectrum	50
E_{∞}	one dimensional turbulence kinetic energy	51
F	flatness factor	51
F_u	flatness factor of u	51
F_v	flatness factor of v	51
f	focus length	39
	frequency	31
	friction factor	42
f_K	Kolmogorov frequency	66
H	hole-size	21
K	hole-size	80
k	parameter of Blackwelder and Kaplan's detection method	13
	wavenumber	31
N	number of detections	74
n	exponent	54
	integer	76
P	static pressure	7
R	correlation factor	43
	nozzle radius	61
	tube radius	7
$R_{uu}(\Delta z)$	two-point spatial correlation of u	11
Re	Reynolds number	44
Re_D	Reynolds number based on U_{av} and D	7
	Reynolds number based on U_c and D	28
Re_{θ}	Reynolds number based on U_{av} and θ	7

Re_θ	Reynolds number based on U_∞ and θ	10
S	skewness factor	51
S_u	skewness factor of u	51
S_v	skewness factor of v	51
s	integration variable	68
t	time	6
	total duration signal	77
T_B	mean burst period	14
T_d	mean time between successive detections	66
t_d	time interval between successive detections	73
T_g	mean time between successive coherent uv-groups	102
t_g	time interval between successive coherent uv-groups	102
t_i	total time uv-signal spent in quadrant i excluding hole (i = 1, 2, 3 or 4) or in hole (i = 5)	80
t_j	total time uv-signal spent in quadrant j (j = 1, 2, 3 or 4)	101
T_m	averaging time of Blackwelder and Kaplan's detection method	13
T_{mg}	averaging time of modified version of Blackwelder and Kaplan's detection method	83
t_n	time midway between beginning and end of detection	69
	beginning of detection	70
t_o	total time uv-signal spent outside hole	112
U, V, W	Eulerian Cartesian velocity components	10
	\bar{U} , \bar{V} , \bar{W} time-mean values	7
\underline{U}	instantaneous velocity vector	60
u, v, w	turbulence velocity components of U, V and W respectively	10
	u' , v' , w' root-mean-square turbulence velocity components	11
U_{av}	average flow velocity in tube cross section	7
\bar{U}_{max}	time-mean flow velocity at tube axis	7
U_c	average bulge velocity	19
U_e	nozzle exit velocity	28
U_{eff}	effective velocity component X-wire	60
U_∞	free stream velocity	10
u_e'	u' at centerline of jet nozzle	61
u'_{max}	jet exit boundary layer maximum of u'	61

u_τ	wall friction velocity	5
var	variance of streamwise turbulence velocity component	68
$W(k,U)$	wavenumber-convection velocity spectrum	31
x, y, z	Cartesian coordinates	5
y_1	wall distance measuring point laser	57
y_w	wall distance hydrogen bubble wire	57
y^*	jet exit wall distance	60
$-\rho\overline{uv}$	Reynolds stress	43
$-\rho\overline{uv}_d$	Reynolds stress due to detections	77
$-\rho\overline{uv}_g$	Reynolds stress due to coherent uv-groups	104
$-\rho\overline{uv}_i$	Reynolds stress due to quadrant i excluding hole (i = 1, 2, 3 or 4) or to hole (i = 5)	80
$-\rho\overline{uv}_{i,d}$	Reynolds stress of quadrant i excluding hole (i = 2 or 4) due to detections of Blackwelder and Kaplan's method	81
$-\rho\overline{uv}_j$	Reynolds stress due to quadrant j (j = 1, 2, 3 or 4)	108
$-\rho\overline{uv}_o$	Reynolds stress outside hole	112
Δt	time interval	6
Δt_d	total detection time	77
Δt_g	total detection time of coherent uv-groups	104
$\Delta t_{i,d}$	total time uv-signal spent in quadrant i excluding hole (i = 2 or 4) due to detections of Blackwelder and Kaplan's method	81
Δz	spanwise separation	11
∂	partial differential operator	15
δ	boundary layer thickness	6
$\delta_{0,99}$	boundary layer thickness	35
δ^*	displacement thickness	35
ϵ	dissipation per unit mass and time	66
η	dimensionless radial jet distance	108
	Kolmogorov frequency	66
θ	momentum thickness	7
λ	dissipation length scale	66
λ_x	streamwise length of low-speed streak	15

λ_z	spanwise low-speed streak spacing	6
ν	kinematic viscosity	5
ρ	density	5
τ	time delay	14
τ_d	maximum time delay between successive detections on one structure	101
τ_w	wall shear stress	5
ϕ	angle between X-wire and velocity vector	60
$\Delta\tau$	enlargment of detection time	76
+	normalized with inner variables u and	5
\wedge	VITA average	68
\sim	VITA average	83
< >	conditional average	69

References

1. Antonia, R.A., [1972]
Conditionally sampled measurements near the outer edge of a
turbulent boundary layer.
J. Fluid Mech., 56, 1
2. Bandyopadhyay, P.R., [1982]
Period between bursting in turbulent boundary layers.
Phys. Fluids., 25, 1751
3. Batchelor, G.K. and Townsend, A.A., [1948 a]
Decay of isotropic turbulence in the initial period.
Proc. R. Soc. London, Ser. A, 193, 539
4. Batchelor, G.K. and Townsend, A.A., [1948 b]
Decay of turbulence in the final period.
Proc. R. Soc. London, Ser. A, 194, 527
5. Blackwelder, R.F. and Eckelmann, H., [1979]
Streamwise vortices associated with the bursting phenomenon.
J. Fluid Mech., 94, 577
6. Blackwelder, R.F. and Kaplan, R.E., [1972]
The intermittent structure of the wall region of a turbulent
boundary layer.
Rep. USCAE 1-22
University of Southern California, Los Angeles
7. Blackwelder, R.F. and Kaplan, R.E., [1976]
On the wall structure of the turbulent boundary layer.
J. Fluid Mech., 76, 89
8. Blackwelder, R.F. and Kovaszny, L.S.G., [1972]
Time scales and correlations in a turbulent boundary layer.
Phys. Fluids, 15, 1545
9. Boelsma, G.H., [1981]
Analoge en numerieke detectie van coherente structuren in een
turbulente grenslaag. (In Dutch)
Delft, University of Technology, afstudeerverslag
10. Bogard, D.G., [1982]
Investigation of burst structures in turbulent channel flows
through simultaneous flow visualization and velocity
measurements.
Purdue University, thesis
11. Boussinesq, J., [1877]
Theorie de l'ecoulement tourbillant.
Mem. pres. acad. sci. Paris, 23, 46
12. Brodkey, R.S., Wallace, J.M. and Eckelmann, H., [1974]
Some properties of truncated signals in boundary shear flows.
J. Fluid Mech., 63, 209
13. Brown, G.L. and Roshko, A., [1974]
On density effects and large structure in turbulent mixing
layers.
J. Fluid Mech., 64, 775
14. Brown, G.L. and Thomas, A.S.W., [1977]
Large structure in a turbulent boundary layer.
Phys. Fluids, 20, S243

15. Bruun, H.H., [1977]
A time-domain analysis of the large-scale flow structure in a circular jet.
Part 1. Moderate Reynolds number.
J. Fluid Mech., 83, 641
16. Cantwell, B.J., [1975]
A flying hot-wire study of the turbulent near wake of a circular cylinder at a Reynolds number of 140000.
Ph.D. Thesis, California Institute of Technology
17. Cantwell, B.J., [1981]
Organized motion in turbulent flow.
Ann. Rev. Fluid Mech., 13, 457
18. Chevray, R. and Tutu, N.K., [1978]
Intermittency and preferential transport of heat in a round jet.
J. Fluid Mech., 88, 133
19. Clauser, F.H., [1956]
The turbulent boundary layer.
Adv. in Appl. Mech., 4, 1
20. Comte-Bellot, G., Sabot, J. and Saleh, I., [1979]
Detection of intermittent events maintaining Reynolds stress.
Proceedings of the Dynamic Flow Conference 1978.
Sijthoff & Noordhoff, the Netherlands.
21. Corino, E.R. and Brodkey, R.S., [1969]
A visual investigation of the wall region in turbulent flow.
J. Fluid Mech., 37, 1
22. Corrsin, S., [1943]
Investigations of flow in an axially symmetric heated jet of air.
NACA Wartime Rep. W-94
23. Corrsin, S. and Kistler, A., [1954]
The free boundaries of turbulent flows.
NACA Tech. Note No. 3133
24. Crow, S.C. and Champagne, F.H., [1971]
Orderly structure in jet turbulence.
J. Fluid Mech., 48, 547
25. Dimotakis, P.E., Miake-Lye, R.C. and Papantoniou, D.A., [1983]
Structure and dynamics of round turbulent jets.
Phys. Fluids, 26, 3185
26. Durst, F., Melling, A. and Whitelaw, J.H., [1976]
Principles and practice of laser-Doppler anemometry.
Academic Press, New York.
27. Eckelmann, H., [1970]
Experimentelle Untersuchungen in einer turbulenten Kanalströmung mit starken viskosen Wandschichten.
Max Planck Institut für Strömungsforschung, Göttingen, nr. 48
28. Eckelmann, H., [1974]
The structure of the viscous sublayer and the adjacent wall region in a turbulent channel flow.
J. Fluid Mech., 65, 439
29. Eiseley, L., [1979]
Darwin and the mysterious mr. X: New light on the evolutionists.
Dutton, E.P., New York
30. Emmons, H.W., [1951]
The laminar-turbulent transition in a boundary layer. Part 1.
J. Aerosp. Sci., 18, 490
31. Fage, F.A. and Townsend, H.C.H., [1932]
An examination of turbulent flow with an ultramicroscope.
Proc. Roy. Soc. London, Ser. A, 135, 656

32. Falco, R.E., [1977]
Coherent motions in the outer region of turbulent boundary layers.
Phys. Fluids, 20, S124
33. Favre, A., [1946]
Appareil de mesures statistiques de la corrélation dans le temps.
Proc. Int. Congr. Mech., 6th.
34. Favre, A., Gaviglió, J. and Dumas, R., [1957]
Space-time double correlations and spectra in a turbulent boundary layer.
J. Fluid Mech., 2, 313
35. Favre, A., Gaviglió, J. and Dumas, R., [1958]
Further space-time correlations of velocity in a turbulent boundary layer.
J. fluid Mech., 3, 344
36. Fondse, H., Leijdens, H. and Ooms, G., [1983]
On the influence of the exit conditions on the entrainment rate in the development region of a free, round, turbulent jet.
Appl. Sci. Res., 40, 355
37. Freymuth, P., [1966]
On transition in a separated laminar boundary layer.
J. Fluid Mech., 26, 683
38. Godefroy, H.W.H.E. and Kunen, J.M.G., [1984]
Meetmogelijkheden met een laser-Doppler snelheidsmeter, betreffende Reynoldse schuifspanningen in turbulente pijpströmungen.
Delft, Hydraulics Laboratory, S 216-III
39. Grass, A.J., [1971]
Structural features of turbulent flow over smooth and rough boundaries.
J. Fluid Mech., 50, 233
40. Gupta, A.K. and Kaplan, R.E., [1972]
Statistical characteristics of Reynolds stress in a turbulent boundary layer.
Phys. Fluids, 15, 981
41. Gupta, A.K., Laufer, J. and Kaplan, R.E., [1971]
Spatial structure in the viscous sublayer.
J. Fluid Mech., 50, 493
42. Hama, F.R., Long, J.D. and Hegarty, J.C., [1957]
On transition from laminar to turbulent flow.
J. Appl. Phys., 28, 388
43. Head, M.R. and Bandyopadhyay, P.R., [1981]
New aspects of turbulent boundary-layer structure.
J. Fluid Mech., 107, 297
44. Hedley, T.B. and Keffer, J.F., [1974]
Some turbulent/non-turbulent properties of the outer intermittent region of a boundary layer.
J. Fluid Mech., 64, 645
45. Hinze, J.O., [1975]
Turbulence. 2nd ed.
McGraw Hill, New York
46. Hussain, A.K.M.F., [1983]
Coherent structures -reality and myth.
Phys. Fluids, 26, 2816
47. Hussain, A.K.M.F. and Clark, A.R., [1981]
Measurements of wavenumber-celerity spectrum in plane and axisymmetric jets.
AIAA J., 19, 51

48. Hussain, A.K.M.F. and Zaman, K.B.M.Q., [1980]
Vortex pairing in a circular jet under controlled excitation.
Part 2. Coherent Structure dynamics.
J. Fluid Mech., 101, 493
49. Kaplan, R.E. and Laufer, J., [1969]
The intermittently turbulent region of the boundary layer.
Proc. Int. Congr. Mech., 12th, 236
50. Kawaguchi, Y., Yano, T. and Suzuki, K., [1983]
An experimental study on coherent structure in a turbulent
boundary layer disturbed by a cylinder.
Preprints for the Eighth Biennial Symposium on Turbulence.
Missouri-Rolla
ed. Zakin, J.L. and Patterson, G.K.
51. Kim, H.T., Kline, S.J. and Reynolds, W.C., [1971]
The production of turbulence near a smooth wall in a turbulent
boundary layer.
J. Fluid Mech., 50, 133
52. Klebanoff, P.S., [1954]
Characteristics of turbulence in a boundary layer with zero
pressure gradient.
NACA Tech. Note No. 3178
53. Kline, S.J., Reynolds, W.C., Schraub, F.A. and Runstadler, P.W.,
[1967]
The structure of turbulent boundary layers.
J. Fluid Mech., 30, 741
54. Kline, S.J. and Runstadler, P.W., [1959]
Some preliminary results of visual studies of the flow model of
the wall layers of the turbulent boundary layer.
J. Appl. Mech., Ser. E, 26, 166
55. Kolmogorov, A.N. [1941]
The local structure of turbulence in incompressible flow for
very large Reynolds number.
Compt. rend. acad. sci. U.R.S.S., 30, 31
56. Kovaszny, L.S.G., Kibens, V. and Blackwelder, R.F., [1970]
Large-scale motion in the intermittent region of a turbulent
boundary layer.
J. Fluid Mech., 41, 283
57. Kreplin, H.-P. and Eckelmann, H., [1979]
Behavior of the three fluctuating velocity components in the
wall region of a turbulent channel flow.
Phys. Fluids, 22, 1233
58. Lau, J.C. and Fisher, M.J., [1975]
The vortex-street structure of 'turbulent' jets. Part 1.
J. Fluid Mech., 67, 299
59. Lau, J.C., Fisher, M.J. and Fuchs, H.V., [1972]
The intrinsic structure of turbulent jets.
J. Sound and Vib., 22, 379
60. Laufer, J., [1954]
The structure of turbulence in fully developed pipe flow.
NACA Rep. 1174
61. Lawn, C.J., [1971]
The determination of the rate of dissipation in turbulent pipe
flow.
J. Fluid Mech., 48, 477
62. Lu, S.S. and Willmarth, W.W., [1973]
Measurements of the structure of the Reynolds stress in a
turbulent boundary layer.
J. Fluid Mech., 60, 481

63. Ludwig, H. and Tillmann, W., [1949]
 Untersuchungen ueber die Wandschubspannung in turbulenten
 Reibungsschichten.
 Ing.-Arch., 17, 288
64. Maanen, H.R.E. van and Fortuin, J.M.H., [1983]
 Experimental determination of the random lump-age distribution
 in the boundary layer of the turbulent pipe flow using laser-
 Doppler anemometry.
 Chem. Eng. Sci., 38, 399
65. Mizushima, T. and Usui, H., [1977]
 Reduction of eddy diffusion for momentum and heat in
 viscoelastic fluid flow in a circular tube.
 Phys. Fluids, 20, S100
66. Mollo-Christensen, E., [1971]
 Physics of turbulent flow.
 AIAA J., 9, 1217
67. Morrison, W.R.B. and Kronauer, R.E., [1969]
 Structural similarity for fully developed turbulence in smooth
 tubes.
 J. Fluid Mech., 39, 117
68. Narayanan, B. and Marvin, J., [1978]
 On the period of the coherent structure in boundary layers at
 large Reynolds numbers.
 Lehigh Workshop on coherent structure in turbulent boundary
 layers., 380
 ed. Smith, C.R. and Abbot, D.E.
69. Nychas, S.G., Hershey, H.C. and Brodkey, R.S., [1973]
 A visual study of turbulent shear flow.
 J. Fluid Mech., 61, 513
70. Offen, G.R. and Kline, S.J., [1973]
 Experiments on the velocity characteristics of 'bursts' and on
 the interaction between the inner and outer regions of a
 turbulent boundary layer.
 Rep. no. MD-31
 Stanford University, Stanford, California
71. Popovich, A.T. and Hummel, R.L., [1967]
 Experimental study of the viscous sublayer in turbulent pipe
 flow.
 AIChE J., 13, 854
72. Prandtl, L., [1925]
 Bericht ueber untersuchungen zur ausgebildeten Turbulenz.
 Z. angew. Math. und Mech., 5, 136
73. Rao, K.N., Narasimha, R. and Narayanan, M.A.B., [1971]
 Bursting in a turbulent boundary layer.
 J. Fluid Mech., 48, 339
74. Reynolds, O., [1895]
 On the dynamical theory of incompressible viscous fluid and the
 determination of the criterium.
 Philos. Trans. R. Soc. London, Ser. A, 186, 123
75. Runstadler, P.W., Kline, S.J. and Reynolds, W.C., [1963]
 An investigation of the flow structure of the turbulent boundary
 layer.
 Rep. no. MD-8
 Stanford University, Stanford, California
76. Schraub, F.A. and Kline, S.J., [1965]
 A study of the structure of the turbulent boundary layer with
 and without longitudinal pressure gradient.
 Rep. no. MD-12
 Stanford University, Stanford, California

77. Smith, C.R., [1978]
Visualization of turbulent boundary layer structure using a moving hydrogen bubble probe.
Proc. of the Workshop on Coherent Structure of Turbulent Boundary Layer.
Lehigh university, Bethelam, Pennsylvania
78. Smith, C.R., [1983]
A synthesized model of the near-wall behaviour in turbulent boundary layers.
Preprints for the Eighth Biennial Symposium on Turbulence.
Missouri-Rolla
ed. Zakin, J.L. and Patterson, G.K.
79. Smith, C.R. and Metzler, S.P., [1983]
The characteristics of low-speed streaks in the near-wall region of a turbulent boundary layer.
J. Fluid Mech., 129, 27
80. Smith, C.R. and Schwartz, S.P., [1983]
Observation of streamwise rotation in the near-wall region of a turbulent boundary layer.
Phys. Fluids, 26, 641
81. Sreenivasan, K.R., Antonia, R.A. and Britz, D., [1979]
Local isotropy and large structures in a heated turbulent jet.
J. Fluid Mech., 94, 745
82. Suzuki, K. and Kawaguchi, K., [1980]
Measurement of bursting period and test of surface renewal model in a turbulent boundary layer distributed by a cylinder.
ICHMI/IUTAM Symposium on Heat and Mass Transfer and the Structure of Turbulence, Dubrovnik.
83. Talmon, A.M., [1984]
Simultane visualisatie-studie en snelheidsmetingen aan coherente structuren in een turbulente grenslaag. (In Dutch)
Delft, University of Technology, afstudeerverslag.
84. Taylor, G.I., [1915]
Eddy motion in atmosphere.
Philos. Trans. R. Soc. London, Ser. A, 215, 1
85. Taylor, G.I., [1932]
The transport of vorticity and heat through fluids in turbulent motion.
Proc. R. Soc. London, Ser. A, 135, 678
86. Taylor, G.I., [1935]
The statistical theory of turbulence, parts I - IV.
Proc. R. Soc. London, Ser. A, 151, 421
87. Theodorsen, T., [1955]
The structure of turbulence.
In: 50 Jahre Grenzschichtforschung, 55
ed. Gortler, H. and Tollmien, W.
Braunschweig, Vieweg & Sohn
88. Townsend, A.A., [1947]
Measurements in a turbulent wake of a cylinder.
Proc. R. Soc. London, Ser. A, 190, 551
89. Townsend, A.A., [1956]
The structure of turbulent shear flow. 1st ed.
Cambridge Univ. Press., Cambridge
90. Townsend, A.A., [1970]
Entrainment and the structure of turbulent flow.
J. Fluid Mech., 141, 13
91. Townsend, A.A., [1976]
The structure of turbulent shear flow. 2nd ed.
Cambridge Univ. Press., Cambridge

92. Tso, J., Kovasznay, L.S.G. and Hussain, A.K.M.F., [1981]
Search for large-scale coherent structures in the nearly self-preserving region of a turbulent axisymmetric jet.
J. Fluids Eng., 103, 503
93. Ueda, H. and Hinze, J.O., [1975]
Fine structure turbulence in the wall region of a turbulent boundary layer.
J. Fluid Mech., 67, 125
94. Vink, P.J.J., [1981]
Coherente structuren in turbulente stromingen. (In Dutch)
Delft, University of Technology, 3e jaarsverslag
95. Vink, P.J.J., [1982]
Numerieke detectie van coherente structuren in een turbulente grenslaag. (In Dutch)
Delft, University of Technology, 4e jaarsverslag
96. Vink, P.J.J., [1984]
Coherente structuren in een vrije straal. (In Dutch)
Delft, University of Technology, MEAH-32
97. Wallace, J.M., Eckelmann, H. and Brodkey, R.S., [1972]
The wall region in turbulent shear flow.
J. Fluid Mech., 54, 39
98. Weske, J.R. and Plankholt, A.H., [1953]
Discrete vortex systems in the transition range in a fully developed flow in a pipe.
J. Aero. Sci., 20, 717
99. Wille, R., [1963]
Beitraege zur Phaenomenologie der Freistrahlen.
Z. Flugwiss., 11, 222
100. Willmarth, W.W., [1975]
Structure of turbulence in boundary layer.
Adv. in Appl. Mech., 15, 159
101. Willmarth, W.W. and Lu, S.S., [1972]
Structure of the Reynolds stress near the wall.
J. Fluid Mech., 55, 65
102. Wills, J.A.B., [1962]
The correction of hot-wire readings for proximity to a solid boundary.
J. Fluid Mech., 12, 388
103. Winant, C.D. and Browand, F.K., [1974]
Vortex pairing: the mechanism of turbulent mixing-layer growth at moderate Reynolds number.
J. Fluid Mech., 63, 237
104. Wygnanski, I.J. and Champagne, F.H., [1973]
On transition in a pipe
Part 1. The origin of puffs and slugs and the flow in a turbulent slug.
J. Fluid Mech., 59, 281
105. Wygnanski, I.J., Solokov, N. and Friedman, D., [1975]
On transition in a pipe.
Part 2. The equilibrium puff.
J. Fluid Mech., 69, 283
106. Wygnanski, I.J., Solokov, N. and Friedman, D., [1976]
On the turbulent 'spot' in a boundary layer undergoing transition.
J. Fluid Mech., 78, 785
107. Yeh, H. and Cummins, H.Z., [1964]
Localized fluid flow measurements with He-Ne laser spectrometer.
Appl. Phys. Lett., 4, 176

108. Zaman, K.B.M.Q. and Hussain, A.K.M.F., [1980]
Vortex pairing in a circular jet under controlled excitation.
Part 1. General jet response.
J. Fluid Mech., 101, 449

Appendix A
DESCRIPTION OF A TURBULENT BOUNDARY LAYER

Two regions or layers can be distinguished in a turbulent flow along a smooth rigid wall:

- (1) a region close to the wall -the wall or inner layer- where the wall directly influences the flow through the action of the viscous stress,
- (2) the remaining part of the boundary layer -the outer or intermittent layer (in pipe and channel flow this region is called the core region)- where the wall only indirectly affects the flow through the wall shear stress τ_w .

The characteristic length and velocity scale in the wall layer are the friction length ν/u_τ and the friction velocity u_τ . These scales are the so-called inner parameters of the turbulent boundary layer.

$$[u_\tau = \sqrt{\tau_w/\rho} \text{ (}\rho \text{ is the density of the flow).}$$

ν is the kinematic viscosity of the flow.]

The turbulence characteristics of the outer layer are dominated by the free stream velocity U_∞ and the boundary layer thickness δ ; the outer parameters of a turbulent boundary layer.

In the wall layer of the turbulent boundary layer three subregions can be distinguished:

- (1) the viscous sublayer, the region closest to the wall where the viscous stresses are considerably greater in magnitude than the Reynolds stresses,
- (2) the buffer layer, the region beyond the viscous sublayer where the viscous stresses and the Reynolds stresses are of the same order of magnitude,
- (3) the logarithmic layer, the region bounded by the buffer layer where the viscous stresses are negligibly small in comparison with the Reynolds stress.

In the viscous sublayer ($0 < y^+ < 5$) the following relation holds

$$\bar{u}/u_\tau = yu_\tau/\nu,$$

and in the logarithmic layer ($y^+ > 30$)

$$\bar{u}/u_\tau = A^{10} \log y^+ + B.$$

For the coefficients A and B many values have been proposed, Clauser [1956] proposed for boundary layer flows the values $A = 5.6$ and $B = 4.9$.

The logarithmic layer is supposed to be ended at the point where the velocity distribution does not agree anymore with the logarithmic relation. If the Reynolds number of the flow is great enough, the logarithmic region can extend to $y^+ = 500$.

The logarithmic layer and the outer layer together are called the velocity defect region.

Appendix B
DESCRIPTION OF AN AXISYMMETRIC JET

In a free, round, turbulent jet a number of regions are distinguished. Usually a jet is divided into two main regions (fig. 100):

- (1) the region of about the first 70 diameters is called the development region,
- (2) the remaining part of a jet is called the fully developed region or the region of complete self-preservation.

Commonly two subregions are defined in the development region (fig. 100):

- (1) the region of the first 5 diameters is called the mixing layer region,
- (2) the region between about 10 and 70 diameters is called the region of partial self-preservation.

In the mixing layer region a two-dimensional mixing layer is found 'wrapped around' the jet axis. This mixing layer is developing into a three-dimensional flow, in which firstly the time-mean velocity profile becomes self-preserving (the region of partial self-preservation) and further downstream the profiles of other turbulence quantities attain the state of self-preservation (the fully developed region).

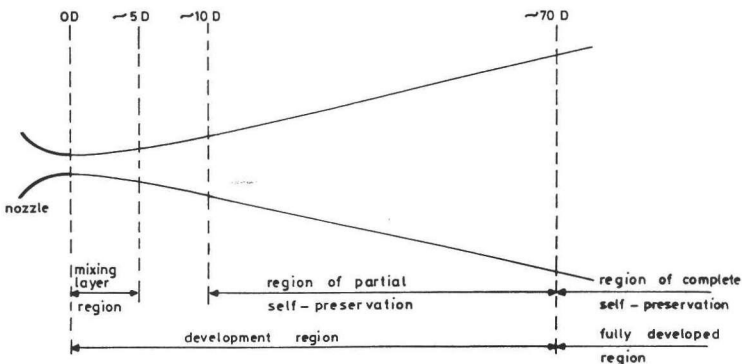


Figure 100: Flow regions in a turbulent jet.

SAMENVATTING

Visualisatie-onderzoek heeft in turbulente stromingen het bestaan van zg. coherente structuren aan het licht gebracht. Daar deze methode vooral kwalitatieve informatie over structuren geeft, wordt met Eulerse detectie-methoden geprobeerd om kwantitatieve gegevens over deze structuren te verzamelen.

In dit onderzoek is de objectiviteit van een aantal Eulerse detectie-methoden bestudeerd, nl. van de detectie-methode van Ueda en Hinze, van de methode van Blackwelder en Kaplan en van een methode die een uitbreiding is van de methode van Blackwelder en Kaplan. Hiervoor zijn meetsignalen uit een turbulente grenslaag en een turbulente pijpstroming gebruikt. De resultaten geven echter aan dat deze methoden niet objectief zijn. De gemiddelde tussentijd van opeenvolgende detecties, de verdeling van de tussentijden en de conditioneel gemiddelde hoofdstroomsnelheid blijken nl. sterk afhankelijk te zijn van de parameterwaarden die in deze methoden gebruikt worden. De verdeling van detectie-tussentijden blijkt ook een andere vorm te hebben dan een visueel bepaalde verdeling van 'burst'-tussentijden. De bijdrage van detecties aan de Reynoldsspanning blijkt niet veel groter te zijn dan op grond van de gedetecteerde tijdfractie verwacht mag worden. De conclusie lijkt derhalve gewettigd, dat deze detectie-methoden niet erg geschikt zijn voor het bemeten van coherente structuren.

Daar blijkt, dat de autocorrelatie-methode maar een gedeelte van de meettijd toegepast kan worden, moet voor deze methode hetzelfde geconcludeerd worden.

Teneinde te kunnen onderzoeken of Eulerse detecties samenvallen met visuele detecties van structuren is visualisatie-onderzoek gecombineerd met laser-Doppler metingen in een turbulente waterstroming. Visualisatie is uitgevoerd met de zg. waterstofbelletjes-methode. Detecties volgens de methode van Blackwelder en Kaplan blijken slechts voor een klein gedeelte samen te vallen met visueel waargenomen 'bursts'. Detecties volgens de zg. tweede kwadrant-methode, waarbij alleen bepaalde bijdragen aan de Reynoldsspanning behorend tot tweede kwadrant van het u-v vlak beschouwd worden, blijken wel

erg goed overeen te komen met visuele detecties van 'ejections'. Als verondersteld wordt dat snel na elkaar voorkomende Eulerse detecties reacties zijn op een structuur, dan blijken zelfs 'bursts' gedetecteerd te kunnen worden.

De kwadranten-methode geeft alleen in die gebieden van een straal waar vooral de invloed van de naburige rand merkbaar is, relevante informatie over structuren, omdat deze methode de structuren niet onderscheidt naar beginpunt en orientatie.

ACKNOWLEDGEMENT

The author wishes to express his gratitude to prof.dr.ir. G. Ooms whose guidance and encouragement made this work possible.

Thanks are also extended to the other members of the Laboratory for Aero- and Hydrodynamics of the Delft University of Technology for their assistance and advice during the investigations.

The author is specially indebted to the former students G.H. Boelsma, A.M. Talmon, P.J.J Vink and A. Westen.

Many thanks are due to ir. H.W.H.E. Godefroy of the Delft Hydraulics Laboratory, for giving the author the opportunity to measure in turbulent flows the instantaneous Reynolds stress with laser-Doppler equipment.

The author wants to thank Mr. H.G.M. Linskens for making the drawings and Mrs. E.A. Kunen-Ashton for correcting the manuscript.

LEVENSBERICHT

De schrijver werd op 6 september 1953 geboren te Venray.

Van 1966 t/m 1972 bezocht hij het Boschveldcollege te Venray, alwaar hij zijn middelbare schoolopleiding afsloot met het eindexamen gymnasium β .

In laatstgenoemde jaar begon hij te studeren aan de afdeling Luchtvaart- en Ruimtevaarttechniek van de T.H. te Delft. Daar studeerde hij in juli 1978 af bij de vakgroep Theoretische en Experimentele Aerodynamica.

Van augustus 1978 t/m december 1979 vervulde hij zijn militaire dienstplicht als reserve-officier bij de Koninklijke Luchtmacht.

Van januari 1980 t/m januari 1984 was hij in dienst bij de afdeling Werktuigbouwkunde van de T.H. te Delft. In die tijd werd bij de vakgroep Stromingsleer dit onderzoek uitgevoerd.

In juni 1984 trad hij in dienst bij TNO in Delft.

Stellingen

1. Methoden die coherente structuren detecteren in snelheids-signalen dienen vergeleken te worden met visualisatie-onderzoek teneinde te kunnen controleren of en zo ja welke structuren gedetecteerd worden.
2. De detectie-methode van Blackwelder en Kaplan detecteert geen "bursts" maar langzame stroomstromingen.
3. De door Ueda en Hinze gemeten waarde voor de dimensieloze "burst"-periode [$T_B U_\infty / \delta = 4.7$] is een eigenschap van hun detectie-methode.
4. In haar huidige vorm draagt ontwikkelingshulp meer bij aan de ontwikkeling van het gevende dan van het ontvangende land.
5. De bewapeningswedloop dient aangepakt te worden bij de wortel van het probleem, de research en ontwikkeling.
6. Het belang dat aan de televisie toegekend wordt - getuige het gekrakeel over satelliet-, betaal- en kabeltelevisie, komt in een vreemd daglicht te staan, als bedacht wordt dat de kijker het gebodene gelaten over zich heen laat gaan - getuige het α -ritme dat de hersenen produceren tijdens het televisie kijken.
7. Economisch belang gebiedt onderscheid te maken tussen beroepsverkeer op het water en pleziervaart wat voorrang op wegverkeer betreft.
8. De parlementaire enquête naar het RSV-debâcle leert dat de overheid een onverantwoord risico neemt door aan een bedrijf in moeilijkheden financiële steun te verlenen zonder tegelijkertijd toezicht op de bedrijfsvoering uit te oefenen.

9. Wetenschappelijk onderzoek van promovendi aan universiteiten en technische hogescholen dreigt in de verdrinking te komen door de invoering van de twee-fasenstructuur.
10. In openbaar vervoer kan men niet zwart rijden.

Delft

J.M.G. Kunen

